Deterimination of Focal Depths of Earthquakes in the Mid-Oceanic Ridges from Amplitude Spectra of Surface Waves

by

YI-BEN TSAI

B. S., National Taiwan University
(1962)

M. S., National Central University
(1965)

SUBMITTED IN PARTIAL FULFILLMENT
OF THE REQUIREMENTS FOR THE
DEGREE OF DOCTOR OF
PHILOSOPHY

at the

MASSACHUSETTS INSTITUTE OF TECHNOLOGY
June, 1969

Signature of Author _____
Department of Earth and Planetary Sciences

Certified by _____
Thesis Supervisor

Accepted by _____
Chairman, Departmental Committee on Graduate Students

ABSTRACT

Deterimination of Focal Depths of Earthquakes in the Mid-Oceanic Ridges from Amplitude Spectra of Surface Waves

by

Yi-Ben Tsai

Submitted to the Department of Earth and Planetary Sciences in partial fulfillment of the requirement for the degree of Doctor of Philosophy.

A method based on the normal mode theory for surface waves excited by a slip dislocation in a multilayered elastic medium is successfully developed for determining the focal depths of remote earthquakes with known fault plane solutions. After examining various possible sources of uncertainty and testing on several earthquakes, the method is shown to be dependable for studying earthquakes with magnitude $m_b \leq 6$.

Since the amplitude spectra of surface waves are used in this method, not only the focal depth but also the seismic moment of the equivalent double couple system of an earthquake can be determined.

32 earthquakes with known fault plane solutions and in the three major mid-oceanic ridge systems of the world are studied by this method. Our results can be summarized as the following:

(1) All strike-slip earthquakes from the east Pacific rise, the Gulf of California, the San Andreas fault, the Mendocino fracture zone, the Blanco fracture zone and the Queen Charlotte Island fault occurred at depths within 10 km excluding the water depth. This similarity of focal depth distribution strongly supports Wilson's (1965a,b) ideas that the San Andreas fault is a transform fault, and that the east Pacific rise extends through the tectonic features mentioned and terminates at the Queen Charlotte Island fault.

All the strike-slip earthquakes from the mid-Atlantic and the mid-Indian ocean ridges were also characterized by extremely shallow focal depths.

(2) All 16 dip-slip earthquakes studied in this paper occurred systematically at greater depths --- from about 30 to 65 km. This evidence suggests that the thickness of the lithosphere beneath the central ridges is at least 65 km.

(3) By using Aki's (1967) scaling law for seismic spectrum, the observed seismic moments are translated to the surface wave magnitude Ms and compared with the body wave magnitude m_b. The results show that all earthquakes, whether dip-slip or strike-slip, follow the same Ms-versus-m_b relationship as that observed for earthquakes in the western United States. This similarity of the Ms-versus-m_b relationship again supports the idea that the seismicity in the western United States is closely related to the east Pacific rise. It also implies that the low stress drop observed for earthquakes on the San Andreas fault probably characterizes those earthquakes on the mid-oceanic ridges too.

The surprisingly uniform pattern in focal depth distribution and the unique Ms-versus-m_b relationship existing among earthquakes in all three major mid-oceanic ridges are strong evidence for the concept of new global tectonics. (Isacks, et. al., 1968).

Thesis Supervisor: Keiiti Aki
Title: Professor of Geophysics

Acknowledgments

I am deeply grateful for the extremely inspiring advice given by Professor Keiiti Aki during the writing of this thesis. In fact, I have learned from him the joy of being a seismological worker.

I am also indebted to Professor Frank Press. His suggestion on using the radiation patterns of surface waves to study the transform faults has been influential in defining problems for this thesis.

Very valuable assistance and advice provided by other persons are greatly appreciated, among them are many of my fellow graduate students.

I owe whatever I may accomplish to my parents, my wife Chu-jen and her parents. My parents have struggled hard to provide me an opportunity for higher learning for which they were denied. My wife's affection and understanding have made this opportunity much more meaningful and fruitful. Her parents' encouragement is another important source of inspiration I have received constantly.

My wife's drafting and Mrs. Shu-Mei Chung's typing have made the appearance of this thesis possible. I thank both of them.

The work of this thesis was supported partly by the Air Force Office of Scientific Research under contract AF49(638)-1632, and partly by the National Science Foundation under Grant GA-4039.

Table of Contents

		page
Abstract		2
Acknowledgments		4
Table of Contents		5
Chapter 1 -	INTRODUCTION	7
Chapter 2 -	EXCITATION OF SURFACE WAVE DUE TO DISLOCATION SOURCES IN A MULTILAYERED MEDIUM	10
2.1	The Fourier spectra of surface waves due to a point source in a layered half-space	11
2.2	Effects of the crustal thickness under continents on the excitation of Rayleigh waves	26
2.3	Effects of the water depth over oceans on the excitation of Rayleigh waves	30
2.4	Variations of the amplitude spectrum of surface waves due to a small uncertainty on the fault-plane solutions	33
2.5	The effects of finiteness of a source on the amplitude spectrum of surface waves	40
2.6	The Fourier spectrum of the source time function	45
Chapter 3 -	EQUALIZATION OF THE OBSERVED AMPLITUDE SPECTRUM OF SURFACE WAVES	49
3.1	Correction for the instrumental response	50
3.2	Corrections for the geometrical spreading and attenuation	51
3.3	Measurements on the attenuation coefficient of Rayleigh waves by the two-station method	55
3.4	Tests on the proposed method for focal depth determination	64
Chapter 4 -	THE FOCAL DEPTHS AND THE SEISMIC MOMENTS OF EARTHQUAKES ON THE MID-OCEANIC RIDGES	77
4.1	Earthquakes on theeast Pacific rise, in the Gulf of California, western North American and the northeast Pacific region	80
4.2	Earthquakes on the mid-Atlantic ridge	102
4.3	Earthquakes on the mid-Indian ocean ridge	113
4.4	The focal depths of earthquakes on the mid-oceanic ridges	129
4.5	Interpretation of the seismic moment data	131

Table of Contents (Cont.)

	page
Chapter 5 - SUMMARY AND DISCUSSIONS	135
5.1 On the method	135
5.2 On the results	137
5.3 Future studies	139
References	140

CHAPTER 1

Introduction

Recently, seismological evidence (Sykes, 1967) has provided a strong support for the hypotheses of sea-floor spreading, transform faults and continental drift. This evidence may be summarized briefly as the following:

Seismic activity on a fracture zone is confined almost exclusively to the section between the displaced ridges. Earthquakes in this zone are characterized by predominantly strike-slip motion. On the other hand, earthquakes located on the ridge crests are characterized by predominantly dip-slip motion. The inferred axes of maximum tension for these dip-slip faults are approximately perpendicular to the local strike of the ridges.

Unfortunately, the evidence mentioned above does not include information on the tectonics of ridges in three space dimensions because of the lack of adequate method to determine the focal depth of remote earthquakes. The purpose of the present paper is to fill in such information by determining the focal depths of earthquakes on the mid-oceanic ridges using the amplitude spectra of surface waves.

The focal depths of remote earthquakes such as those from the mid-oceanic ridges can not be accurately determined by travel time data alone. For example, Basham and Ellis (1969) have recently pointed out that the USCGS depths determined on a least-squares basis from P-travel times are, conservatively,

not considered more reliable than ± 50 km. Various authors have attempted to use depth phases such as pP or sP for focal depth determination. But this approach has some serious shortcomings when it is used for shallow earthquakes. LaCoss (1969) using depth phases at LASA to determine focal depths of nearly 200 events found that sP or pP was correctly picked for only 42 - 57% of all earthquakes. Basham and Ellis (1969) used a non-linear "P-Detection" polarization filter to isolate compressional and shear phases of 41 seismic events recorded at Western Alberta. They were able to detect the pP phase for only 25 of the 41 events. The accuracy of focal depths determined for these 25 earthquakes was about ± 15 km. From these two examples we notice that the depth phases were available for only less than 60% of all earthquakes studied. Furthermore, it is almost impossible to identify these phases for very shallow earthquakes. Since most earthquakes from the mid-oceanic ridges are remote and presumedly shallow, these classical approaches can not give accurate determination of their focal depths.

The method used in the present paper is based on the normal mode theory for surface waves excited by a slip dislocation in a realistic, multilayered earth model. This method was first proposed by Yanovskaya (1958). She and several other authors such as Ben-Menahem (1961), Harkrider (1964), Haskell (1964), Ben-Menahem and Harkrider (1964) and Saito (1967) solved the theoretical problems behind the method. We shall

here solve the practical problems encountered in the application of the method to actual earthquakes. The method will be applied to surface waves with periods 10 to 50 seconds from earthquakes with known fault plane solutions and with magnitudes smaller than about 6.5.

In the following chapters, several factors affecting the accuracy of the method will be first investigated in details. The applicability of the method will be tested using the data from earthquakes with known depths. We shall then apply this method to determine focal depths of more than thirty earthquakes in the three major mid-oceanic ridge systems of the world. The results will be discussed in the light of the theory of new global tectonics (Isack, et. al., 1968).

CHAPTER 2

Excitation of surface waves due to dislocation sources in a multilayered medium

The Fourier spectrum of surface waves due to a dislocation source in a layered half-space may be specified as a product of the following three factors:

a. the spatial factor which is a complex function determined by the focal depth, the structure of the layered medium and the orientation of the equivalent force system of the dislocation source;

b. the temporal factor which is the Fourier transform of the source time function; and

c. the finiteness factor which is derived from the simplified assumption that the rupture propagates along the fault plane with a unform speed over a finite distance.

In order to elucidate how the Fourier spectrum of surface waves may be used to determine the focal depths of earthquakes, each of these factors is examined in the following sections.

2.1 The Fourier spectra of surface waves due to a point source in a layered half-space.

Excitation of Surface waves due to point sources in a layered half-space has been studied by several authors, such as Haskell (1964), Harkrider (1964), Ben-Menahem and Harkrider (1964) and Saito (1967). These studies were all based upon the normal mode theory of surface waves in multilayered medium due to point force systems. Here we shall follow Saito's results.

The mechanism of earthquakes has been investigated extensively using fault plane solutions based on the first motions of P and polarization of S waves. A large number of such fault plane solutions now exist. Wickens and Hodgson (1967) give a collection of those from before 1962, and many more have since been made using the long period WWSSN stations. All reliable solutions obtained so far are consistent with a double couple source. Furthermore, recent theoretical studies by Knopoff and Gilbert (1960), Maruyama (1963), Haskell (1964) and Burridge & Knopoff (1964) show that the equivalency of a slip dislocation along a fault to a double couple in the absence of the fault is valid not only in the static elastic field but also in the dynamic elastic field. Thus for the purpose of calculating the excitation of surface waves due to an earthquake, we shall represent the earthquake source by an equivalent point double couple. The moment of either component couple of the equivalent double couple is defined as seismic moment (Aki, 1966). For the time being, we assume that the seismic moment

m(t) varys as a step function in time, i.e.

$$\begin{aligned} m(t)&=0 \qquad \text{when } t < 0 \\ m(t)&=M \qquad \text{when } t \geq 0 \end{aligned} \tag{1}$$

More sophisticated source time functions shall be discussed in a latter section.

Now let us define the coordinate and the fault plane geometry in Figure 1. The fault is assumed to strike in the X direction and to be located at depth h. The dip angle d is measured downward from the positive Y direction. The slip angle S is measured counterclockwise from a horizontal line on the fault plane. r and ϕ represent the distance and the azimuth from the epicenter to a point P on the free surface. ϕ is measured counterclockwise from the fault strike.

According to Saito (1967), the Fourier spectrum of displacement due to Love waves observed at P can be written as

$$\begin{aligned} L_\phi(\omega, r, \phi/h, d, s) = {} & \frac{M Y_1(0)}{4\omega C U I_1}\left(\frac{2C}{\pi\omega r}\right)^{1/2} e^{-i\left(\frac{\omega r}{C}-\frac{3\pi}{4}\right)} \\ & \cdot\left\{\frac{\omega Y_1(h)}{C}(\sin d \cos s \cos 2\phi - \tfrac{1}{2}\sin 2d \sin s \sin 2\phi) \right. \\ & \left. + i\frac{Y_2(h)}{\mu(h)}(\cos 2d \sin s \cos\phi + \cos d \cos s \sin\phi)\right\} \end{aligned} \tag{2}$$

where C is the phase velocity and U the group velocity of Love waves at angular frequency ω . I_1 in equation (2) is defined by

$$I_1 = \int_{-\infty}^{0} \rho(z)\, y_1^2(z)\, dz \tag{3}$$

$Y_1(z)$ and $y_2(z)$ in equations (2) and (3) are the normal mode solutions satisfying the equations

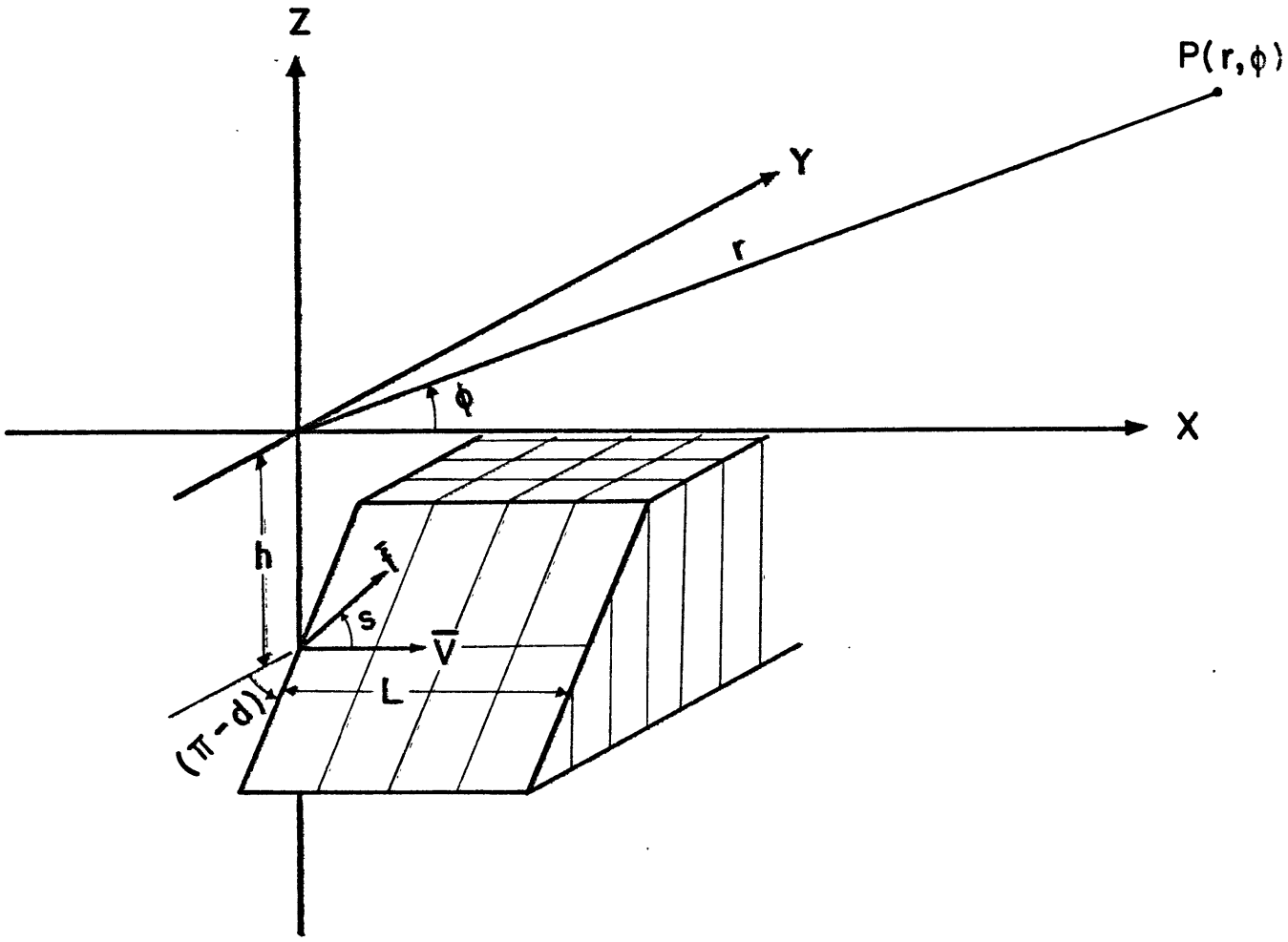

FIG. 1. Coordinate and fault plane geometry.

$$\begin{bmatrix} \frac{dy_1}{dz} \\ \frac{dy_2}{dz} \end{bmatrix} = \begin{bmatrix} 0 & \frac{1}{\mu(z)} \\ \frac{\omega^2}{c^2}\left[\mu(z) - c^2\rho(z)\right] & 0 \end{bmatrix} \begin{bmatrix} y_1 \\ y_2 \end{bmatrix} \tag{4}$$

and the boundary conditions

$$y_2(0)=y_2(-\infty)=y_1(-\infty)=0 \tag{5}$$

where $\rho(z)$ is density and $\mu(z)$ is rigidity of the medium at depth z.

Similarly, the Fourier spectrum of displacement due to Rayleigh waves observed at P can be written as

$$R_z(\omega,r,\phi/h,d,s)= \frac{M\, Y_1(0)}{4\omega C U I_1}\left(\frac{2C}{\pi\omega r}\right)^{1/2} e^{-i\left(\frac{\omega r}{C}-\frac{\pi}{4}\right)}$$

$$\cdot\left\{\frac{\omega\, Y_3(h)}{C}\left[\frac{1}{2}\,\frac{3\lambda(h)+2\mu(h)}{\lambda(h)+2\mu(h)}\sin 2d \sin s - \tfrac{1}{2}\sin 2d \sin s \cos 2\phi - \sin d \cos s \sin 2\phi\right] + \frac{Y_2(h)}{\lambda(h)+2\mu(h)}\sin 2d \sin s + i\,\frac{Y_4(h)}{\mu(h)}\left[\cos d \cos s \cos\phi - \cos 2d \sin s \sin\phi\right]\right\} \tag{6}$$

for the vertical component and

$$R_r(\omega,r,\phi/h,d,s)=Y_3(0)\, R_z(\omega,r,\phi/h,d,s)e^{-i\frac{\pi}{2}} \tag{7}$$

for the radial component. C and U in equation (6) are phase velocity and group velocity, respectively, at angular frequency ω . I_1 in (6) is defined as

$$I_1= \int_{-\infty}^{0}\rho(z)\left[Y_1^{\,2}(z) + y_3^{\,2}(z)\right] dz \tag{8}$$

$Y_1(z)$, $Y_2(z)$, $Y_3(z)$ and $Y_4(z)$ are the normal mode solutions satisfying the equations

$$\begin{bmatrix} \frac{dY_1}{dz} \\ \frac{dY_2}{dz} \\ \frac{dY_3}{dz} \\ \frac{dY_4}{dz} \end{bmatrix} = \begin{bmatrix} 0 & \frac{1}{\lambda(z)+2\mu(z)} & \frac{\omega}{c}\left[\frac{\lambda(z)}{\lambda(z)+2\mu(z)}\right] & 0 \\ -\omega^2\rho(z) & 0 & 0 & \frac{\omega}{c} \\ -\frac{\omega}{c} & 0 & 0 & \frac{1}{\mu(z)} \\ 0 & -\frac{\omega}{c}\left[\frac{\lambda(z)}{\lambda(z)+2\mu(z)}\right] & -\omega^2\rho(z)+\frac{4\omega^2}{c^2}\frac{\mu(z)[\lambda(z)+\mu(z)]}{\lambda(z)+2\mu(z)} & 0 \end{bmatrix} \begin{bmatrix} Y_1 \\ Y_2 \\ Y_3 \\ Y_4 \end{bmatrix} \qquad (9)$$

and the boundary conditions

$$Y_2(0)=Y_4(0)=Y_1(-\infty)=Y_2(-\infty)=Y_3(-\infty)=Y_4(-\infty)=0 \qquad (10)$$

$\rho(z)$, $\mu(z)$ and $\lambda(z)$ in equations (9) are density, rigidity and the Lame' constant, respectively, of the medium at depth z.

All the normal mode solutions Y's must be continuous at any depth including the layer interfaces and the depth at which the source is located. Both the system of equations (4) and (5) and the system of equations (8) and (9) are eigenvalue problems and can be solved either by Haskell's (1953) matrix method or by the Runge-Kutta method of numerical integrations (Takeuchi et. al. 1964). Once the phase velocity is determined against an angular frequency ω , the normal mode solutions Y's can easily be calculated by means of equations (4) or (9). All Y's are normalized in such a way that $Y_1(0)=1$.

The group velocity U is then calculated by the following formula (Takeuchi et. al. 1962):

(a) for Love waves

$$U=I_2/CI_1 \tag{11}$$

where I_1 is defined by equation (3) and

$$I_2=\int_{-\infty}^{0}\mu(z)\,Y_1^2(z)\,dz \tag{12}$$

(b) for Rayleigh waves

$$U=\frac{2(I_2+I_5)\omega+C(I_3+I_6)}{2\omega CI_1} \tag{13}$$

where I_1 is defined by equation (8) and

$$I_2=\int_{-\infty}^{0}\lambda(z)\,Y_3^2(z)\,dz \tag{14}$$

$$I_3=-2\int_{-\infty}^{0}\lambda(z)\,Y_3(z)\left(\frac{dy_1}{dz}\right)\,dz \tag{15}$$

$$I_5=\int_{-\infty}^{0}\mu(z)\left[Y_1^2(z)+2\,Y_3^2(z)\right]\,dz \tag{16}$$

$$I_6=2\int_{-\infty}^{0}\mu(z)\,Y_1(z)\left(\frac{dy_3}{dz}\right)\,dz \tag{17}$$

Once the phase velocity, group velocity and the normal mode solutions Y's at angular frequency ω are obtained for a medium, it is easy to calculate the Fourier spectrum of Love waves by equation (2) and that of Rayleigh waves by equations (6) and (7) due to a dislocation point source. The source parameters present in these equations are the dip angle d, the slip angle S and the focal depth h. Another source parameter, i.e. the seismic moment M, enters these equations simply as a scalar factor. Thus, either the phase spectrum or the shape of the amplitude spectrum of surface waves can be used to

determine the focal depth h of an earthquake if its fault-plane solution is known. In the present paper, the amplitude spectrum shall be used because in this way we shall be able to obtain simultaneously the seismic moment and the focal depth of an earthquake. The phase spectrum shall be used in the future to study the regional variations of the phase velocity of surface waves.

In calculating the theoretical surface wave amplitude spectrum, we shall choose the frequently used Gutenberg model (Dorman, et. al. 1960) for the continental paths and the Harkrider-Anderson model (1966) for the oceanic paths.

The layer parameters of the Gutenberg model are given in Table 1. The crust of this model consists of two layers with an equal thickness of 19 km.

The layer parameters of the Harkrider-Anderson model are given in Table 2. The uppermost portion of this model consists of a 5-km water layer, an 1-km sedimentary layer and an oceanic crustal layer of 5km. As compared with the Gutenberg continental model, the Harkrider and Anderson oceanic model has a shallower and more pronounced low-velocity zone in addition to a thinner crustal wave guide.

Each layer in Table 1 and Table 2 is assumed to be homogeneous.

The effects of the crustal thickness in the continental model and the effects of the water depth in the oceanic model upon the amplitude spectrum of surface waves shall be discussed later.

TABLE 1. Layer Parameters of the Gutenberg Model Used in This Paper.

Depth (km)	ρ (g/cm^3)	α (km/sec)	β (km/sec)
0-19	2.74	6.14	3.55
19-38	3.00	6.58	3.80
38-50	3.32	8.20	4.65
50-60	3.34	8.17	4.62
60-70	3.35	8.14	4.57
70-80	3.36	8.10	4.51
80-90	3.37	8.07	4.46
90-100	3.38	8.02	4.41
100-125	3.39	7.93	4.37
125-150	3.41	7.85	4.35
150-175	3.43	7.89	4.36
175-200	3.46	7.98	4.38
200-225	3.48	8.10	4.42
225-250	3.50	8.21	4.46
250-300	3.53	8.38	4.54
300-350	3.58	8.62	4.68
350-400	3.62	8.87	4.85
400-450	3.69	9.15	5.04
450-500	3.82	9.45	5.21
500-600	4.01	9.88	5.45
600-700	4.21	10.30	5.76
700-800	4.40	10.71	6.03
800-900	4.56	11.10	6.23
900-1000	4.63	11.35	6.32

TABLE 2. Layer Parameters of the Oceanic Model Used in This Paper.

Depth (km)	ρ (g/cm^3)	α (km/sec)	β (km/sec)
0-5	1.030	1.520	0.0
5-6	2.100	2.100	1.000
6-11	3.066	6.410	3.700
11-20	3.400	8.110	4.606
20-25	3.400	8.120	4.616
25-40	3.400	8.120	4.610
40-60	3.370	8.010	4.560
60-80	3.370	7.950	4.560
80-100	3.370	7.710	4.400
100-120	3.330	7.680	4.340
120-140	3.330	7.777	4.340
140-160	3.330	7.850	4.340
160-180	3.330	8.100	4.450
180-200	3.330	8.120	4.450
200-220	3.330	8.120	4.450
220-240	3.330	8.120	4.450
240-260	3.330	8.120	4.450
260-280	3.350	8.120	4.450
280-230	3.360	8.120	4.450
300-320	3.370	8.120	4.450
320-340	3.380	8.120	4.450
340-360	3.390	8.240	4.500
360-370	3.440	8.300	4.530
370-390	3.500	8.360	4.560

TABLE 2.-Continued

Depth (km)	ρ (g/cm^3)	α (km/sec)	β (km/sec)
390-415	3.684	8.750	4.795
415-435	3.880	9.150	5.040
435-445	3.900	9.430	5.217
445-465	3.920	9.760	5.400
465-490	3.933	9.765	5.400
490-515	3.948	9.775	5.400
515-540	3.960	9.780	5.400
540-565	3.988	9.784	5.400
565-590	4.022	9.788	5.400
590-615	4.056	9.792	5.400
615-640	4.090	9.796	5.400
640-665	4.120	9.800	5.400
665-690	4.165	10.163	5.600
690-715	4.212	10.488	5.800
715-740	4.257	10.818	6.100
740-765	4.300	11.120	6.200
765-790	4.475	11.135	6.205
790-815	4.633	11.150	6.210
815-840	4.797	11.165	6.218
840-865	4.940	11.180	6.230
865-890	4.943	11.224	6.250
890-915	4.945	11.267	6.275
915-940	4.948	11.310	6.297
940-965	4.950	11.350	6.322
965-990	4.952	11.392	6.340

Several examples are given here to illustrate how the amplitude spectrum of surface waves varys with the focal depth. Figure 2 shows the Rayleigh wave amplitude spectrum between periods 10 and 50 seconds from a vertical strike-slip fault ($d=90^{o}$, $s=0^{o}$) buried at various depth h within the Gutenberg model. Figure 3 shows the corresponding Love wave amplitude spectrum. The seismic moment is assumed to be a unit step function in time, i.e. M=1 dyne-cm in equation (1). The observation point is at the azimuth of 30^{o} from the strike and 2000 km away from the epicenter. The number accompanying each curve in the figures indicates the focal depth in kilometers.

Figure 2 suggests that the Rayleigh wave amplitude spectrum in periods 10 to 50 seconds depends very strongly on the focal depth of an earthquake. This is particularly evident for focal depth less than 100 km. The spectral node on each curve is caused by the sign reversal of Y_3 in equation (6). Thus, the Rayleigh wave amplitude spectrum in this frequency range may be used to determine the focal depths of shallow earthquakes. Fortunately, the prospect of such an approach is strengthened by the fact that surface waves from shallow earthquakes of medium magnitudes are most clearly recorded in this frequency range by the WWSSN long period seismographs.

Excitation of Love waves in the continental model also varys with the focal depth as shown in Figure 3. However, the dependence is weak for focal depth less than 20 km because the normal mode solutions y's decay very slowly with depth in this portion. In other words, the Love wave amplitude spectrum can

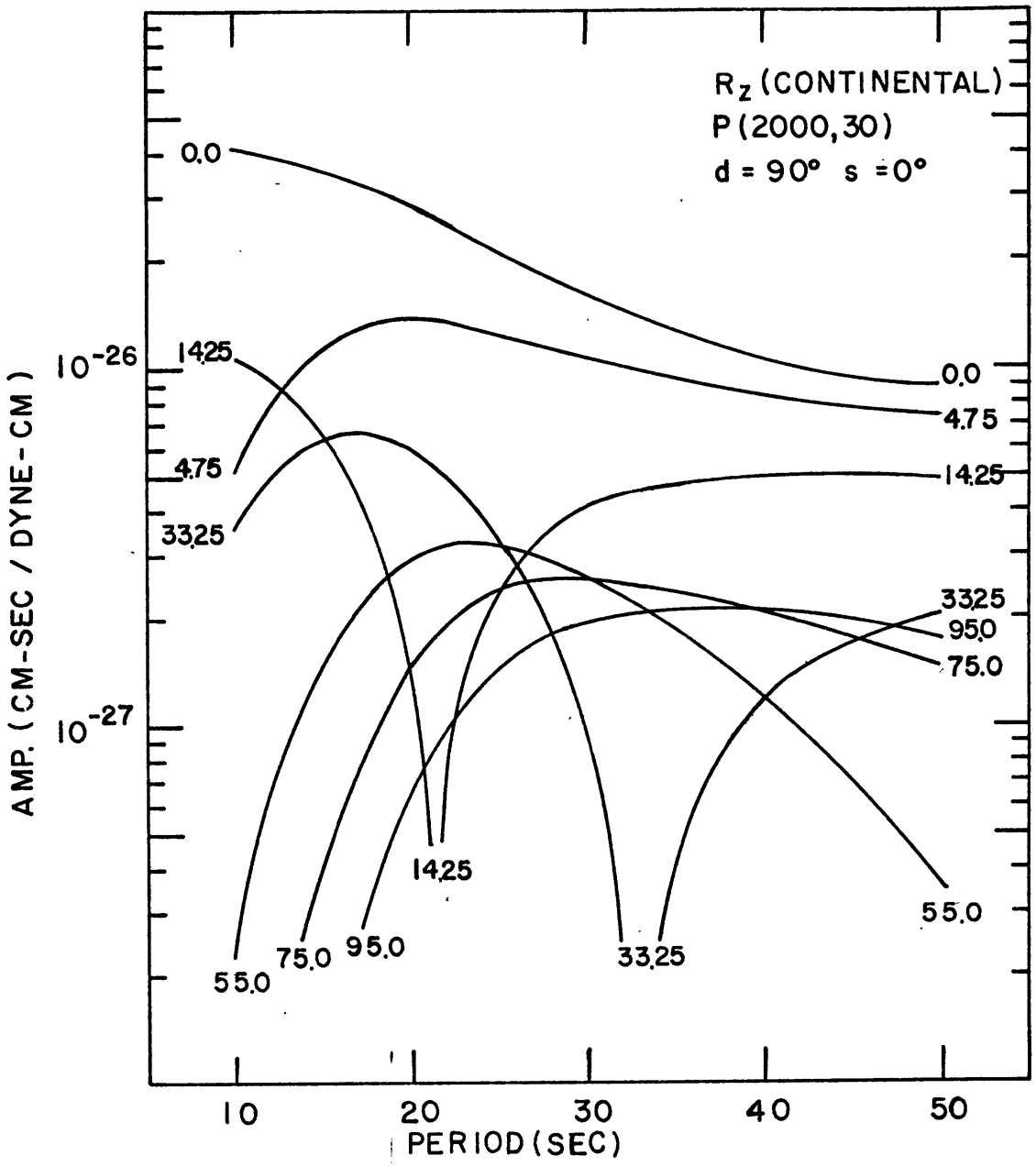

FIG. 2. Amplitude spectrum of Rayleigh waves from a vertical strike-slip fault in the Gutenberg continental earth model.

not effectively be used to determine the focal depth of a very shallow earthquake.

Figure 4 shows the Love wave amplitude spectrum at the ocean floor excited by a vertical strike-slip fault buried in the oceanic model at various depth measured from the ocean floor. Figure 5 shows the corresponding Rayleigh wave amplitude spectrum. As shown in Figure 5, the Rayleigh wave amplitude spectrum again depends strongly on the focal depth of an earthquake located at depth less than 100 km. On the contrary, Figure 4 shows that the Love wave amplitude spectrum varys very little with the focal depth when the earthquake is less than 100 km deep. The effect of focal depth in this case would appear in periods shorter than 10 seconds which are outside our frequency range.

In the present paper we are interested in determining the focal depths of many strike-slip earthquakes occurred on the fracture zones and presumed to be shallow. We shall use primarily the Rayleigh wave amplitude data. Love waves shall be used only as a supplement when required. Another disadvantage we may have in using Love wave data results from the fact that Love waves suffer greater scattering due to lateral inhomogeneities in the crust and the upper mantle.

It should be mentioned that the strong dependence of Rayleigh wave amplitude spectrum on the focal depth exists not only for a vertical strike-slip fault as shown in the examples but also for other types of fault as will be shown later.

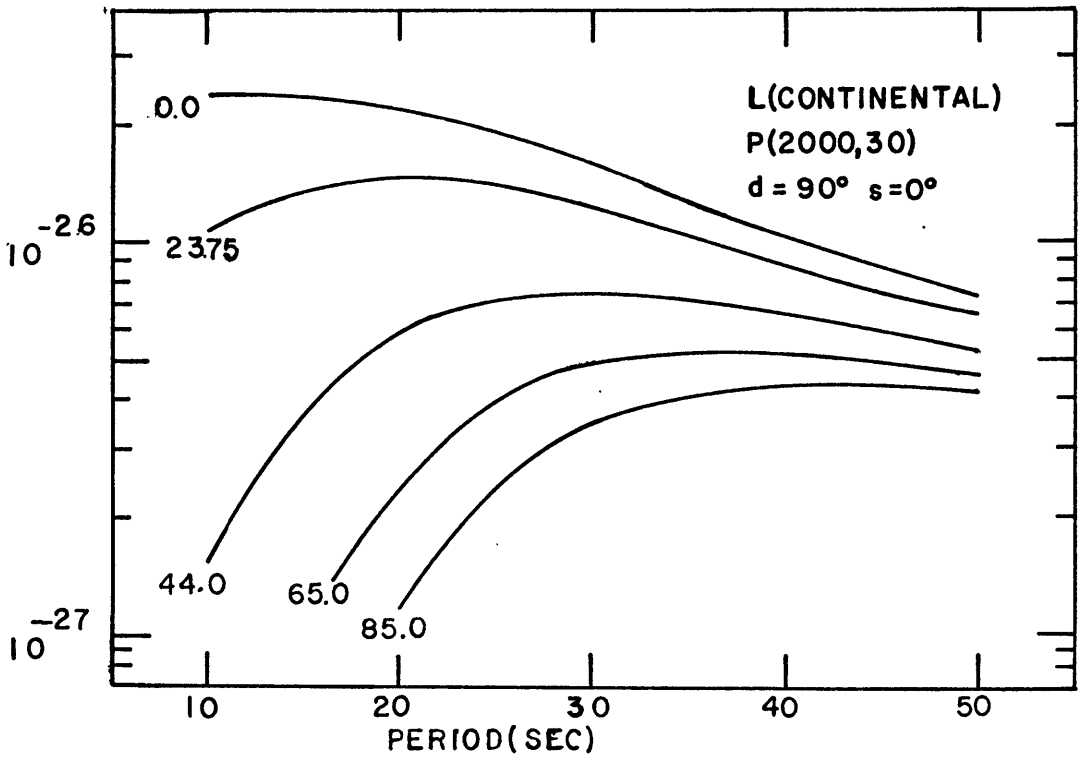

FIG. 3. Amplitude spectrum of Love waves from a vertical strike-slip fault in the Gutenberg continental earth model.

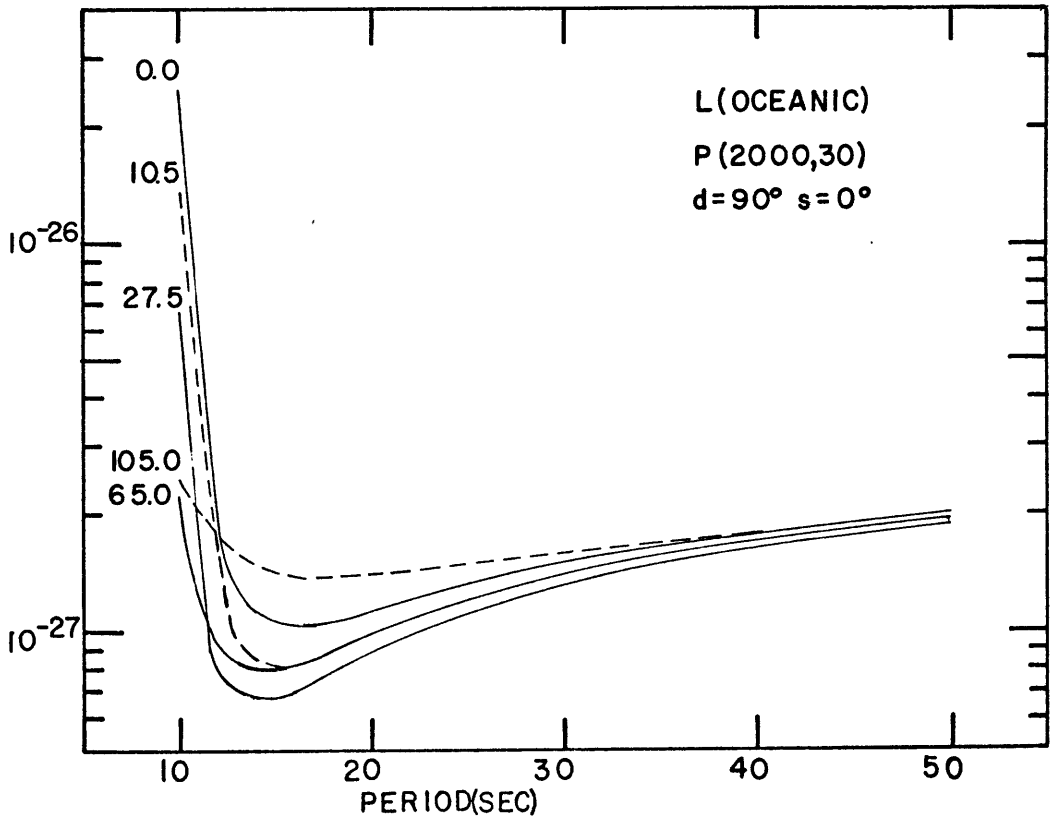

FIG. 4. Amplitude spectrum of Love waves from a vertical strike-slip fault in the Harkrider-Anderson oceanic earth model.

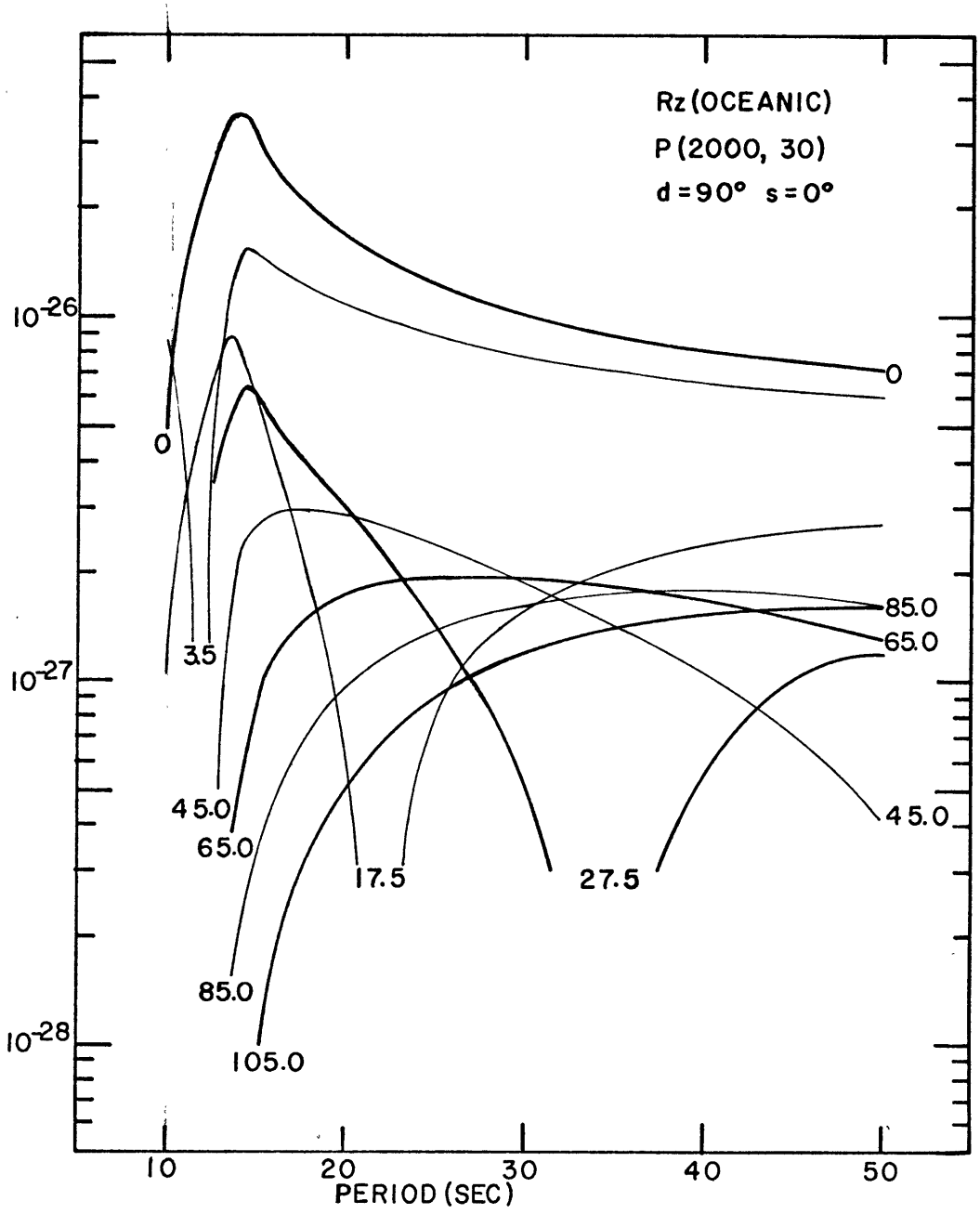

FIG. 5. Amplitude spectrum of Rayleigh waves from a vertical strike-slip fault in the Harkrider-Anderson oceanic earth model.

2.2 Effects of the crustal thickness under continents on the excitation of Rayleigh waves

It is well known that the crustal thickness under continents varys from one place to another. We shall now examine how the excitation of Rayleigh waves is affected by changing the crustal thickness of the Gutenberg continental model. We have calculated the amplitude spectrum of Rayleigh waves for two continental models with a crust of 24 km in one and 48 km in another. The Rayleigh wave amplitude spectrum from a strike slip fault is shown in Figure 6 for a focal depth of 6km and in Figure 7 for a focal depth of 65 km. The number attached to each curve in the figures corresponds to the crustal thickness in km. Figure 6 and Figure 7 suggest that the effect of the crustal thickness on the Rayleigh wave amplitude spectrum is minor no matter whether the fault is within or below the crust. The same remark can also be made about a pure dip-slip fault dipping at 45°, as shown in Figure 8 and Figure 9. Therefore we shall use the Gutenberg model with a crust of 38 km for all continental paths without regard to possible variations of the crustal thickness over individual paths.

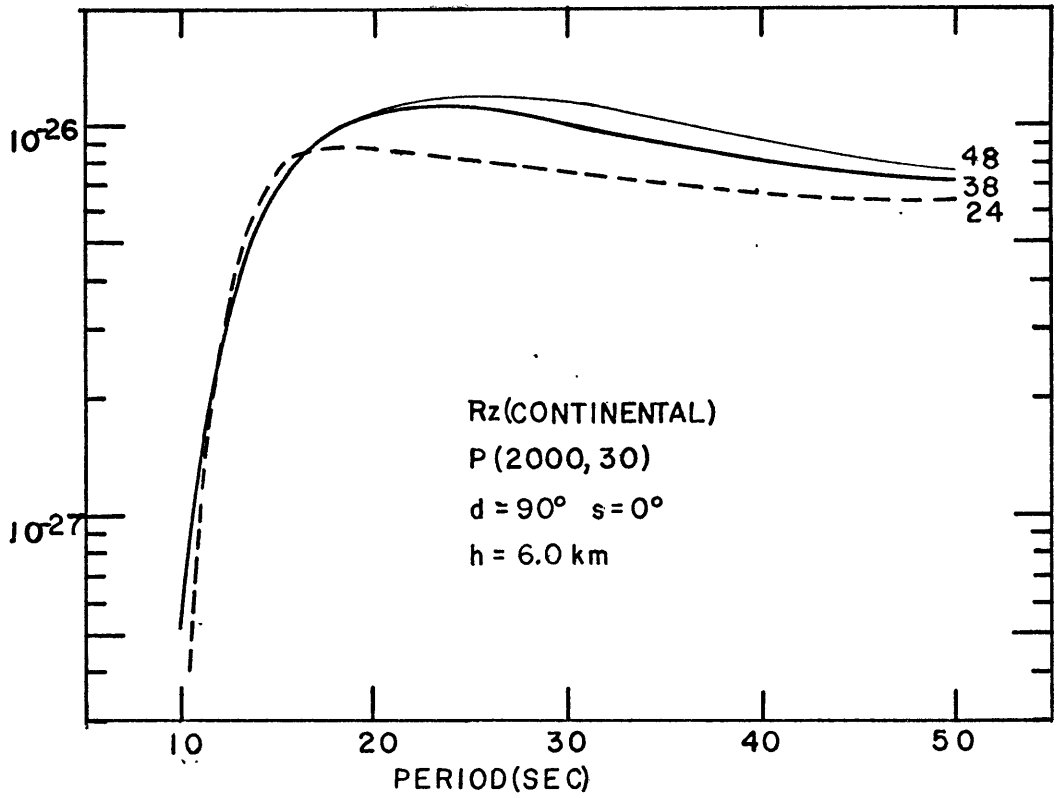

FIG. 6. Effect of crustal thickness of the continental model on the amplitude spectrum of Rayleigh waves for focal depth 6 km.

FIG. 7. Effect of crustal thickness on the Rayleigh wave amplitude spectrum for focal depth 65 km.

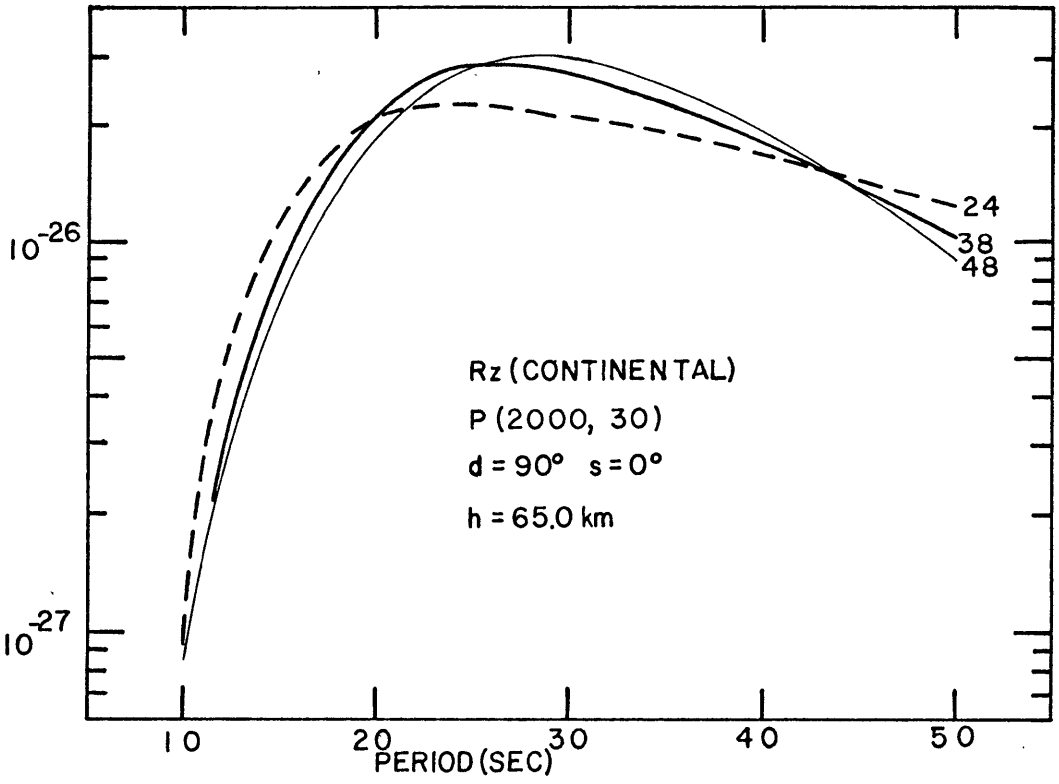

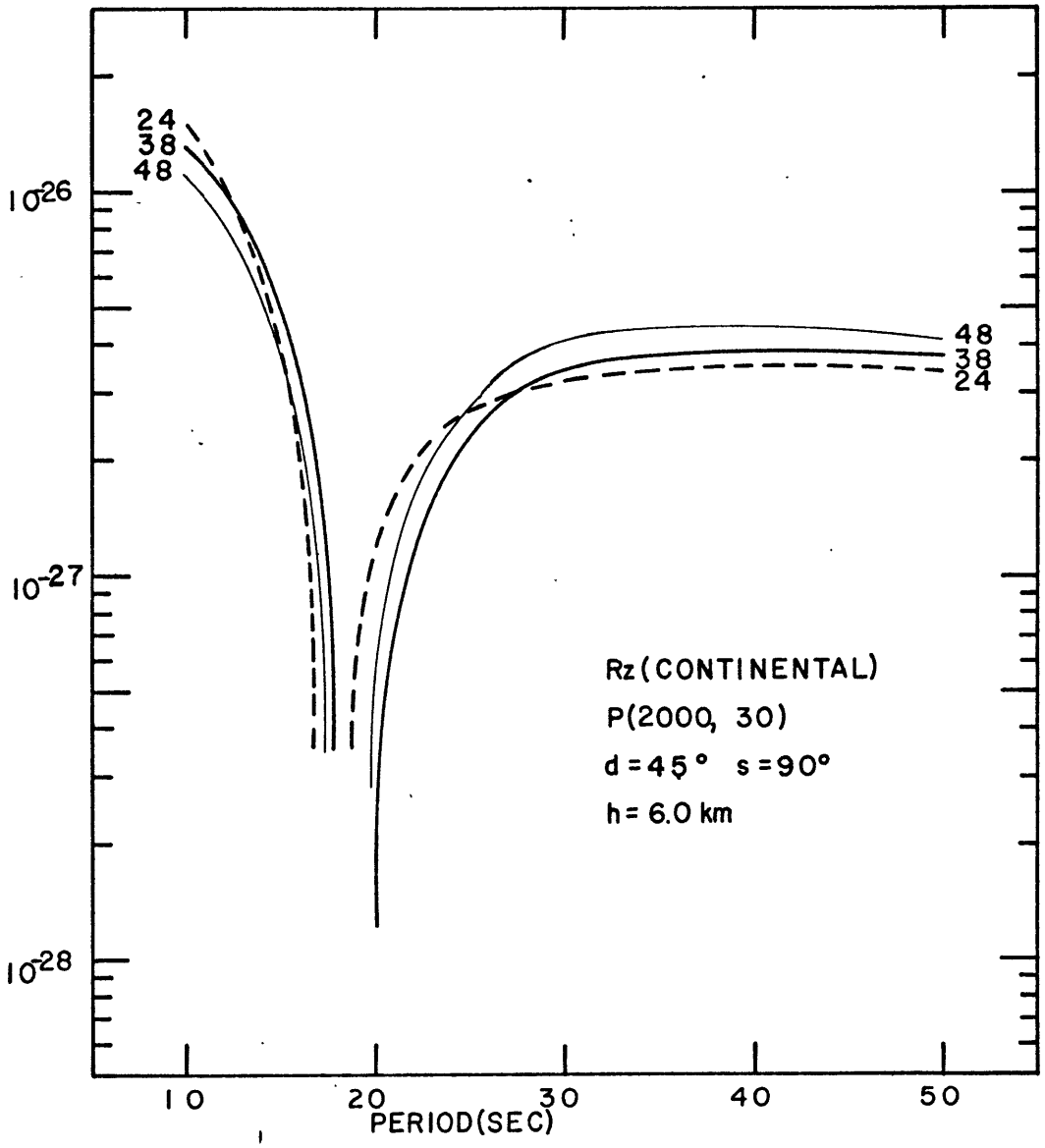

FIG. 8. Effect of crustal thickness on the Rayleigh wave amplitude spectrum from a dip-slip fault at depth 6 km.

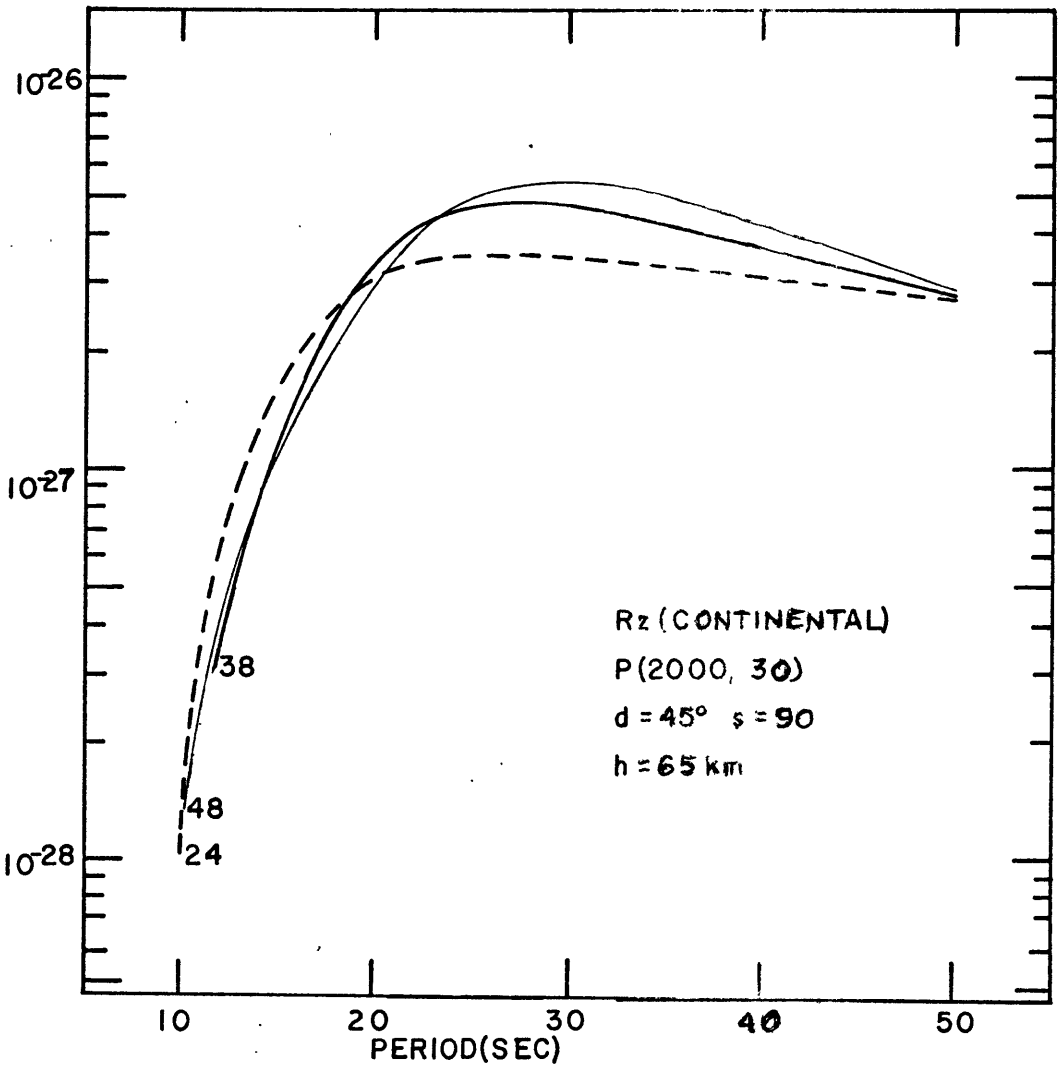

FIG. 9. Effect of crustal thickness on the Rayleigh wave amplitude spectrum from a dip-slip fault at depth 65 km.

2.3 Effects of the water depth over oceans on the excitation of Rayleigh waves

In the oceanic model given in Table 2, the water depth is assumed to be 5 km. Since different oceanic paths may have different water depth, it is necessary to examine how the excitation of Rayleigh waves varys with the water depth. For this purpose, let us reduce the water depth from 5 km to 3 km in the oceanic model and recalculate the normal mode solutions. The Rayleigh wave amplitude spectrum from a vertical strike-slip fault calculated for this modified model and that calculated for the original model are compared in Figure 10. The same comparison is shown in Figure 11 for a pure dip-slip fault dipping at 45^{o}. Two focal depths are assumed — 3.5 km for one and 65.0 km for another. In both figures the heavy curves belong to the original model with 5 km water and the light curves to the modified one with 3 km water. Figure 10 and Figure 11 indicate that the Rayleigh wave amplitude spectrum appears to be shifted toward shorter periods by a small amount when the water depth is reduced. Fortunately, the shape of the spectrum remains almost unchanged. This would allow us to use the standard oceanic model to interpret the Rayleigh wave amplitude data over oceanic paths by properly adjusting the theoretical amplitude spectrum along the frequency axis to accomodate with the known water depth.

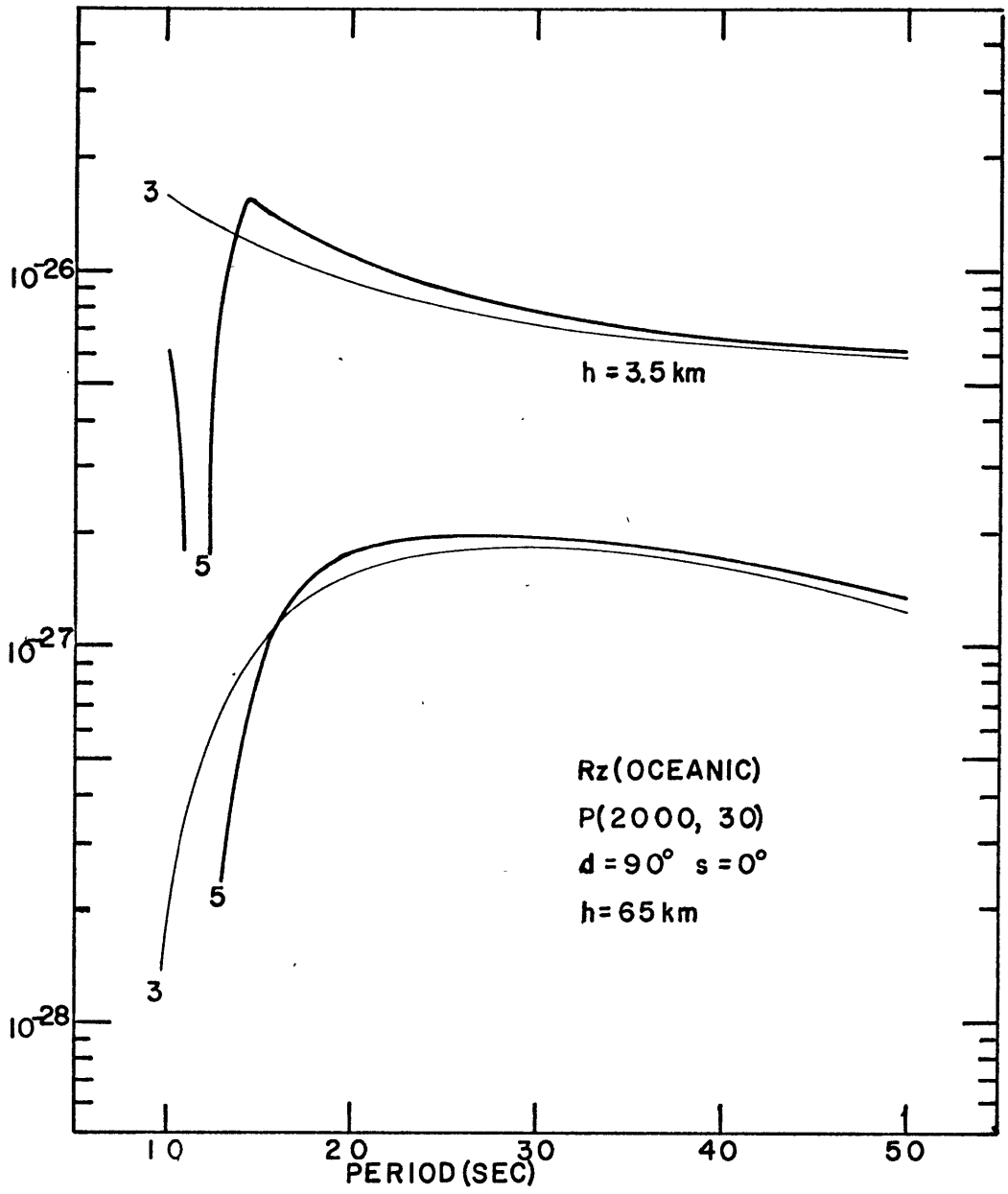

FIG. lo. Effect of ocean depth on the Rayleigh wave amplitude spectrum from a strike-slip fault.

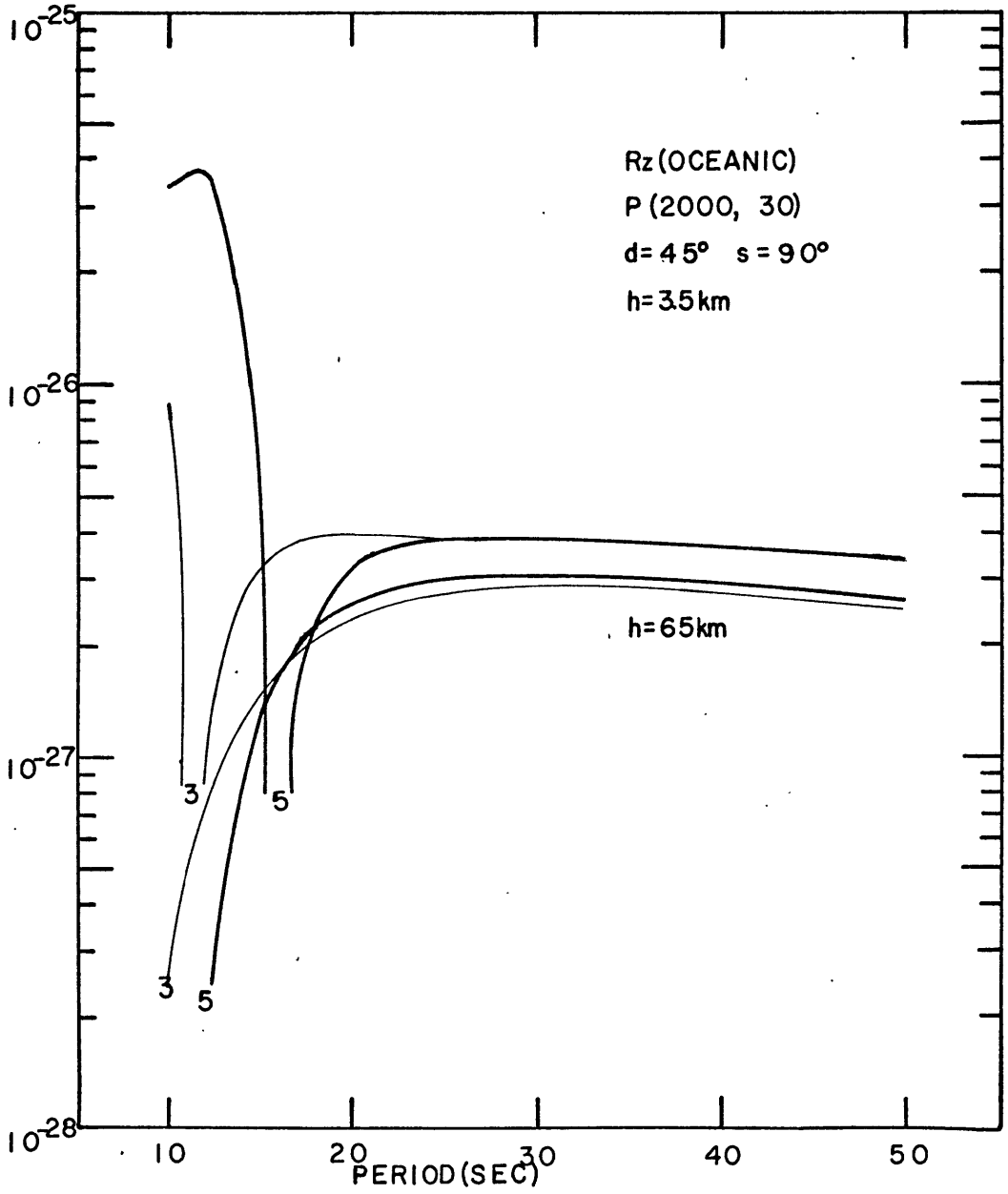

FIG. 11. Effect of ocean depth on the Rayleigh wave amplitude spectrum from a dip-slip fault.

2.4 Variations of the amplitude spectrum of surface waves due to a small uncertainty on the fault-plane solutions

Sykes (1967) made a comparison of focal mechanism solutions for seven earthquakes on the mid-ocean ridges obtained by Stauder and Bollinger (1964a, b; 1965), Stefansson (1966) with those obtained by himself. He found that with the exception of an event preceded by a small forerunner, the strikes and dips of the remaining solutions agree within about 15°, and within less than 5° for some of the best solutions. For a great many other fault-plane solutions based on data obtained at modern long-period seismograph networks such as the WWSSN or the Canadian network, the uncertainty on the strikes and the dips may be comparable to that of these six solutions, i.e. within about 15°.

The variations of the excitation of surface waves due to 15° of uncertainty on the fault-plane solutions are examined here for two cases: a vertical strike-slip fault and a pure dip-slip fault dipping at 45°. In both cases, either the dip angle or the slip angle or both is varied by 15°. We shall consider each case separately at two focal depths in the Gutenberg model. The amplitude spectral variations due to a change of 15° in dip or/and slip of a vertical strike-slip fault at 4.75 km are shown in Figure 12 for Rayleigh waves and in Figure 13 for Love waves. The corresponding spectral variations at focal depth 65 km are shown in Figure 14 for Rayleigh waves and in Figure 15 for Love waves. As suggested

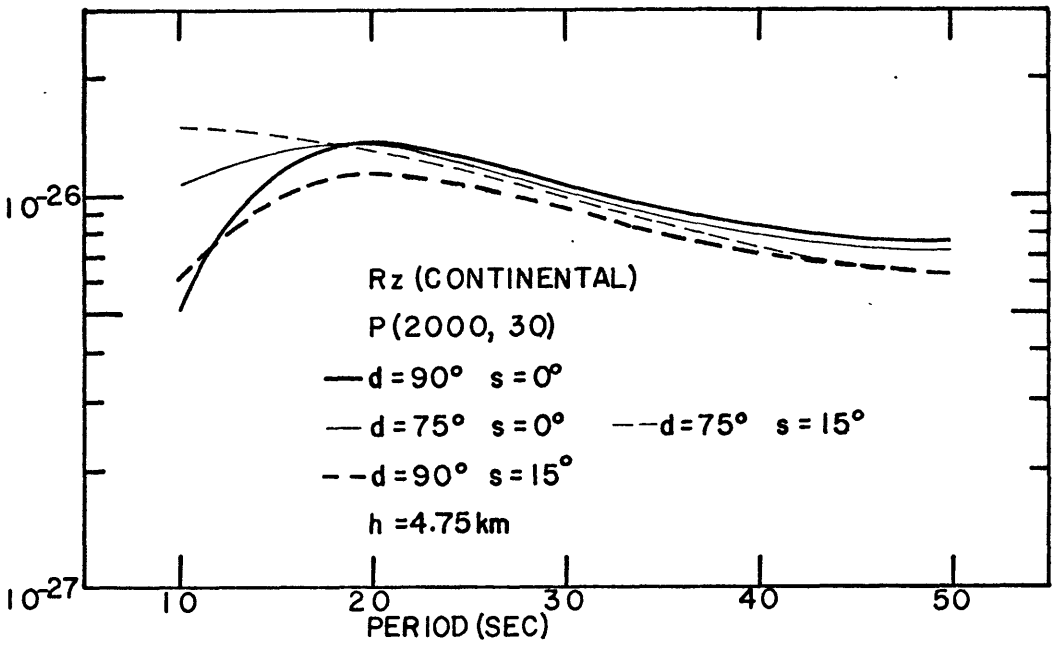

FIG. 12. Variations of the Rayleigh wave amplitude spectrum due to 15 degree change in the dip or/and slip angles.

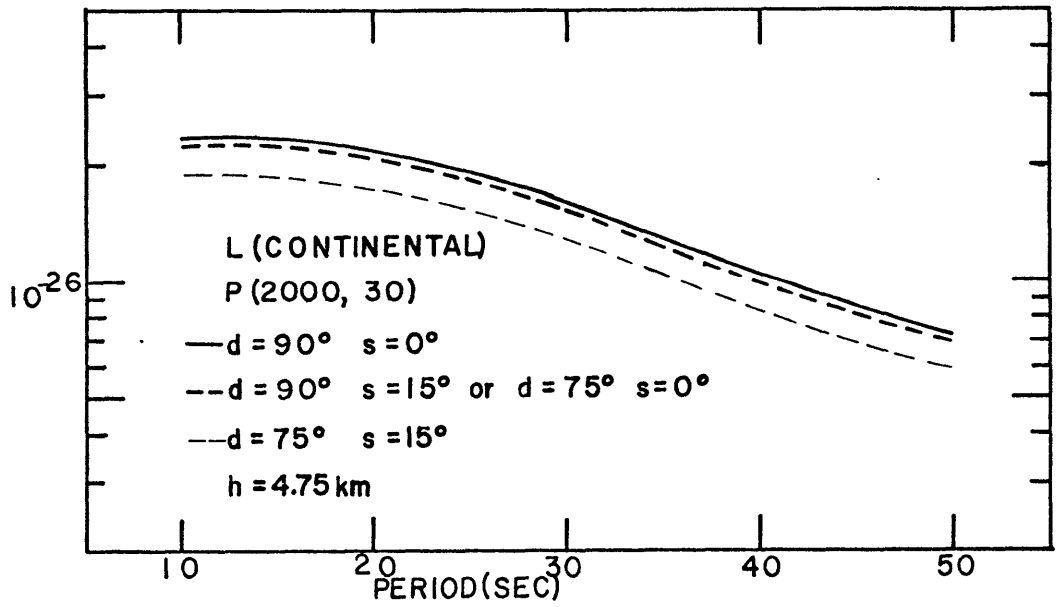

FIG. 13. Variations of the Love wave amplitude spectrum due to 15 degree change in the dip or/and slip angles of a strike-slip fault.

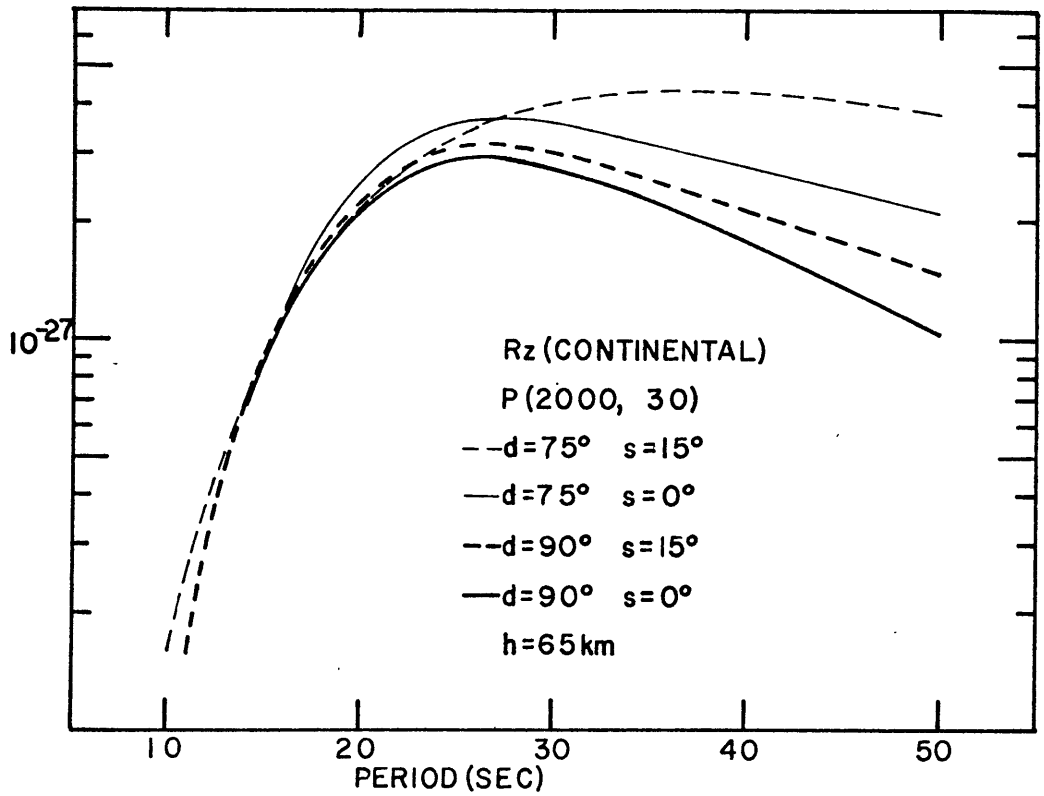

FIG. 14. Variations of the Rayleigh wave amplitude spectrum due to 15 degree change in the dip or/and slip angles of a strike-slip fault at depth 65 km.

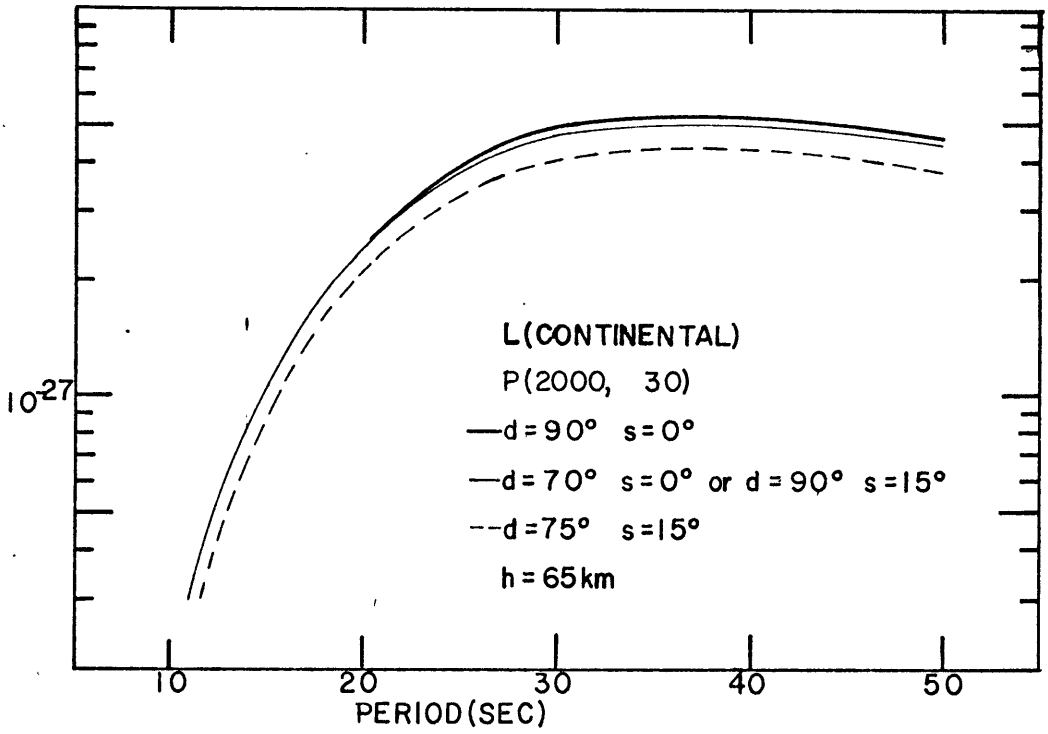

FIG. 15. Variations of the Love wave amplitude spectrum due to 15 degree change in the dip or/slip angles of a strike-slip fault at depth 65 km.

by Figure 13 and Figure 15, the variations of Love waves for both source depths are purely scalar and thus cause no change on the spectral shape. Figure 12 and Figure 14 suggest that the Rayleigh wave spectral node is obscured when either the dip or the slip or both of the vertical strike-slip fault are slightly varied, regardless of its focal depth. This does not, however, mean that the dependence of Rayleigh wave spectrum on focal depth is obscured. On the contrary, the difference between the spectrum from a very shallow earthquake (say at 4.75 km) and that from a deeper earthquake (say at 65 km) is sharpened. This is due to the fact that the spectral node is located in the short-period end when the focal depth is small and moves toward the long-period end when the focal depth is increased. The obscuring of this spectral node will then enhance the spectral components on the short-period end when the fault is close to the surface but will enhance those on the long-period end when the fault is at 50 km or deeper.

For the case of a dip-slip fault, the spectral variations of Rayleigh and Love waves are shown in Figure 16 and Figure 17 when the fault is at depth 4.75 km and in Figure 18 and Figure 19 when the fault is at depth 65 km. From Figure 17 and Figure 19, we again find that Love wave spectrum is affected only by a small scalar factor if the dip or/and the slip of the dip-slip fault at both depths is altered by 15°. For a fault very close to the surface, the Rayleigh wave spectrum is noticeably affected, as shown in Figure 16. Not only the

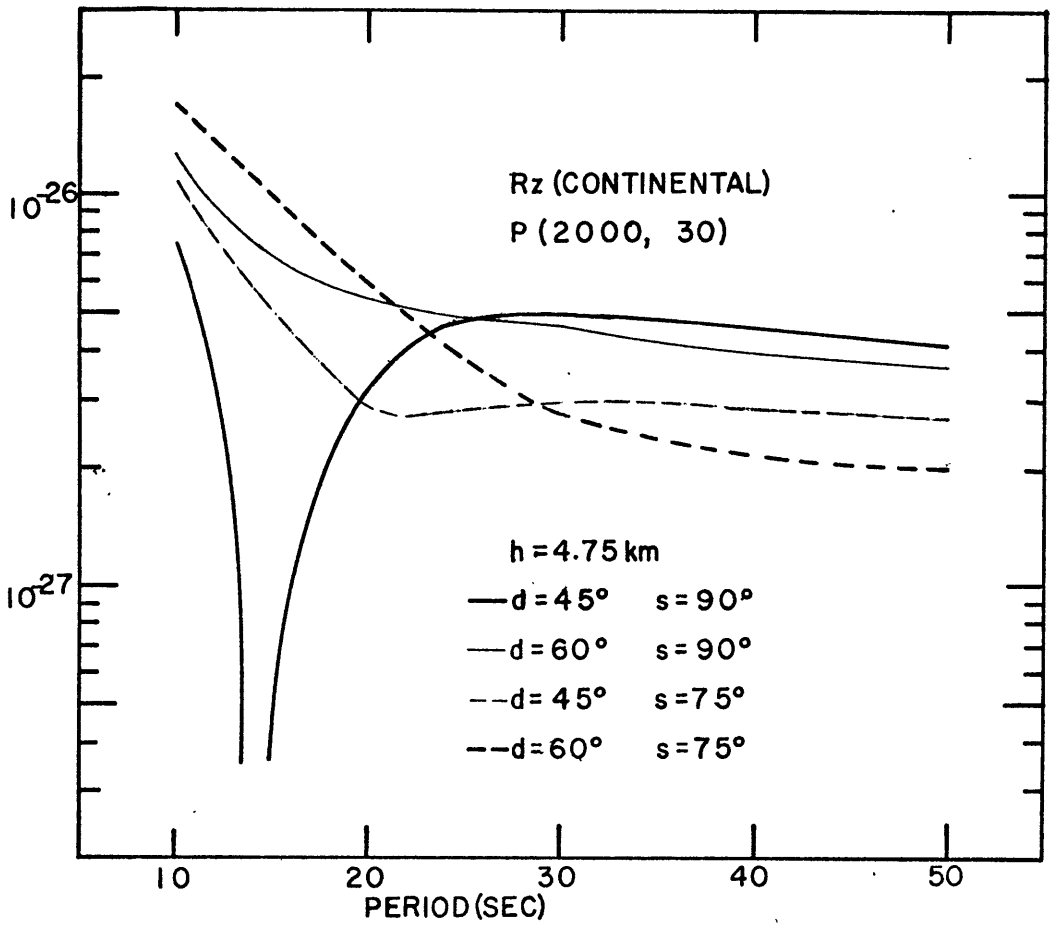

FIG. 16. Variations of the Rayleigh wave amplitude spectrum due to 15 degree change in the dip or/and slip angles of a dip-slip fault at depth 4.75 km.

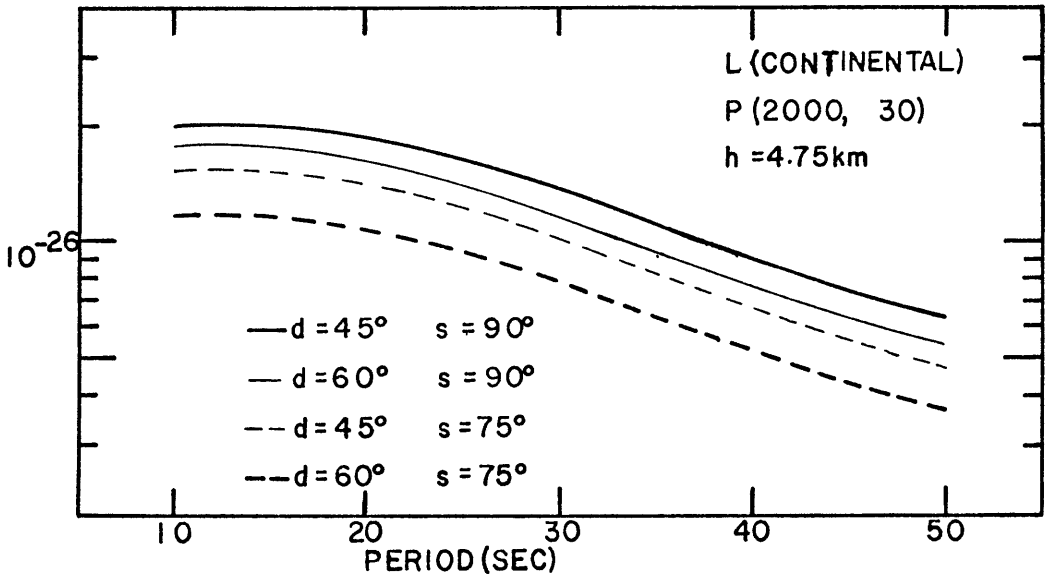

FIG. 17. Variations of the Love wave amplitude spectrum due to 15 degree change in the dip or/and slip angles of a dip-slip fault at depth 4.75 km.

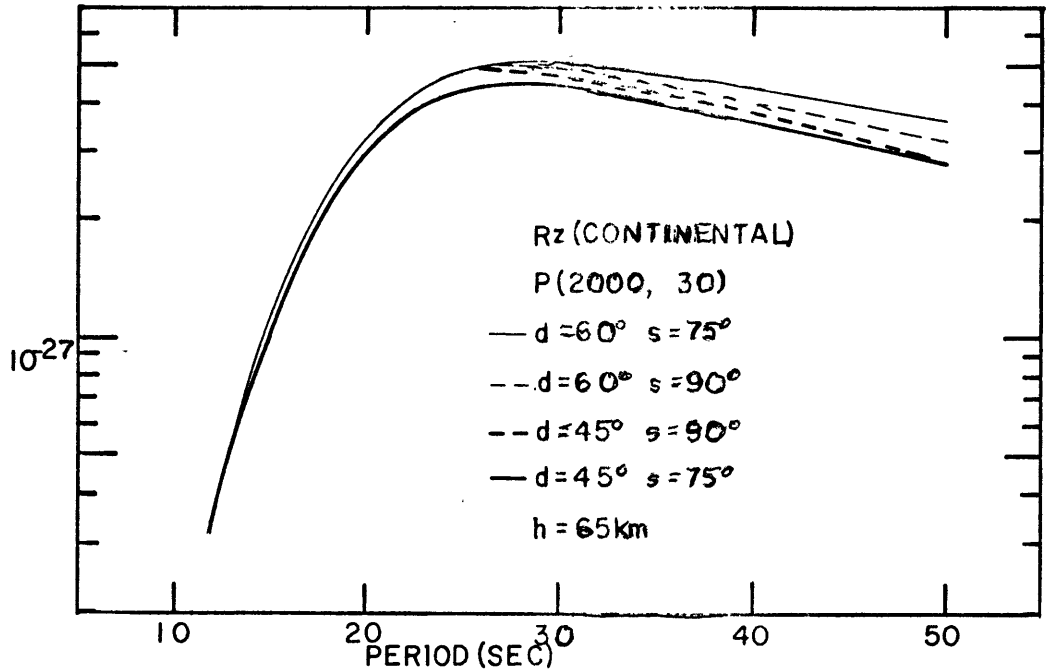

FIG. 18. Variations of the Rayleigh wave amplitude spectrum due to 15 degree change in the dip or/and slip angles of a dip-slip fault at depth 65 km.

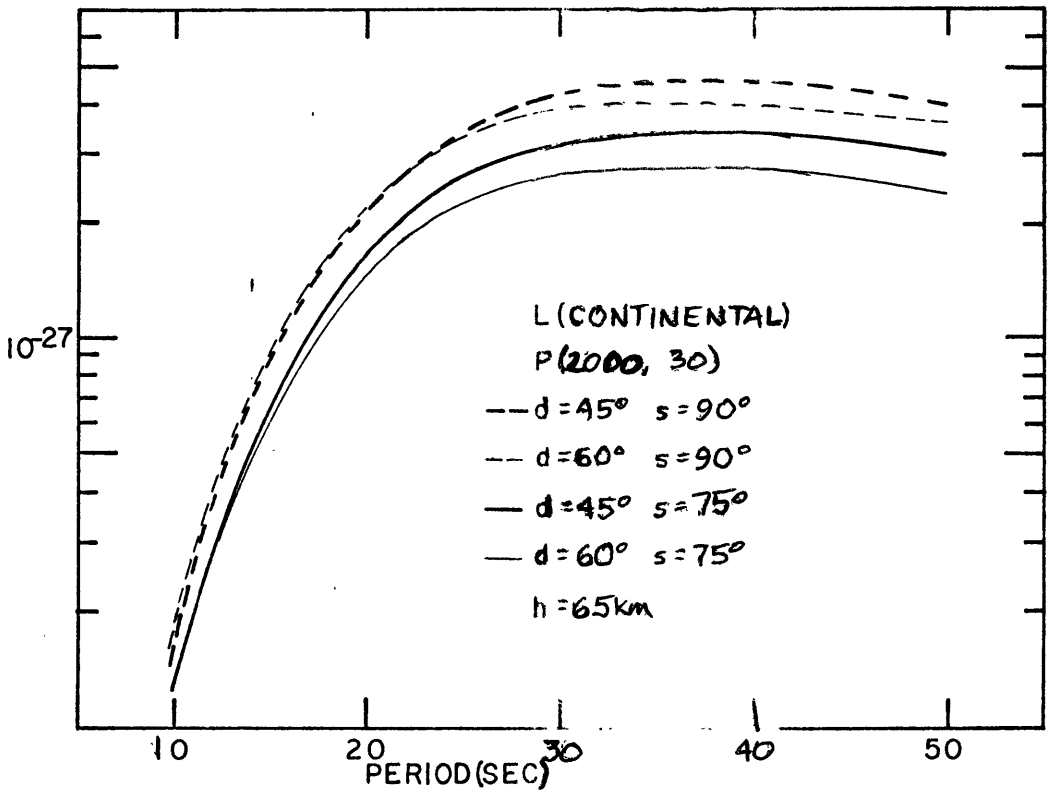

FIG. 19. Variations of the Love wave amplitude spectrum due to change in dip or slip angles.

spectral node is obscured but also the amplitude level is significantly changed. The end effect tends to strengthen the short-period components and weaken the long-period components. On the other hand, Rayleigh waves are affected very little when the fault is at 50 km or deeper. Thus we can conclude this discussion by saying that an uncertainty of about 15° of the dip or the slip or both of a fault-plane solution will not seriously affect the accuracy of our method of depth determination.

2.5 The effects of finiteness of a source on the amplitude spectrum of surface waves

The dependence of amplitude spectrum of seismic waves on source size has been derived semi-empirically by Aki (1967) under the assumption that large and small earthquakes are similar phenomena. This assumption of similarity implies a constant stress drop independent of source size. His results indicate that the ω-square model gives a satisfactory explanation of observed data. According to this model, the shape of the amplitude spectrum of displacement for periods longer than 10 seconds is almost independent of earthquake magnitude for $Ms \leq 5.5$ where Ms is the magnitude defined for surface waves with period of 20 seconds. Even for Ms=6.5 the amplitude at period 10 seconds will be reduced by only a factor of about 2. Since all except four of the earthquakes studied in this paper have magnitudes $m_b \lesssim 6$, the effect of source size on the shape of surface wave amplitude spectrum may be neglected for most of these earthquakes.

The finiteness effect of a source can also be estimated if the length and the rupture velocity of the fault are known. Ben-Menahem (1961) showed that the contribution to the Fourier spectrum of surface waves from a unilateral fault with length L and rupture velocity V may be written as

$$\frac{1}{L}\int_0^L \exp\left\{i\omega\left(t-\frac{x}{V}-\frac{r-x\cos\phi}{C}\right)\right\} dx$$

$$=\left\{\frac{\sin X}{X}\ e^{-iX}\right\}\exp\left\{i\omega\left(t-\frac{r}{C}\right)\right\} \qquad (18)$$

where $X=\frac{\omega L}{2}\left(\frac{1}{V}-\frac{\cos\phi}{C}\right)$, r is the epicentral distance and ϕ the azimuth to a station. C is the phase velocity of the wave.

In order to make a realistic estimation of the amplitude of finiteness factor given in equation (18) some knowledge about the fault length L and the rupture velocity V is required.

A number of shallow earthquakes in various parts of the world have been found to be associated with surface traces of rupture near their epicenters. Several authors have found approximate correlations between the magnitudes (M) of these shocks and the length of the surface traces of rupture. The first empirical relationship of this type was derived by Tocher (1958) for ten California and Nevada shocks. Iida (1959, 1965) has studied about 60 shocks occurring world-wide, using in large part data supplied by Richter (1958) and including those of Tocher. Iida obtained results similar to those obtained by Tocher. Press (1967) found Tocher's curve, although valid for large earthquakes, to be unsatisfactory for shocks of small magnitudes. Press used data of small earthquakes and nuclear explosions to derive a modified relationship between fault length and magnitude of small earthquakes. According to Press'

curve, an event of magnitude 4 will have a linear dimension between 0.1 and 1 km. A seismic source with magnitude 5 has a linear dimension between 0.5 and 5 km. King and Knopoff (1968) added forty-two more shocks with magnitude ranging from 3.6 to 8.5 to this kind of studies. All the results obtained so far are summarized in Figure 20 which is taken from the paper by King and Knopoff (1968) with no data points included. Their data show that the Imperial shock of 1966 was undoubtedly a very exceptional case. As for the Parkfield main shock of 1966, if the surface wave magnitude of 6.4 (Wu, 1968), instead 5.5 is used, the deviation from the curve of Press (1967) would be significantly reduced. Thus, for the moment, we shall follow Press' curve and calculate the amplitude of the transfer function in equation (18) by taking L=10 km for an earthquake of magnitude M=6.0 which is the upper limit for most of the earthquakes studied in this paper (Table 3 to Table 5)

As for the rupture velocity, it varys between 3 and 4 km/sec as derived from detailed studies of several major shallow earthquakes by the methods of phase equalization, radiation pattern, and directivity (Ben-Menahem, 1967). An average rupture velocity of 2.2 km/sec has been determined by Eaton (1967) for the Parkfield, 1966 earthquake using the data obtained at the Gold Hill station which was in the fault zone 20 km southeast of the epicenter. This is believed to be the only rupture speed obtained so far by a method not associated with surface wave or free oscillation data. In order to make an estimate of

maximum effect due to the finiteness of sources, we shall choose the smaller rupture velocity, i.e. 2.2 km/sec in our calculations.

Figure 21 gives the factor of $\left|\frac{\sin X}{X}\right|$ for Rayleigh waves in the Gutenberg continental model. Two azimuths (ϕ = 45^{o} and 135^{o}) corresponding to the lobe directions of a vertical strike-slip fault are considered. From this figure, we find that the effect of finiteness is negligible on the forward quadrants of the propagating fault. Even on the backward quadrants, the effect is limited to periods less than 20 seconds or so. This is believed to be a maximum estimate of finiteness effect because the rupture velocity used here is on the lower end of most observed values and the length of fault on the longest end. A greater rupture velocity, say 3 km/sec, would reduce this effect significantly. Based on this evidence the finiteness factor shall be neglected in our interpretation of those events whose fault length and rupture speed are not known.

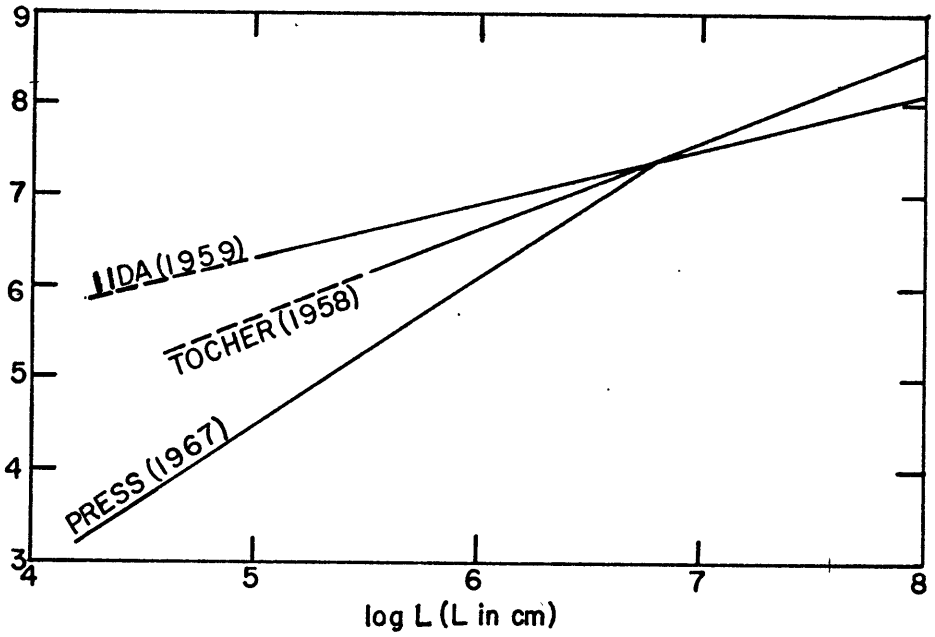

FIG. 2o. Earthquake magnitude versus fault length.

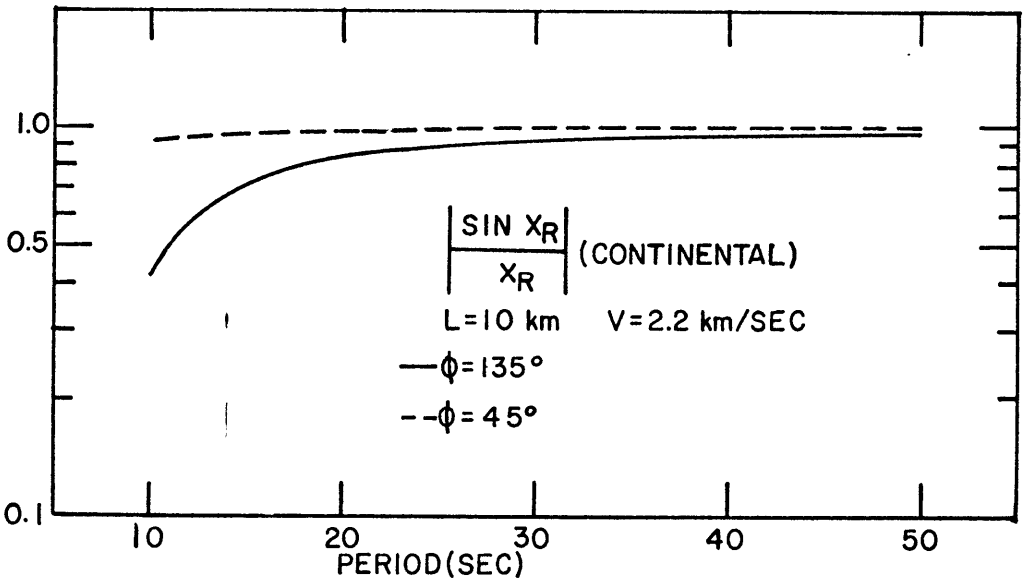

FIG. 21. Effect of finiteness on the Rayleigh wave amplitude spectrum.

2.6 The Fourier spectrum of the source time function

In all calculations we have made so far, a unit step source time function defined by equation (1) (with M=1 dyne cm) is assumed. Although this function has been found to be consistent with most observed surface wave data from shallow earthquakes (Ben-Menahem, 1967), other functions have been proposed to represent the source behavior in time. Among these are a ramp function and a function varying as

$$\begin{aligned} m(t)&=0 && \text{when } t < 0 \\ m(t)&=M(1-e^{-t/\tau}) && \text{when } t \geq 0 \end{aligned} \qquad (20)$$

As shown in Figure 22a, these two functions are comparable to each other. Thus we shall consider here only the latter one.

The Fourier spectrum of the function defined by equation (20) can be written as

$$\mathfrak{M}(\omega)=\left(\frac{M}{i\omega}\right)\left(\frac{1}{1+i\omega\tau}\right) \qquad (21)$$

This spectrum differs that of a step function defined in equation (1) only by a simple factor $\left(\frac{1}{1+i\omega\tau}\right)$. The amplitude of this factor is shown in Figure 22b for several values of τ. It is found that this correction factor is almost uniform for periods between 10 and 50 seconds if τ is less than 1 second. In case of τ =10 seconds, the correction is significant over the whole period range from 10 to 50 seconds.

Ben-Menahem and Toksöz (1963) used the observed phase spectrum of the source time function to obtain a τ =22 seconds for the Kamchatka earthquake of November 4, 1952 which had a magnitude of 8¼ and a fault length of 700 $\pm$ 50 km. Hirasawa (1965) determined the rise time of the Niigata earthquake (M=7.5),

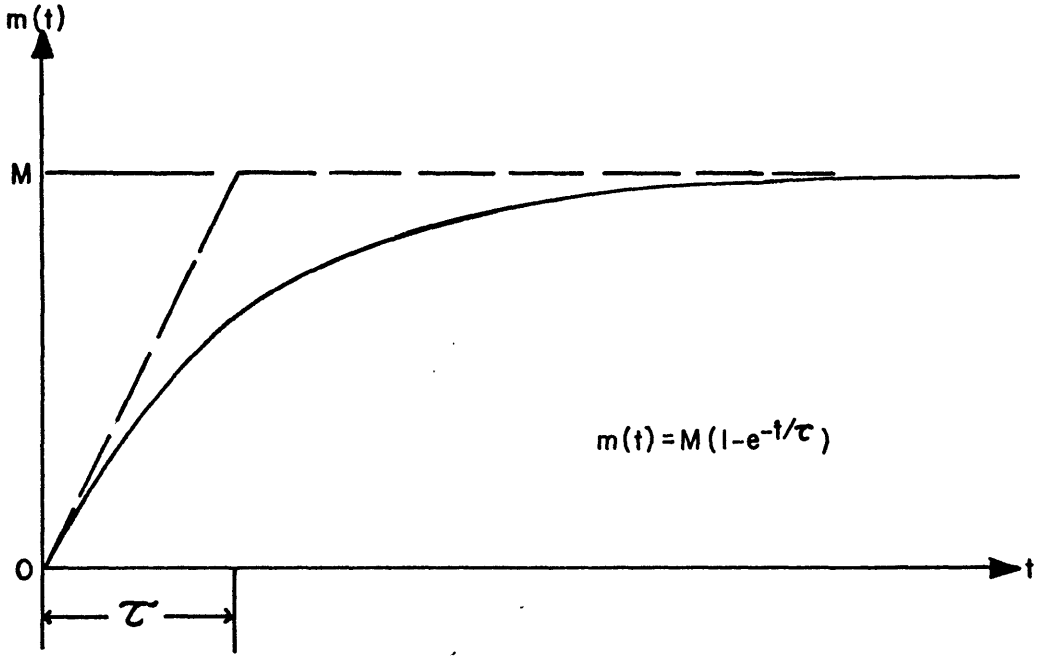

FIG. 22a. A source time function.

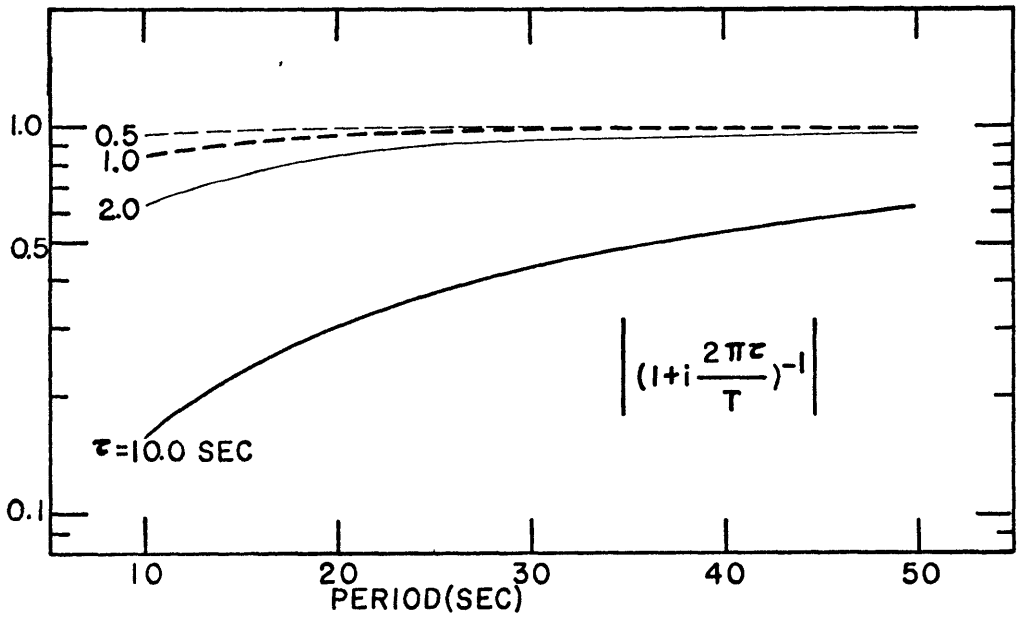

FIG. 22b. The Fourier amplitude ratio between the source time function shown in FIG. 22a and the step function given by Eq. (1).

June 16, 1964 as 2 to 4 seconds by equalizing the wave energy in a finite frequency range obtained from the observed P wave to that theoretically expected. According to Aki (1966) and Hirasawa (1965), this earthquake was caused by a dip-slip fault with a total length between 80 to 100 km. Haskell (1969) used a two-stage ramp source time function to explain the acceleration pulse measured by the strong-motion accelerometer near the fault of the Parkfield earthquake of June 28, 1966. His results showed that the rise time is about 0.9 second. Aki (in press) used a slightly different technique to obtain 0.4 second for the rise time of the same earthquake. The Parkfield earthquake has a fault length of almost 40 km and a surface wave magnitude of 6.4. Although there is still no observation on the rise time of smaller earthquakes, it seems reasonable to say that the rise time for an earthquake with magnitude 6.0 or less and with a fault length of about 10 km may be well within one second. Based on this evidence we may conclude that for most earthquakes studied in the present paper, the source time function can satisfactorily be represented by a step function as defined in equation (1).

After having considered each factor that contributed to the source spectrum of an earthquake, we feel that the theoretical amplitude spectrum of surface waves calculated on the assumption that the source is a point in space and a step function in time can be used to interpret data obtained from earthquakes with magnitude 6.0 or smaller without serious errors. For the determination of focal depths by this method, the current

uncertainty of 15° or less on the dips or/and the slips of the fault plane solutions for shallow earthquakes seems to be tolerable.

The foregoing discussions are concerned with the theoretical part of the proposed method. We shall consider now the observational part in next chapter with the aid of several testing cases.

CHAPTER 3

Equalization of the observed amplitude spectrum of surface waves

As a surface wave train spreads out on its way to a recording station, its Fourier spectrum is modified by:

(a) attenuation due to the anelasticity of the earth's crust and upper mantle;

(b) scattering due to the lateral inhomogeneity present over the propagation path;

(c) dispersion, geometrical spreading and the polar phase shift over a spherical earth; and

(d) the filtering effect of the recording instrument. The process of removing these distorting effects is known as the amplitude and phase equalization of the surface wave spectrum.

In the present study the amplitude equalization method (Toksöz, et. al., 1964; Aki, 1966; Tsai and Aki, 1969) shall be used. By applying this method to an earthquake with known fault-plane solution its focal depth and seismic moment can be determined simultaneously.

In the following sections, we shall first describe the method and then use several examples to illustrate its applicability and limitations.

3.1 Correction for the instrumental response

In the present paper we shall use the WWSSN long-period seismograms.

Attempts have been made to choose an appropriate procedure of correcting for the instrumental response. The magnification curve calculated from appropriate instrument constants by Hagiwara's formula (1958) was compared with those obtained from analysing the calibration trace on the corresponding record for many stations.

In general, the agreement between these two were quite close at long periods but not at short periods, probably due to some contamination of the calibration trace by microseismic noises. Thus, we shall make the instrumental correction through the magnification curve calculated by Hagiwara's formula with a proper choice of the following instrument constants:

Seismometer: To=15 or 30 seconds; ϵ_o =0.93

Galvanometer: T_g=100 seconds; ϵ_g=1.00

magnification	6000	3000	1500	750	375
coupling coefficient	0.805	0.204	0.047	0.013	0.003

3.2 Corrections for the geometrical spreading and attenuation

After the observed amplitude spectrum of displacement is corrected for the instrumental response by the method described in previous section, it should further be corrected for the geometrical spreading and attenuation by the following relation:

$$A_o(\omega)=A_r(\omega)\left[\frac{R_o \sin \Delta_r}{r_o}\right]^{1/2} e^{\eta(\omega) r} \qquad (22)$$

where $A_r(\omega)$ is the amplitude observed at the station r km (or Δ_r degree) from the epicenter; $\eta(\omega)$ is the attenuation coefficient at angular frequency ω ; $A_o(\omega)$ is the equalized amplitude at r_o km on a flattened earth; and R_o is the earth's radius in km. We shall choose r_o =2000 km.

The equalized amplitude $A_o(\omega)$ corresponds to the displacement spectral density observed at r_o on a flat, non-dissipative earth.

The correction for attenuation enters equation (22) through the attenuation coefficient $\eta(\omega)$. Data on $\eta(\omega)$ of Love waves are almost non-existing for periods between 10 and 50 seconds (Sato, 1967).

As for Rayleigh waves, there have been some measurements of $\eta(\omega)$ in the past. Arkhangel'skaya and Fedorov (1961) measured $\eta(\omega)$ between 22-24 sec using R_1 to R_5 observed at Moscow. They also gave a fairly complete list of $\eta(\omega)$ data

for periods less than 30 seconds reported by various authors. Press (1964) measured Q_R=325 at period 12 seconds from LRSM records of Nevada nuclear explosions. A more systematic measurement of $\eta(\omega)$ was made by Tryggavason (1965). He used the WWSSN records of a nuclear explosion near Novaya Zemlya in his study. Tsai and Aki (1969) made a measurement of $\eta(\omega)$ over periods between 15 and 50 seconds from the WWSSN records of the Parkfield, California earthquake of June 28, 1966. Data from all these measurements are summarized in Figure 23. The curve on the figure is Tryggavason's (1965) would-wide average value. Even with the added data, his curve is still valid. These results seem to suggest that the attenuation coefficient $\eta(\omega)$ (not Q) of Rayleigh waves can be approximated by a constant over period range from 50 seconds down to about 15 seconds for the present purpose. For periods shorter than 15 seconds, there is indication of increasing attenuation toward short periods. However, the large variability of the data for the short periods would make any further intepretations less meaningful.

It should be pointed out here that all the data mentioned above have been obtained on a world-wide basis and may not be suitable for use in the present study because the propagation paths are selectively chosen so that each path lies almost entirely in one type of the crustal structure, that is either oceanic or continental. Therefore we shall make measurements of Rayleigh wave attenuation over paths which are entirely oceanic or entirely continental. The results are presented

in next section.

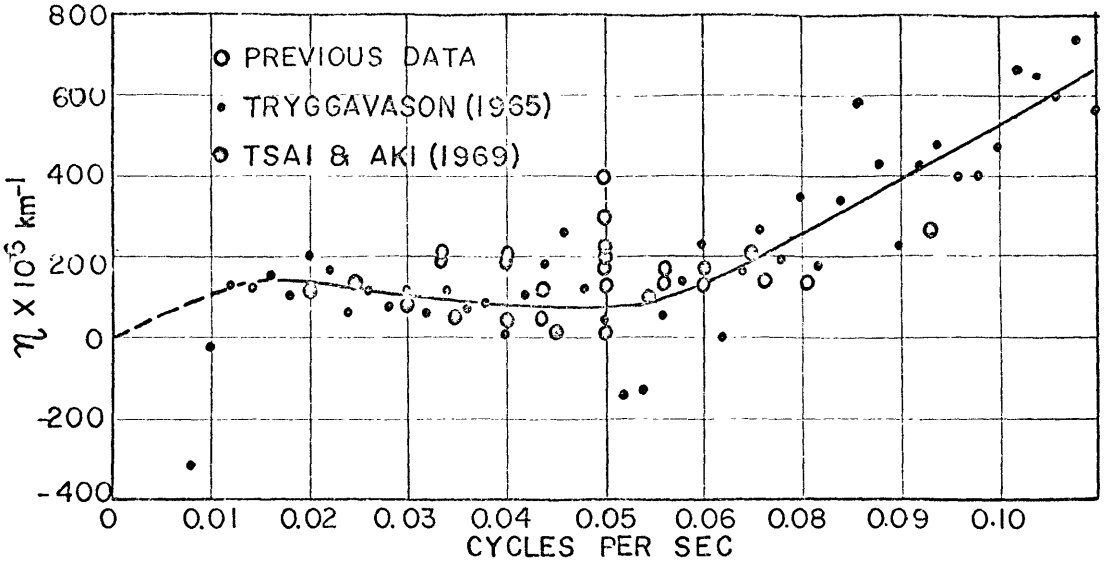

FIG. 23. Summary of the observed attenuation coefficient of Rayleigh waves in periods less than 50 sec.

3.3 Measurements on the attenuation coefficient of Rayleigh waves by the two-station method

The attenuation coefficient $\eta(\omega)$ over the path between a pair of stations nearly on the same great circle can be calculated by

$$\eta(\omega) = \frac{1}{(r_2 - r_1)} \ln\left[\frac{A_1(\omega)}{A_2(\omega)} \left(\frac{\sin \Delta_1}{\sin \Delta_2}\right)^{1/2}\right] \qquad (23)$$

where $A_1(\omega)$ and $A_2(\omega)$ are the amplitudes at frequency ω observed at station 1 and station 2, respectively. The epicentral distance of the first station is designated as r_1 km (Δ_1 degree), the second as r_2 km (Δ_2 degree).

By this method, the source effect can be removed. The uniformity and the availability of the WWSSN long-period records may eventually prove that the two-station method is capable of providing regional attenuation coefficients of surface waves.

Measurements of $\eta(\omega)$ have been made for Rayleigh waves over three paths —— one oceanic (KIP-BKS) and two continental (BOZ-WES and GSC-BLA). The sources were three earthquakes from the Solomon Islands area:

(a) July 17, 1965, 12:47:48.7 GMT m_b=6.4

(b) November 27, 1965, 12:01:51.5 GMT, m_b=6.0

(c) January 13, 1967, 13:48:11.7 GMT, m_b=6.0

Let us now examine the data from each path more carefully.

(1) The east Pacific basin between KIP (Honolulu) and BKS (Berkeley):

The path is oceanic almost all over its entire length of 3880 km except a short portion before reaching BKS where the ocean-continent boundary is crossed. Unfortunately we were able to make only one measurement because the records of the remaining two events were not available at one of the two stations. The observed amplitude spectra at both stations and the corresponding amplitude ratio are shown in Figure 24a and Figure 24b, respectively. In Figure 24a, the epicentral distance and the azimuth at the source, measured clockwise from due north, of the great-circle path leading to each station are also given in the parenthesis following the station code. From this figure, we can see that the general form of the spectrum has been well maintained along its path from KIP to BKS. The phenomenum is again illustrated by the lack of frequency dependence of the amplitude ratio as shown in Figure 24b. The data for periods below 16 seconds or so are much scattered because of their lower amplitude level. The attenuation coefficient $\eta(\omega)$ obtained from this measurement has a constant value of 168×10^{-6} km^{-1} for periods from 10 to 50 seconds. This is quite similar to the world-wide average value for periods longer than 15 seconds as shown in Figure 23. As far as our data are concerned, there appears no systematic increase of attenuation for periods shorter than 15 seconds which was observed by Tryggavason (1965). It is probable that scattering and reflections at crossing boundaries between oceans and continents were responsible for at least part of the attenuation observed by Tryggavason. Although we have no similar

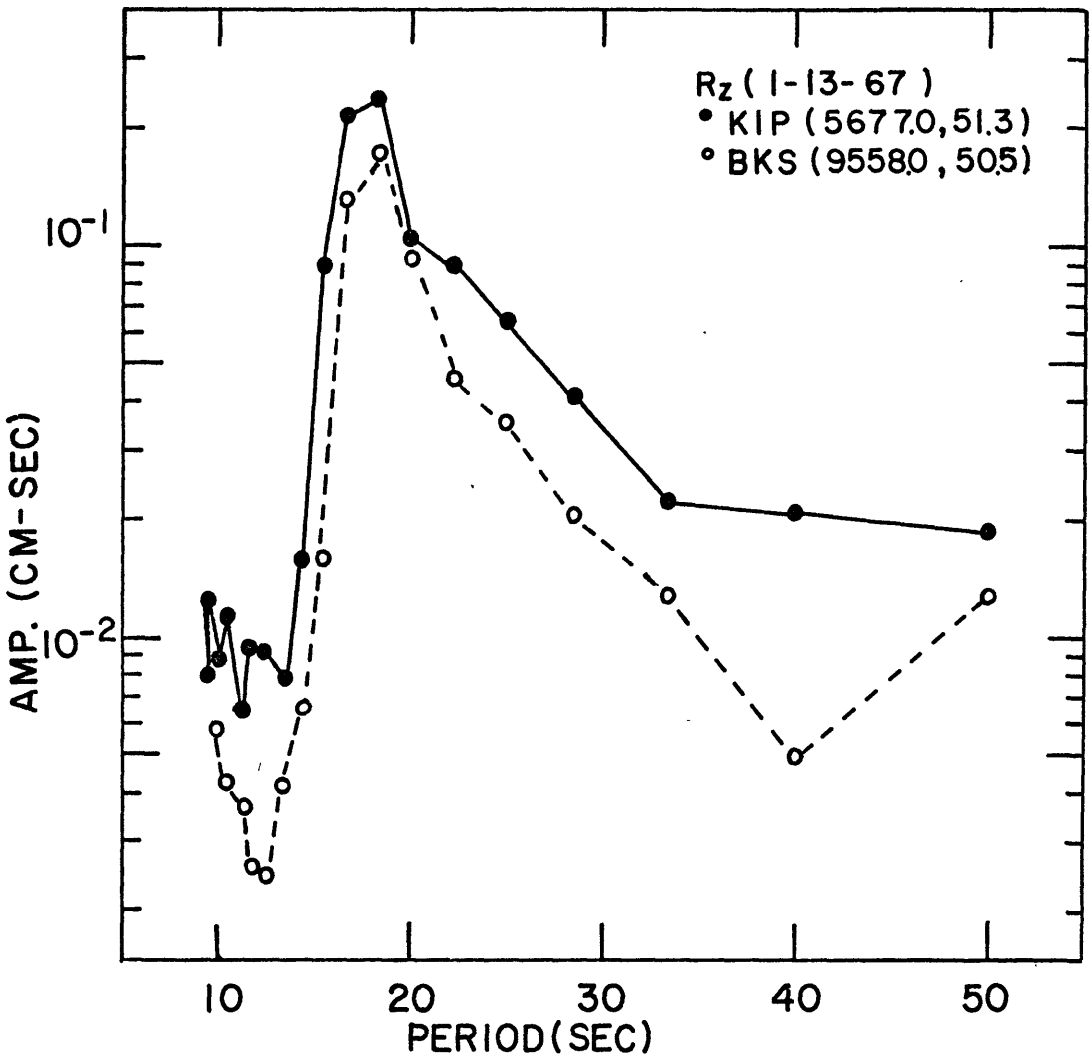

FIG. 24a. The observed Rayleigh wave amplitude spectrum at KIP and BKS.

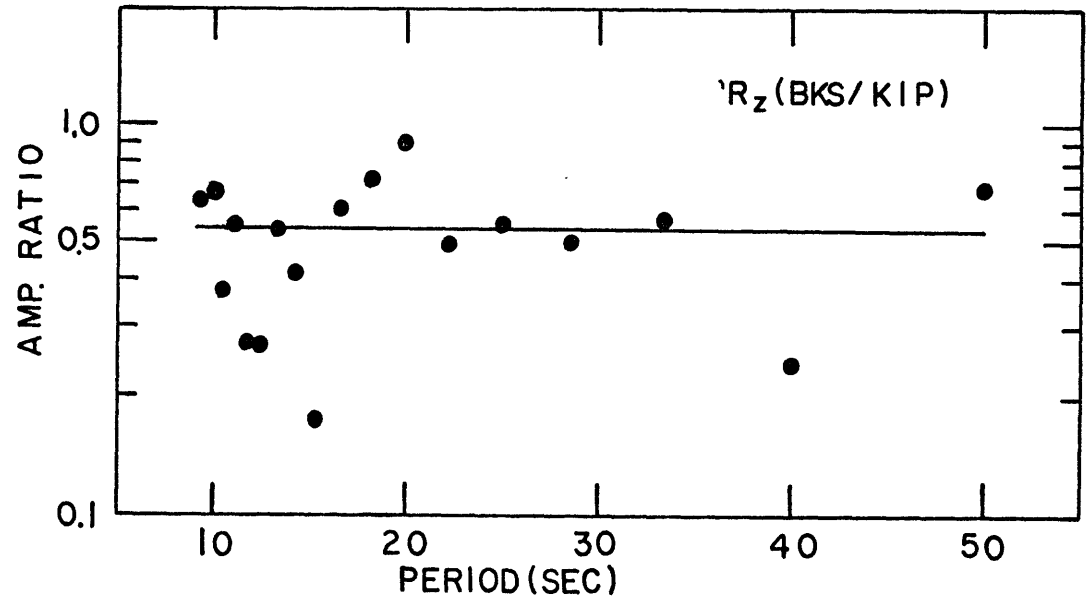

FIG. 24b. The amplitude ratio between BKS and KIP.

measurements over other oceans, the close agreement between our measurement of the Pacific basin ($\eta(\omega)=168 \times 10^{-6}$ km^{-1}) and those made by Gutenberg (1935) over the Atlantic (η = 100 - 150 x 10^{-6} km^{-1} at T=20 seconds) and over the Pacific and the Arctic (η =150 -250 x 10^{-6} km^{-1} at T=20 seconds) suggests that $\eta(\omega)=168 \times 10^{-6}$ km^{-1} may be representive for most ocean basins. Most of our oceanic paths are quite similar to that between KIP and BKS in the sense that shortly before the waves reach the recording stations on land, they all have to cross the ocean-continent boundary. Thus, the attenuation coefficient $\eta(\omega)$ measured from KIP to BKS appears to be applicable to them at least for the first approximation.

(2) Southern United States between GSC (South California) and BLA (Virginia):

This is an exclusively continental path of 3250 km running across the southern part of the United States from the west to the east coast. We have made three measurements on this path. The observed amplitudes an shown in Figure 25a and Figure 25c. The corresponding amplitude ratios from all three measurements are given in Figure 25b. Again the spectrum was distorted very little after the waves had propagated from GSC to BLA for more than 3200 km. The amplitude ratios show no systematic dependence on frequency. From these three measurements we have obtained a constant value of 157 x 10^{-6} km^{-1} for the attenuation coefficient $\eta(\omega)$ in the period range between 10 and 50 seconds. Again, this value is similar to the world-wide average of attenuation.

FIG. 25a. Rz amplitude spectrum at GSC and BLA.

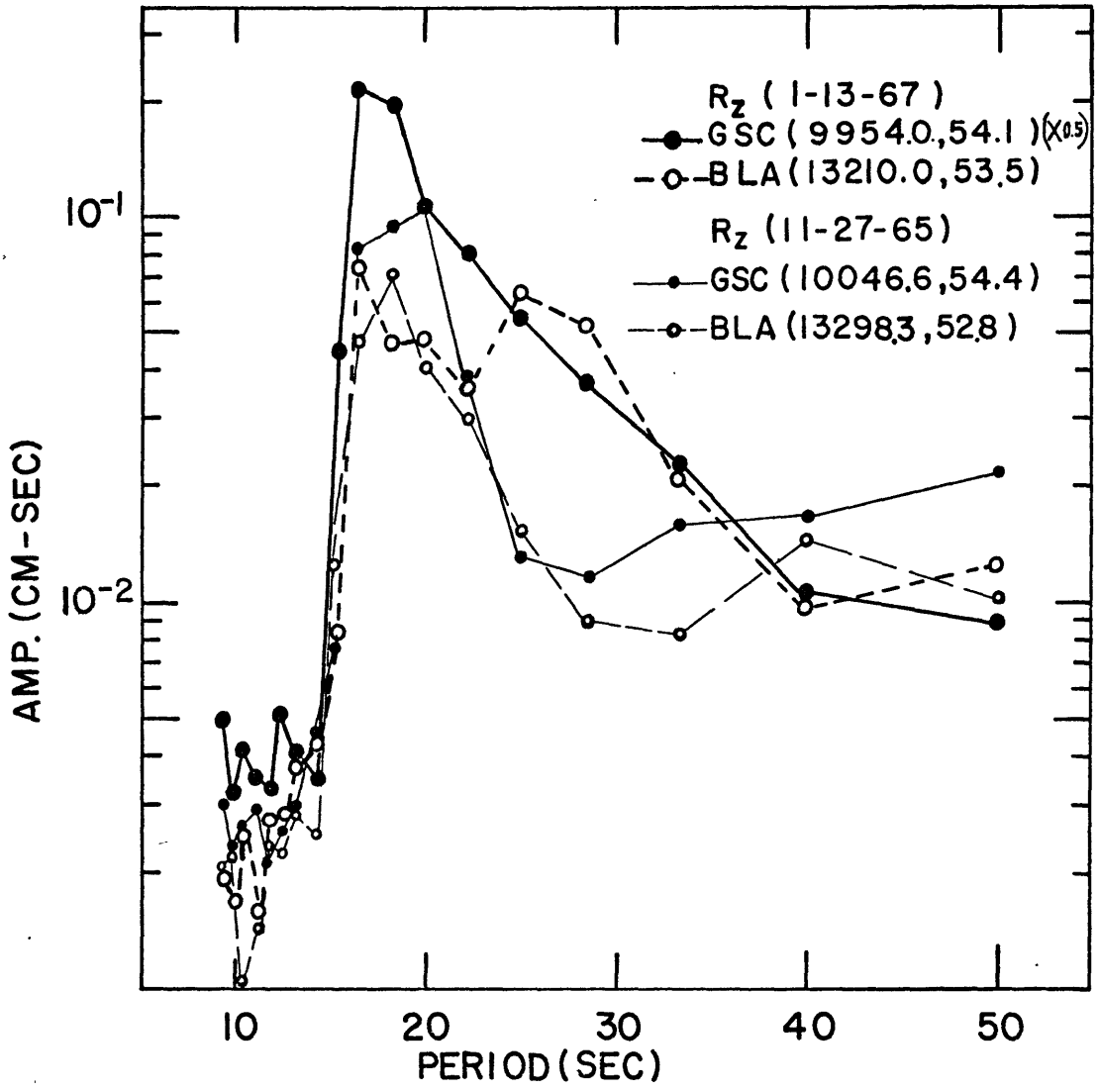

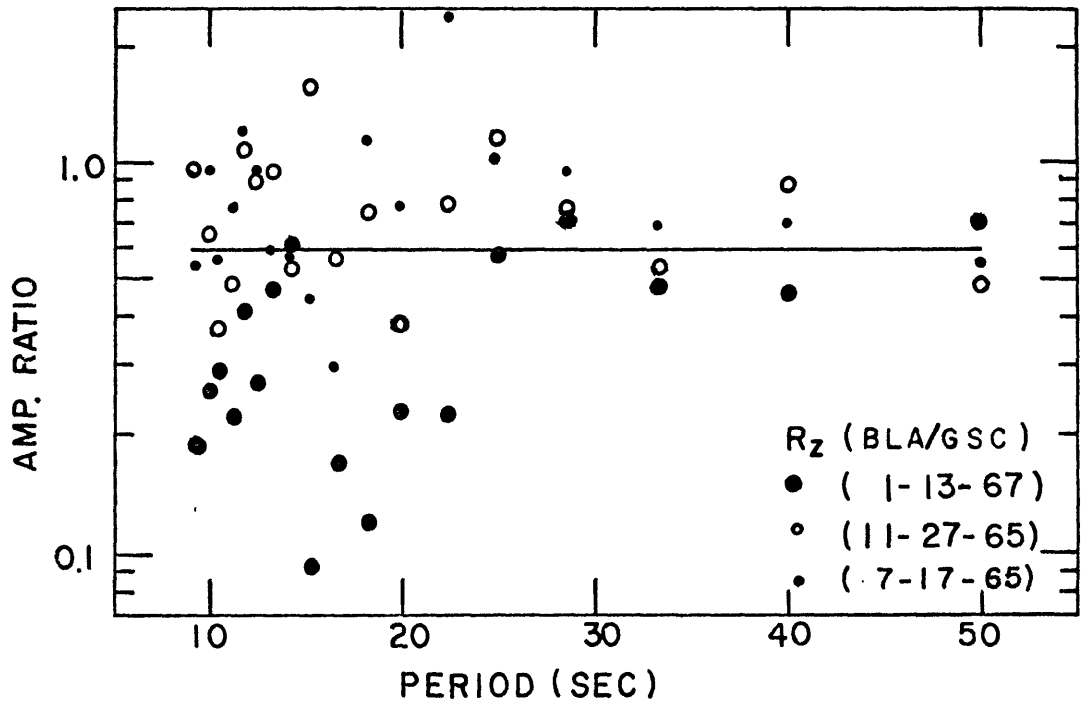

FIG. 25b. Rz amplitude ratios between BLA and GSC.

(3) Northern United States between BOZ (Montana) and WES (Massachusetts):

This is an entirely continental path with a rather uniform crustal structure running from west to east for a distance of 3220 km across northern United States. The observed amplitude spectra from all three events are shown in Figure 26a and Figure 26c. The corresponding amplitude ratios are shown in Figure 26b. These data indicate that the attenuation of Rayleigh waves is nearly frequency independent as we have pointed out already. However, it is interesting to find here that the attenuation coefficient obtained here is only about 52×10^{-6} km^{-1}. This is noticeably lower than most values obtained so far. If this low attenuation is proved to be real, then its geophysical implications may be quite significant. For the moment, we shall not pursue further on this aspect.

In summary, results of all measurements along three different paths appear to indicate that the attenuation coefficient $\eta(\omega)$ is approximately independent of frequency for periods between 10 to 50 seconds. Except one possible low attenuation path, the Rayleigh wave attenuation coefficients obtained from our measurements do not differ much from the world-wide average value. A constant attenuation coefficient $\eta(\omega)$ implies that the quality factor Q_R would be almost inversely proportional with period for $50 \geq T \geq 10$ seconds. This is essentially consistent with the interpretation of Tsai and Aki (1969) that the high Q lithosphere of about 100 km thickness overlies the low Q asthenosphere.

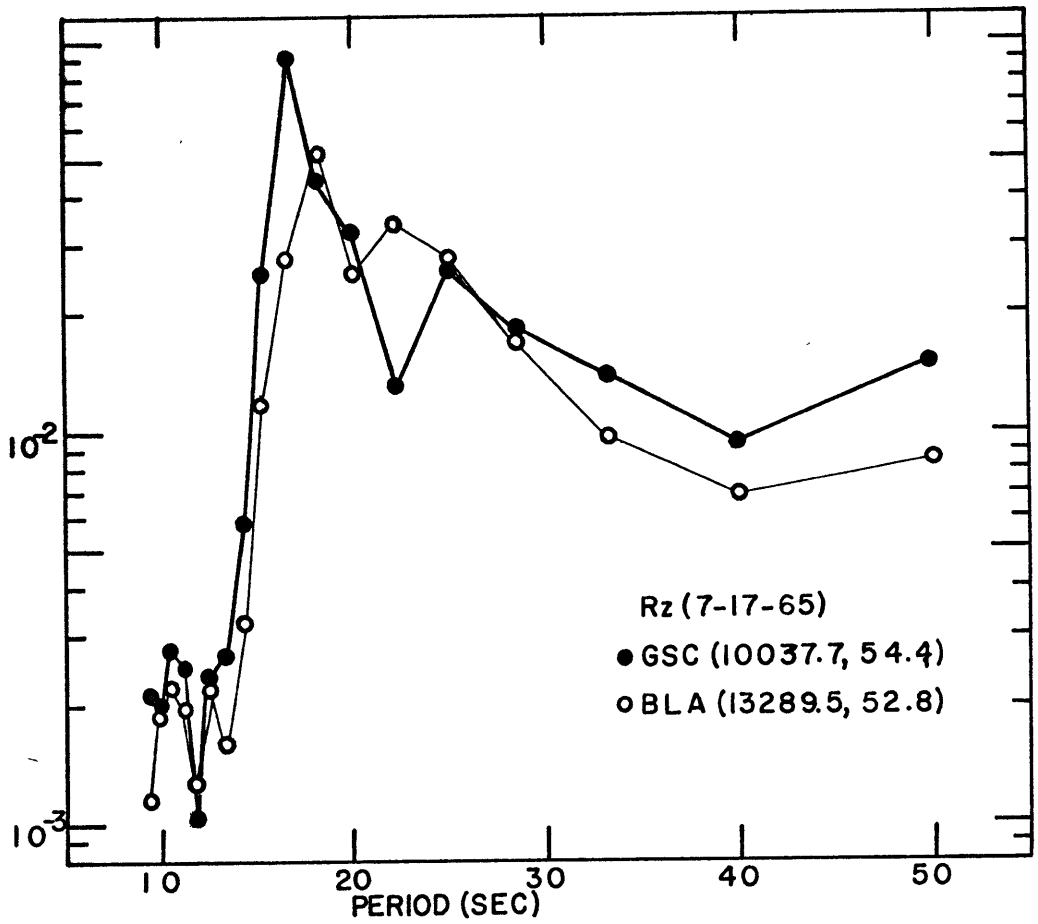

FIG. 25c. Rz amplitude spectrum observed at GSC and BLA.

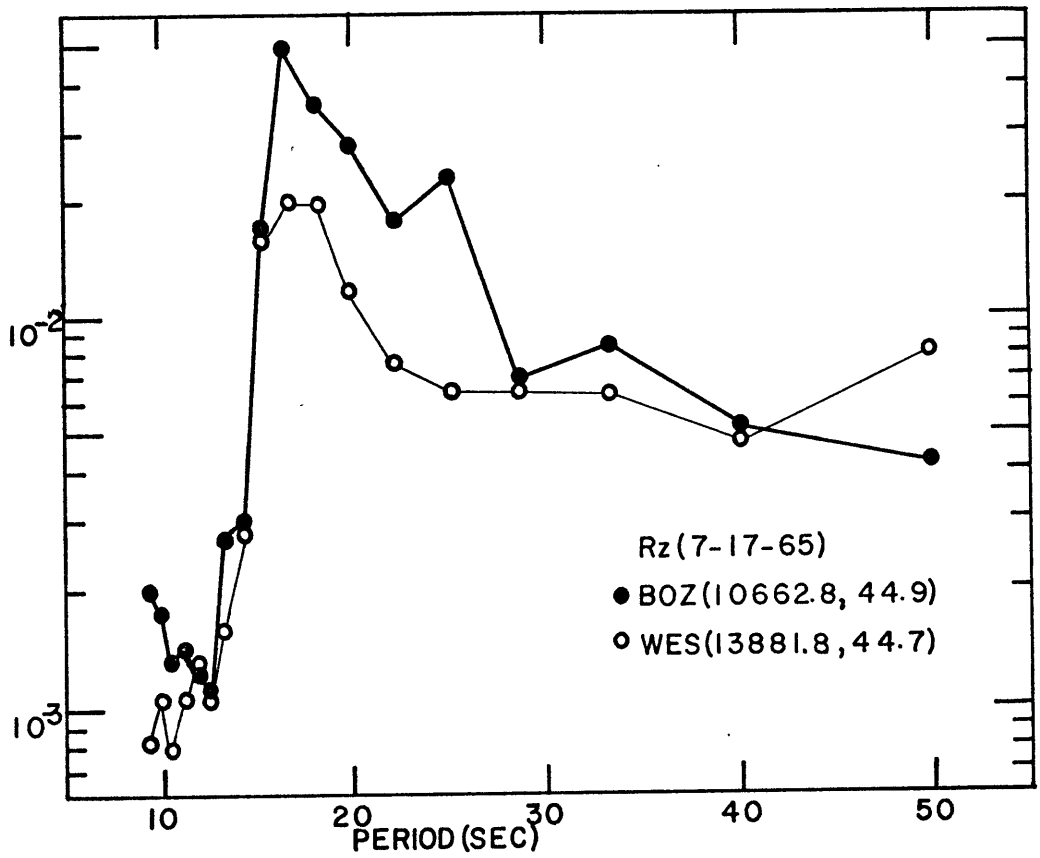

FIG. 26c. Rz amplitude spectrum at BOZ and WES.

FIG. 26a. Rz amplitude spectrum at BOZ and WES.

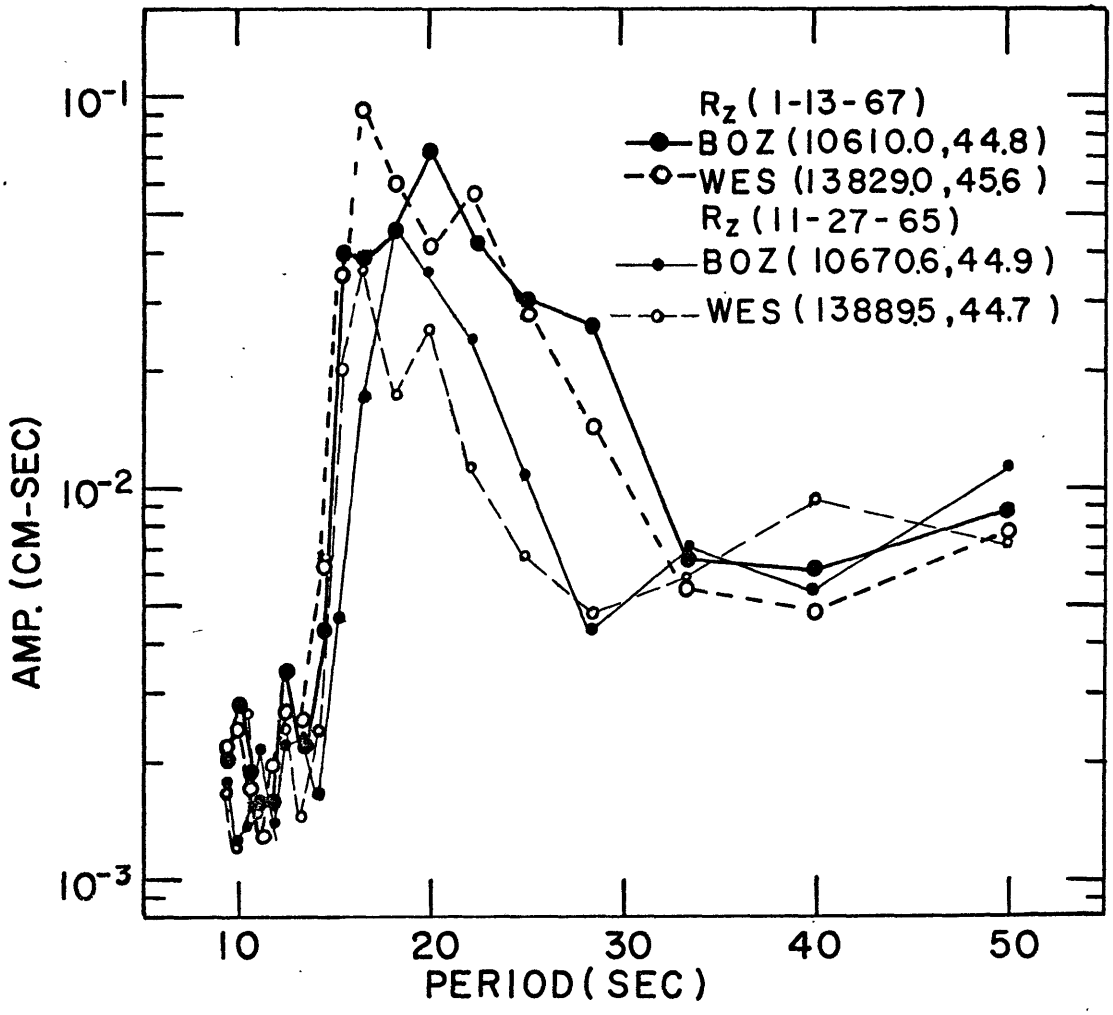

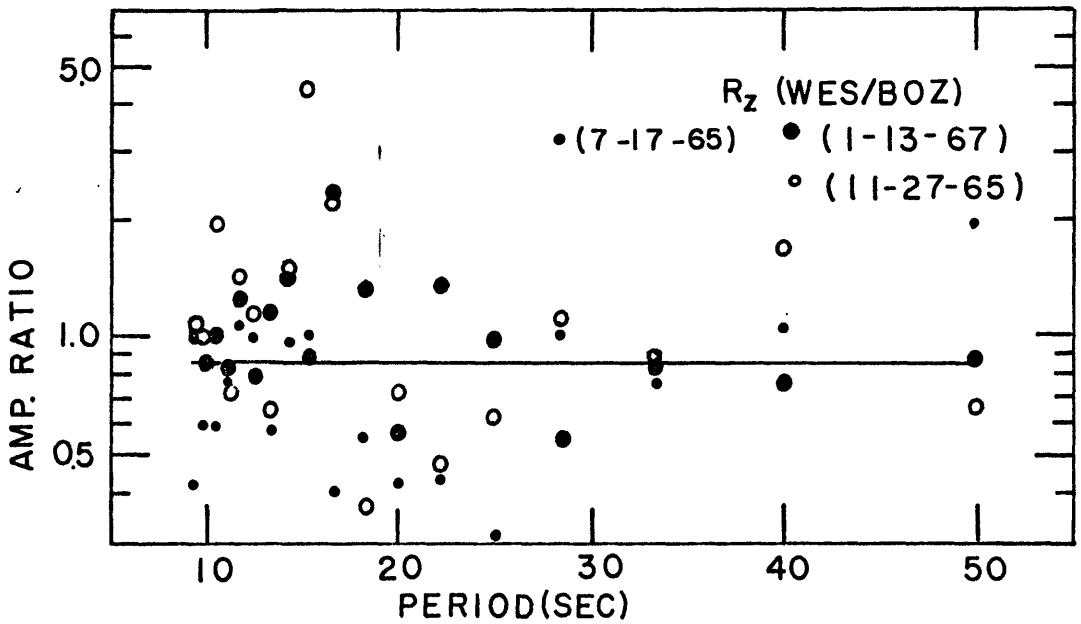

FIG. 26b. Rz amplitude ratios between WES and BOZ.

On the basis of our data given above we may conclude that the attenuation effect on the shape of the Rayleigh wave amplitude spectrum for periods between 10 to 50 seconds may be neglected along a simple path for as long as 3900 km such as the one between KIP and BKS. Thus the correction for attenuation will appear in equation (22) simply as a scalar factor. In other words, it will affect only the seismic moment but not the focal depth determination.

3.4 Tests on the proposed method for focal depth determination

After all major sources of possible uncertainty have been examined, we now believe that the surface wave, especially Rayleigh wave, amplitude spectrum may be used for the determination of the focal depth and the seismic moment. The applicability of the method shall further be tested by several earthquakes whose fault-plane solutions are known and whose focal depths have been determined by independent methods. The following earthquakes appear to be the ideal candidates for such a task:

a. Foreshock, mainshock and aftershock of the Parkfield, California earthquake of June 28, 1966.

b. The Denver earthquake of August 9, 1967. Let us look into the results of these tests in more details.

(1) Test on the main shock, foreshock and aftershock of the Parkfield earthquake of June 28, 1966.

According to McEvilly et. al. (1967), the origin times and locations of these events were the following:

Foreshock June 28, 1966, 04:08:56.2 GMT; 35° 57.6'N, 120° 30.3'W, m_b=5.1

Main shock June 28, 1966, 04:26:13.4 GMT; 35° 57.3'N, 120° 29.9'W, m_b=5.5

Aftershock June 29, 1966, 19:53:25.9 GMT; 35° 56.6'N, 120° 31.5'W, m_b=5.0

The volume of observations collected on this earthquake sequence is quite remarkable. In addition to eight permanent seismograph stations operated in the source area, about 25

temporary stations were employed by various groups for the study of aftershock sequence. Using these data, McEvilly et. al. (1967) studied, among other things, the focal mechanism and the aftershock activity of the sequence. Their results suggested that

a. a right-lateral transcurrent focal mechanism consistent with the San Andreas fault zone was indicated by the P-wave radiation patterns of all the larger shocks, including those three mentioned above, and over 95 percent of the aftershocks. The dip of the fault plane is essentially vertical (85^{o}SW to 88^{o}NE);

b. intense aftershock activity was concentrated closely along the fault zone for approximately 27 km south of the main shock, with sporadic occurience over 45 km. Nearly all the earthquake foci of the sequence lay in the depth range 2-12 km with an averge of about 5 km.

Brown and Vedder (1967), among others, reported surface fracture accompanying the sequence along a 38 km segment of the San Andreas fault zone in the Parkfield-Cholame region.

Eaton (1967) determined the average speed of rupture to be 2.2 km/sec between the main shock epicenter and the Gold Hill Station which was in the fault zone 20 km southeast of the epicenter. This was confirmed by Filson and McEvilly (1967) from Love wave amplitude spectrum of the main shock recorded at Berkeley. In addition, they also determined a fault length of about 30 km for the main shock. Wu (1968)

suggested that the focal depth of the main shock was about 8.6 km based on the Rayleigh waves spectrum of a Canadian Station (SFA). He also suggested that the main shock could have been a series of shocks separated in space and time. Aki (1968) found, by combining the seismic displacement near the fault with the seismic moment, that the fault depth of the main shock was about 3 km within the basement rock. Tsai and Aki (1969) found that a strike trending in N 43°W would give a better fit of the surface wave radiation patterns obtained from the WWSSN long-period records.

Based on these enormous quantity of near-field and far-field data, we can confidently choose the following source parameters:

1. $d=90^{\circ}$, $s=0^{\circ}$, $L=0$ for the foreshock and the aftershock.

2. $d=90^{\circ}$, $s=0^{\circ}$, $L=37$ km, $V=2.2$ km/sec for the Main shock.

The strike is taken, to be in N43°W. And the theoretical amplitude spectrum of surface waves is calculated in the Gutenberg continental model.

For the case of the foreshock and the aftershock, we have chosen Rayleigh waves at ALQ and Love waves at GOL for analysis because they were located close to the lobe direction of the radiation patterns. The observed data are shown in Figure 27a and Figure 27b for the foreshock and in Figure 28a and Figure 28b for the aftershock.

First of all, Rayleigh waves as observed at ALQ and Love waves at GOL from the foreshock are extremely similar to those from the aftershock. This similarity of surface wave spectrum

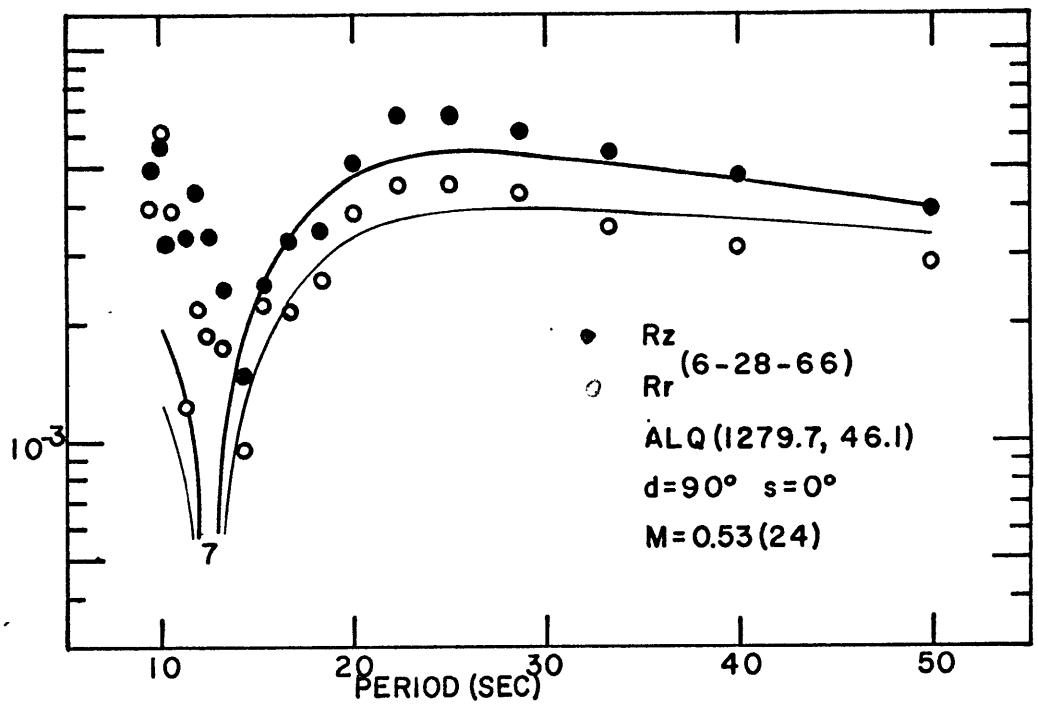

FIG. 27a. Rayleigh wave amplitude spectrum from the foreshock of the June 28, 1966 Parkfield earthquake (event P5') observed at ALQ.

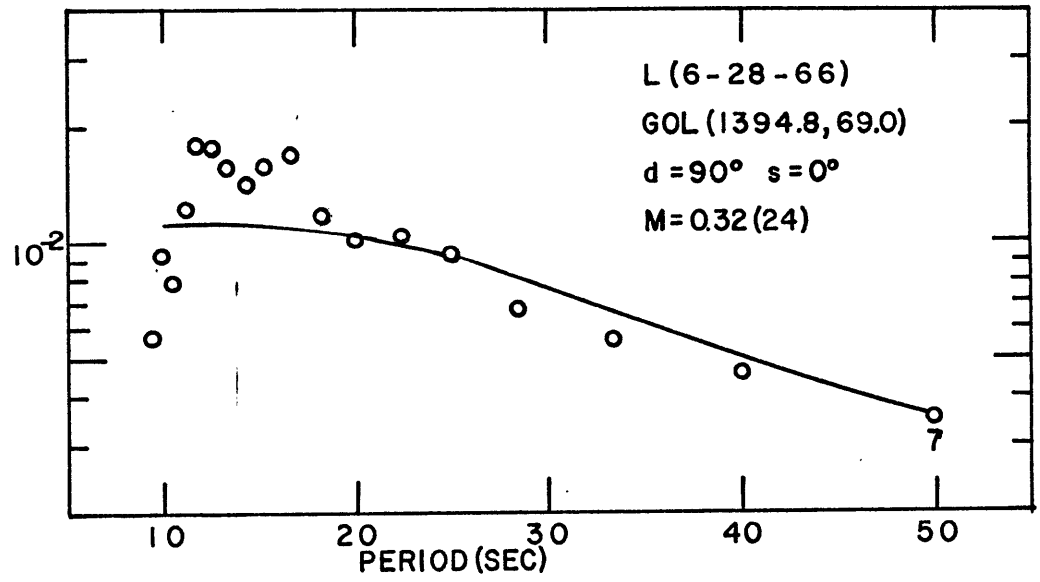

FIG. 27b. Love wave amplitude spectrum observed at GOL from the same event shown in FIG. 27a.

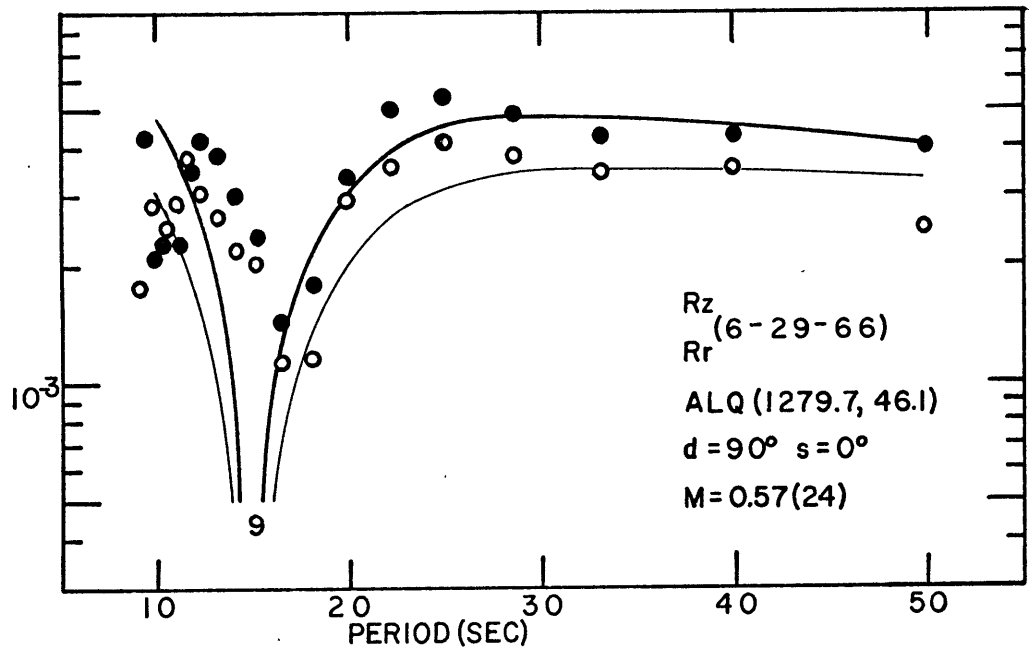

FIG. 28a. Rayleigh amplitude spectrum from the aftershock of the June 28, 1966 Parkfield earthquake (event P6) Observed at ALQ.

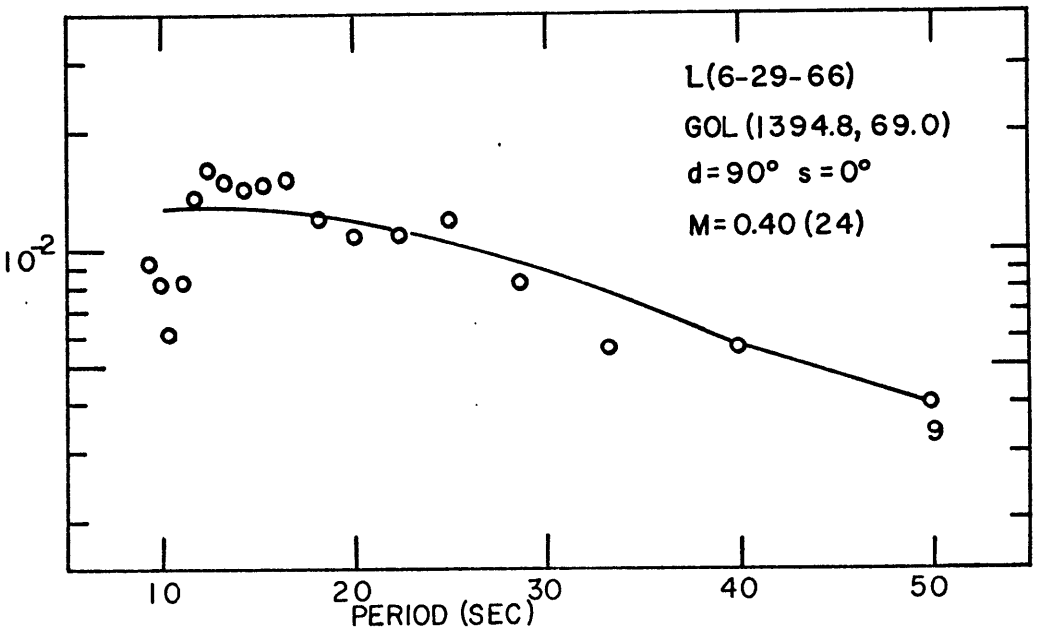

FIG. 28b. Love wave amplitude spectrum from the same event shown in FIG. 28a observed at GOL.

strongly supports the finding that over 95 percent, including the three largest events, of the sequence had the same fault-plane solution (McEvilly, 1967). In Figure 27a, the remarkable spectral node at period about 14 seconds is attributed here to the effect of its focal depth. A focal depth of about 7 km is consistent with the data. It is well known that the finiteness effect can also cause nodes on the amplitude spectrum. We have rejected such a possibility for the present case on the ground that no similar node appears on the Love wave spectrum observed at GOL, as shown in Figure 27b. The theoretical spectrum due to a fault at depth 7 km explains the observed Love wave data equally well. The seismic moment derived from Rayleigh waves (0.53×10^{24} dyne-cm) shows a fairly good agreement with the value derived from the Love wave amplitude spectrum observed at GOL (0.32×10^{24} dyne-cm).

The observed surface wave spectra from the aftershock is shown in Figure 28a and Figure 28b. These data suggest a focal depth of about 9 km for this event. The seismic moment obtained from Rayleigh waves is 0.57×10^{24} dyne-cm as compared to 0.40×10^{24} dyne-cm derived from Love waves. Again the agreement is fairly good.

The focal depths of these two events as indicated by the surface wave amplitude data are within the focal depth distribution of 2 to 12 km of the whole sequence. The USCGS depth determination gave 5 km for both of the foreshock and the aftershock.

The Love wave spectrum at GOL from both the foreshock and

the aftershock suggest that a step function is a good approximation to the source time function because the observed amplitudes in the short-period end near 10 seconds are only slightly lower than the theoretical.

As for the main shock, Rayleigh waves observed at ATL which is close to the lobe direction of the radiation pattern are given in Figure 29. The theoretical spectrum with a focal depth 4 km fits the observed one best. This depth agrees with the one obtained by Aki (1968). The USCGS depth determination gave 4 km for this event.

The seismic moment obtained here is 1.75×10^{25} dyne-cm which is very close to 1.50×10^{25} dyne-cm as obtained by a least squares method from the world-wide data (Tsai and Aki, 1969).

These tests indicate positively that the surface wave amplitude method can be used to determine the focal depth of an earthquake with an uncertainty of a few kilometers if the fault-plane solution of the earthquake is known.

(2) Test on the largest Denver earthquake of August 9, 1967.

This is the largest one of a sequence of earthquakes which are believed to have been triggered by injection of waste fluids into a deep well near Denver, Colorado. Healy et. al. (1968) reported that accurate locations of sixty-two earthquakes which occurred during January and February of 1966 defined an epicentral zone about 10 km long and 3 km wide with its long axis trending N 60°W. With the aid of a very dense network

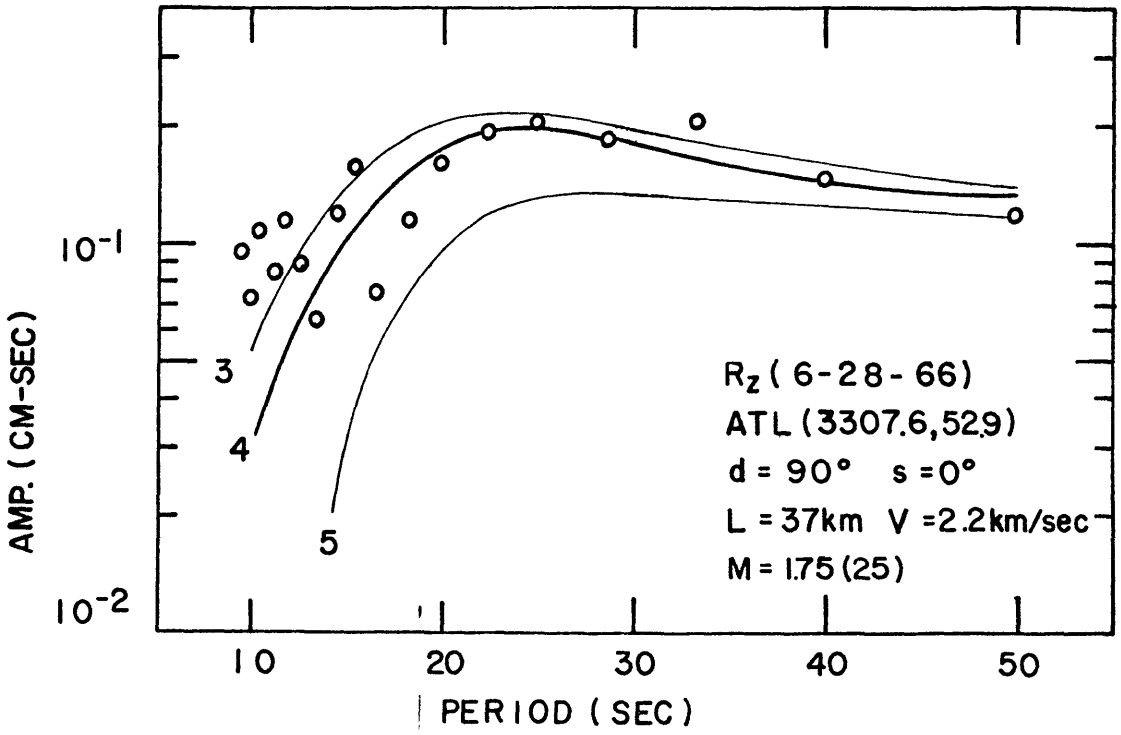

FIG. 29. Rayleigh wave amplitude spectrum from the main shock of the June 28, 1966 Parkfield sequence observed at ATL.

of seismic stations established by the U. S. Geological Survey in the vicinity of the deep well, the accuracy of these earthquake locations were believed to be within 1 km. The depths of these earthquakes ranged from 4.5 to 5.5 km. The largest event of August 9, 1967 fell within this zone too. Major and Simon (1968) studied this event in great details. Using data provided by eight conventional seismograph stations and a large microearthquake array in the epicentral region, they determined the focal depth of this event as 5 km. The origin time was 13:25:07.2 GMT and the Richter magnitude 5.3. With a combination of data from the seismograph network, various strainmeters, tiltimeters, seismoscopes, intensity mapping and field observations in and out the epicentral area, they inferred that the source mechanism of the August 9, 1967 event was a vertical right-lateral strike-slip fault; the rupture probably propagated along the direction N 70^{o}W at a speed of 3 km/sec for about 10 kilometers. In summary, this earthquake is a very suitable candidate for testing our method. The Rayleigh wave amplitude spectrum observed at BKS and at FFC are shown in Figure 30a and Figure 30b, respectively. These data are consistent with the focal mechanism obtained by Major and Simon (1968). The focal depth determined by our method is 5 km which is exactly the same as the one obtained from the near-station travel time data. The two stations also yield the same value for the seismic moment, i.e. 0.18×10^{24} dyne-cm. The Love wave amplitude data from the earthquake observed at

BLC and CHC are given in Figure 31a and Figure 31b, respectively. They are explained equally well by the same focal mechanism used in interpreting the Rayleigh wave data. The seismic moment is determined as 0.16×10^{24} dyne-cm at BLC and 0.14×10^{24} dyne-cm at CHC which agree closely with the one obtained previously from the Rayleigh waves. The finiteness effect in this case is not significant. Again the observed Love wave spectrum suggests that a step function in time for the source is a good approximation because there is no evidence of amplitude decrease for shorter periods in the frequency range studied here. (See Figure 22b for comparison). The agreement between the observed and the theoretical surface wave spectra is in general poorer at those stations located near the nodal directions of radiation than at other stations located near the lobe directions.

In summing up the result of these tests, we can confidently say that the surface wave amplitude spectrum in period range between 10 and 50 seconds can be used to determine the focal depth of an earthquake with known fault-plane solution. For simple paths such as the one from the epicenter of the Parkfield earthquake to ATL (Georgia) the attenuation effect on the amplitude spectral shape can be neglected without causing serious errors for a distance as long as 3000 km. The assumed step function in time for the source appears to be a good approximation as evidenced by the observed Love wave amplitude spectrum from three smaller tested earthquakes. From these tests we have also learned that the finiteness

FIG. 30a. Rz amplitude spectrum from the Denver August 9, 1967 event observed at BKS.

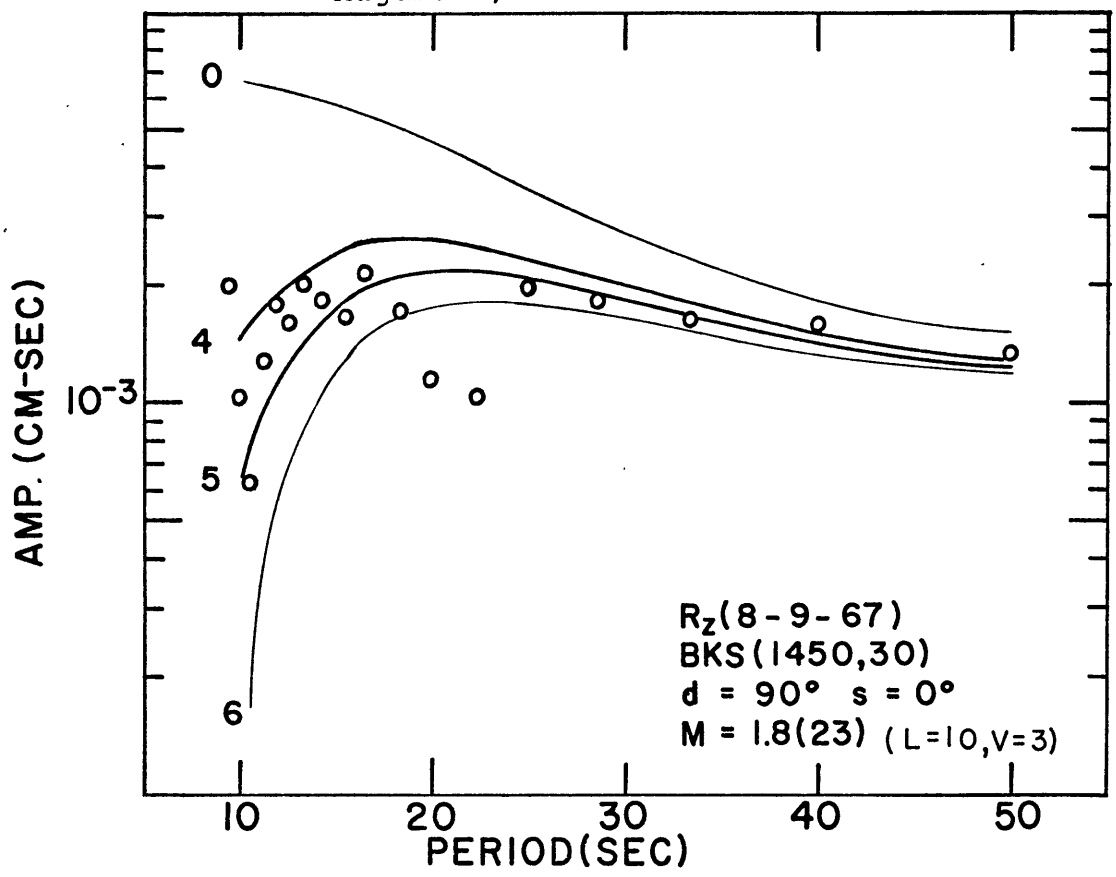

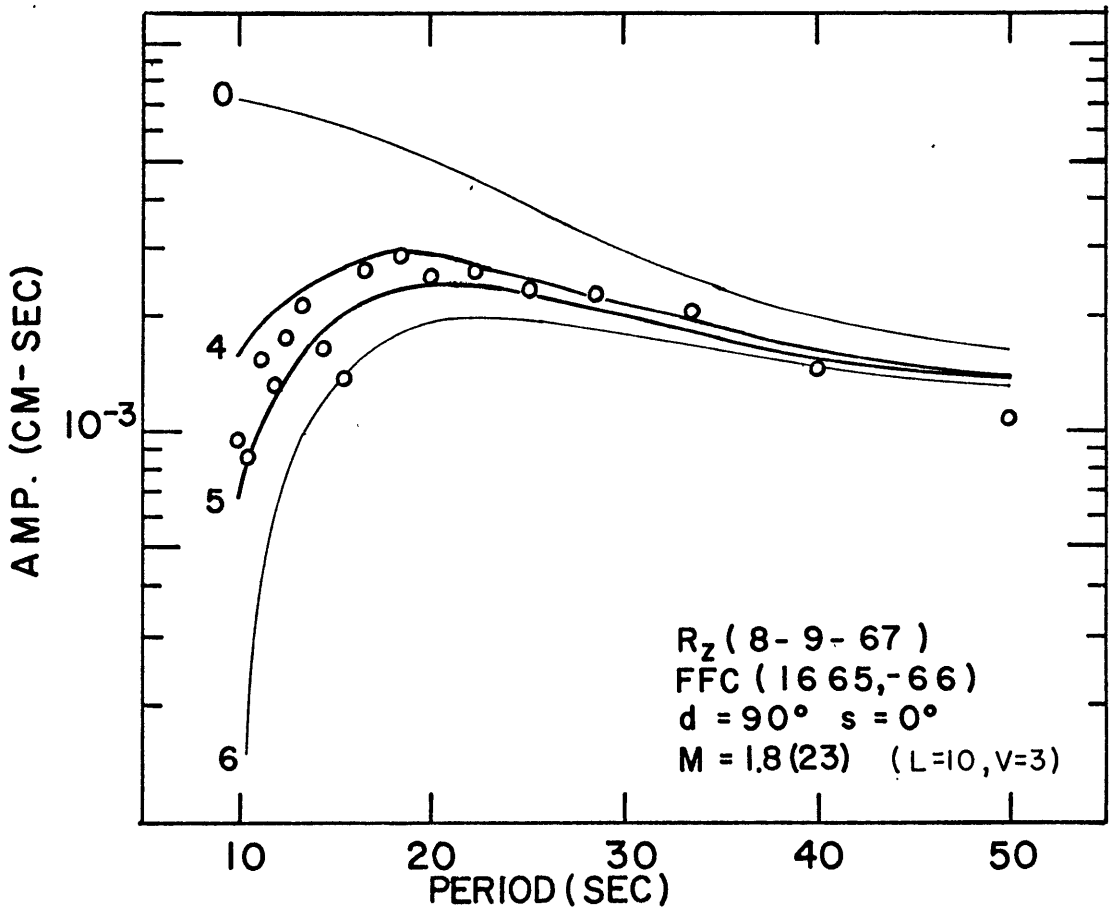

FIG. 30b. Rz of the same event observed at FFC.

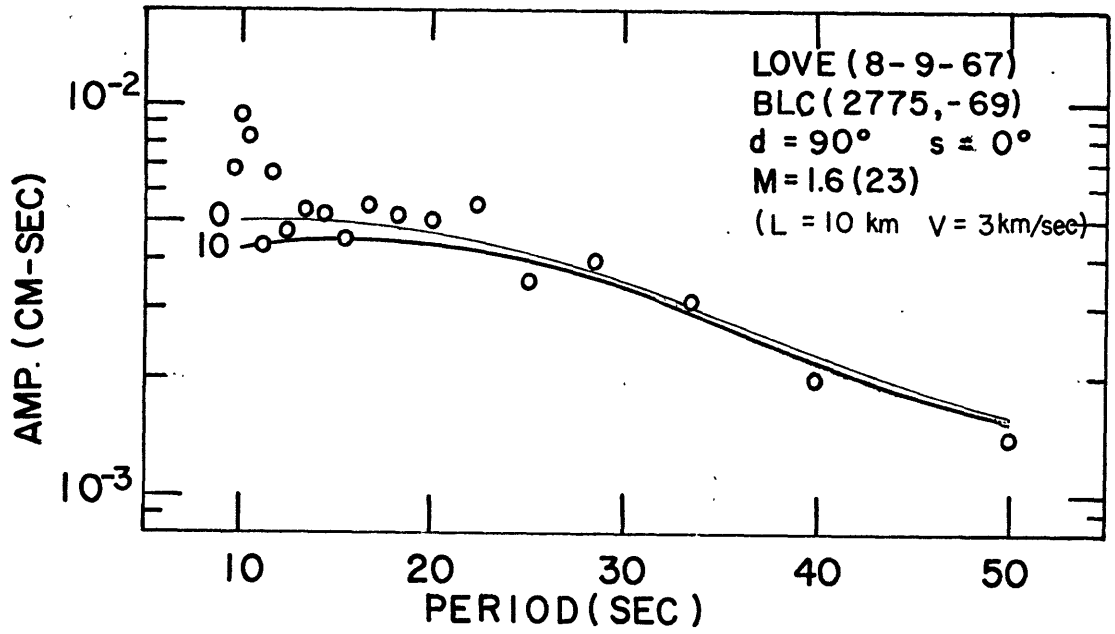

FIG. 31a. Love wave amplitude spectrum from the Denver earthquake of August 9, 1967 observed at BLC.

FIG. 31b. LOVE wave amplitude spectrum from the same event observed at CHC.

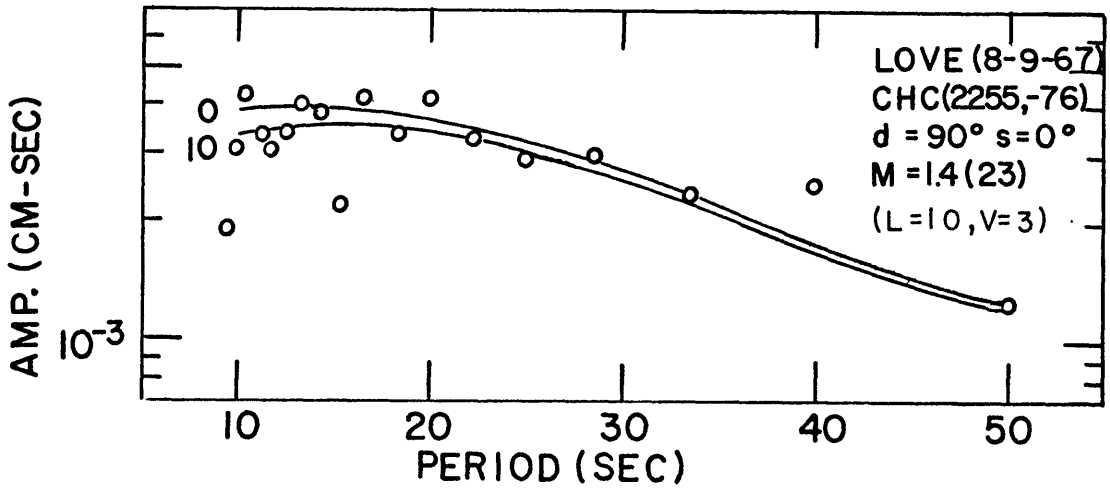

effect is negligible for earthquakes with magnitude up to 5.3. Finally, it must be emphasized that those stations lying on simpler paths from the source and near the lobe directions of radiation should be used for the analysis.

After the validity of the method has been substantiated by the result of several tests, we shall now proceed to apply it to determine the focal depths of many earthquakes on the mid-oceanic ridges.

CHAPTER 4

The focal depths and the seismic moments of earthquakes on the mid-oceanic ridges

During the last few years since the World-Wide Staudardized Seismograph Network (WWSSN) was installed, Focal mechanisms of many earthquakes on the mid-oceanic ridges and on the extension of this ridge system into western North America have been studied. The results indicate that there are two principal types of mechanism for earthquakes on the mid-oceanic ridges (Sykes, 1967). Earthquakes on fracture zones are characterized by predominantly strike-slip motion; earthquakes located on the crest of the ridge but apparently not situated on fracture zones are characterized by predominantly dip-slip motion. The inferred axes of maximum tension for these latter events are approximately perpendicular to the local strike of the ridge. Unfortunately, the locations of these earthquakes in the third dimension, i.e. depth, were not well determined because of insufficient or inexistent travel time data from near stations. Therefore, we shall apply the surface wave amplitude method to determine the focal depths for 32 of these earthquakes whose fault plane solutions are known. At the same time the seismic moment of each event is also obtained. We shall choose those events whose magnitudes are 6.0 or less so that the finiteness effect may be neglected. Care is taken also on the nature of wave path when the stations are selected. We used records for which the wave path is predominantly oceanic or continental. An important factor in making such

selections practicable is the availability of seismograph records from the WWSSN stations. The earthquakes to be studied here were located on three principal mid-oceanic ridge systems, namely, the mid-Atlantic ridge, the mid-Indian Ridge and the East Pacific Rise with its extension into the Gulf of California, western North America and the Northeast Pacific Region.

For each earthquake we first derived from its known fault plane solution the following parameters:

a. the strike of one of the two nodal planes measured in clockwise direction from the north and designated by ϕ_o ,

b. the dip angle d of the same nodal plane as defined in Figure 1 and

c. the slip angle s on the same nodal plane which is also defined in Figure 1.

We then use these fault plane parameters to calculate the theoretical amplitude spectrum of Love waves by equation (2) and that of Rayleigh waves by equations (6) and (7) for each station. In the computations we represent the medium structure either by the Gutenberg continental model (see Table 1.) or by the Harkrider-Anderson oceanic model (see Table 2), depending on the nature of the paths. The theoretical spectrum is then compared with the equalized amplitude spectrum observed at each station to determine the focal depth and the seismic moment of the earthquake.

As pointed out in the preceding chapter, the attenuation effect may be approximated by a scalar factor independent of frequency. Thus in the process of focal depth determination

we neglect the correction for attenuation. The correction for attenuation is made afterward for the determination of seismic moment. In the following sections, the seismic moment M shown in each figure of amplitude spectra for individual stations is not yet corrected for attenuation.

Now let us look at the results.

4.1 Earthquakes on the east Pacific rise, in the Gulf of California, western North American and the northeast Pacific region.

We have studied 15 earthquakes along this ridge system. The fault-plane solutions for these events were studied by Sykes (1967), Bolt et. al. (1968), and Tobin and Sykes (1968). A Summary of locations and other pertinent data of these earthquakes are listed in Table 3.

1. Event P1: This was an event of magnitude 5.8 occurred on April 3, 1963 and located on the Eltanin fracture zone in the southeast Pacific. The fault plane solution for this earthquake was obtained by Sykes (1967) as a strike-slip faulting on a steeply dipping plane with the same strike as the fracture zone. Thus, we have the following fault parameters for this event: $d=90^{o}$ (dip angle), $s=180^{o}$ (Slip angle) and $\phi_o=294^{o}$ (Strike direction measured clockwise from the north).

The Rayleigh wave amplitude spectrum as observed at WEL ($r=4364.4$ km, oceanic) is shown in Figure 33. The entire path was in the south Pacific basin with ocean depth about 5 km. The observed data indicate that the focal depth was 3.5 km beneath the ocean floor and the seismic moment was 0.64×10^{25} dyne-cm before correction for attenuation. The listed USCGS depth was 33 km.

2. Event P2: This was located off the west coast of Mexico on the Rivera fracture zone. The fault plane solution as obtained by Sykes (1967) indicated a predominantly strike-slip fault and gave the following source parameters:

TABLE 3 Earthquakes in the Pacific rise and its northern extension

Event	Long.	Lat.	Date Day	Mo	Yr	Time Hr	Min	Sec	Strike	Dip	Slip	Figure number	Station code	Epidistance (km)	Focal depth (km)	M(uncorrected) (10^{25} dyne-cm)	M(corrected) (10^{25} dyne-cm)	Magnitude Ms	USCGS Depth (km)	m_b	ISC Depth (km)	m_b	Reference
P1	128.2 W	54.40S	03	04	63	14	47	50.4	294	90	180	33	WEL	4364.4	4	0.64	1.33	6.30	33	5.8			Sykes (1967)
P2	107.18W	18.87S	06	12	65	11	34	48.9	112	90	4	34	AFI	7956.4	4	3.60	13.72	6.88	20	5.9			Sykes (1967)
P3	108.75W	21.26N	22	05	66	07	42	42.9	133	90	0	35a	GOL	2069.6	5	0.16	0.22	5.60	53	5.5			Sykes (1968)
P3	"	"	"	"	"	"	"	"	"	"	"	35b	ALQ	1532.8	5	0.13	0.17	5.50					
P4	108.65W	21.36N	23	05	66	11	51	27.3	133	90	0	36a	ALQ	1520.4	5	0.20	0.25	5.65	58	5.6			Sykes (1968)
P4	"	"	"	"	"	"	"	"	"	"	"	36b	GOL	2059.1	5	0.26	0.36	5.80					
P4	"	"	"	"	"	"	"	"	"	"	"	36c	RCD	2568.9	4	0.21	0.31	5.74					
P5'	120.6 W	35.80N	28	06	66	04	08	54.7	317	90	0	27a	ALQ	1279.7	7	0.53×10^{-1}	0.65×10^{-1}	5.12	5	5.1			McEvilly et. al. (1967)
P5'	"	"	"	"	"	"	"	"	"	"	"	27b	GOL	1394.8	7	0.32×10^{-1}	0.40×10^{-1}	4.93					
P5	120.5 W	35.95N	28	06	66	04	26	13.4	317	90	0	29	ATL	3307.6	4	1.75	2.94	6.53	4	5.5			McEvilly et. al. (1967)
P6	120.5 W	35.80N	29	06	66	19	53	24.1	317	90	0	28a	ALQ	1279.7	9	0.57×10^{-1}	0.70×10^{-1}	5.15	5	5.0			McEvilly et. al. (1967)
P6	"	"	"	"	"	"	"	"	"	"	"	28b	GOL	1394.8	9	0.40×10^{-1}	0.50×10^{-1}	5.02					
P7	121.64W	37.03N	16	11	64	02	46	42.2	126	70	0	37	GOL	1450.3	5	0.20×10^{-1}	0.25×10^{-1}	4.75	33	5.2	13	4.8	McEvilly (1967)
P8	125.84W	40.35N	16	09	65	04	10	17.4	108	90	0	38a	BOZ	1294.9	5	0.46×10^{-1}	0.56×10^{-1}	5.07	33	5.6			Bolt et. al. (1968)
												38b	MDS	2991.1	5	0.46×10^{-1}	0.74×10^{-1}	5.17					
P9	127.10W	41.50N	18	04	65	06	33	58.8	345	70	-90	39a	RCD	1978.3	55	0.76	1.03	6.21	20	5.6	17±2.0	5.4	Tobin & Sykes (1968) Bolt, et. al. (1968)
												39b	BOZ	1336.8	55	0.69	0.85	6.14					
P10	126.29W	42.93N	20	06	65	18	04	32.1	204	80	-30	40a	RCD	1865.0	33	0.15	0.20	5.57	33	5.6	0	5.5	Bolt, et. al. (1968)
												40b	BOZ	1205.5	33	0.15	0.18	5.52					
P11	126.60W	43.40N	01	10	64	11	00	50.0	170	55	-42	41a	BOZ	1228.8	55	0.13	0.16	5.48	33	6.0	33	5.1	Tobin & Sykes (1968) Bolt, et. al. (1968)
												41b	GOL	1812.9	44	0.93×10^{-1}	0.12	5.36					
P12	127.20W	43.35N	07	07	64	13	44	40.1	123	90	0	42	BOZ	1364.7	5	0.31×10^{-1}	0.38×10^{-1}	4.91	7	5.7	7	5.1	Bolt, et. al. (1968)
P13	129.50W	44.6 N	14	06	65	09	40	09.5	118	90	0	43	BOZ	1407.8	5	0.13	0.16	5.48	7	5.4	7	5.0	Bolt,et. al. (1968)
P14	130.05W	50.83N	31	03	64	09	01	28.9	165	90	0	44	GDH	4350.5	4	0.86	1.69	6.38	15	5.6	15	5.7	Tobin & Sykes (1968)

ϕ_o =112°, d=90°, s=4°.

The Rayleigh wave amplitude spectrum as observed at AFI (r =7956.4 km, oceanic) is shown in Figure 34. The path is unusually long and uniform over the east Pacific basin. The data indicate that the focal depth was about 3.5 km beneath the ocean floor and the seismic moment was 3.6 x 10^{25} dyne-cm. The listed USCGS depth was 20 km for this event. A pP-P time of 2.2 seconds was reported by CPO (Δ =25.3°) which would correspond to a depth of about 8 km.

3. Events P3 and P4: These were two neighboring events located in the southern portion of the Gulf of California, as shown in Figure 32. Their focal mechanisms as reported by Sykes (1968) were predominantly strike-slip faults. The pertinent source parameters were ϕ_o=133°, d=90°, s=0°.

The observed Rayleigh wave amplitude spectra at GOL (r =2069.6 km, continental) and at ALQ (r =1532.8 km, continental) for event P3 are shown in Figure 35a and Figure 35b, respectively. These two stations were almost on the same continental path. GOL was about 530 km farther away from the epicenter than ALQ. As shown in the Figures, the observed data at both stations indicate the same focal depth of 5 km. The seismic moment obtained at GOL is 0.16 x 10^{25} dyne-cm as compared to 0.13 x 10^{25} dyne-cm at ALQ. This close agreement suggests that the anomalous station effect including instrumental error and site condition may be negligible.

As for event P4, similar observations are made on Rayleigh

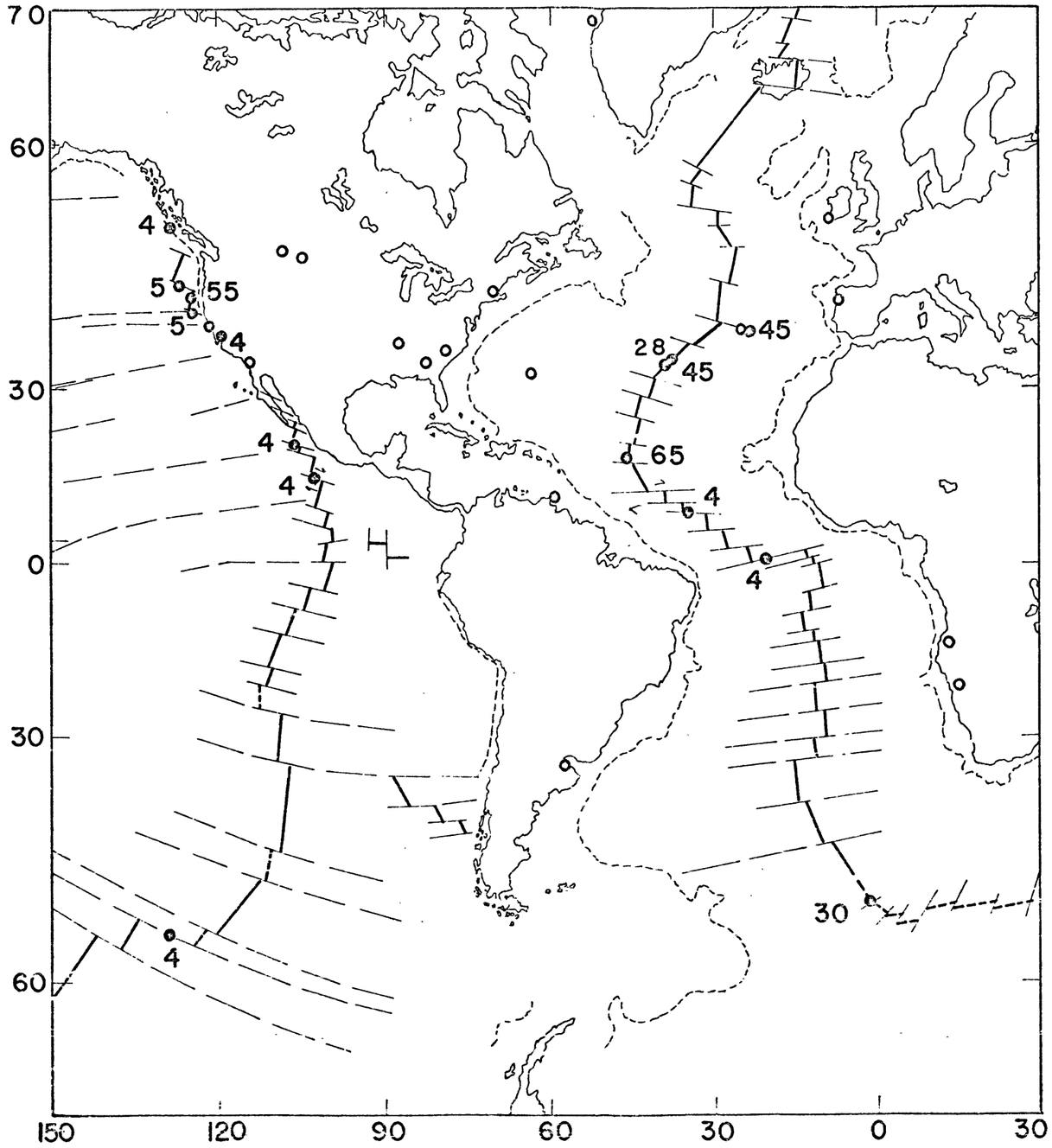

FIG. 32. Locations and focal depths of the earthquakes in the mid-Atlantic ridge and in the east Pacific rise, the Gulf of California, the San Andreas fault and the N.E. Pacific region.

FIG. 33. Rz from event P1 observed at WEL.

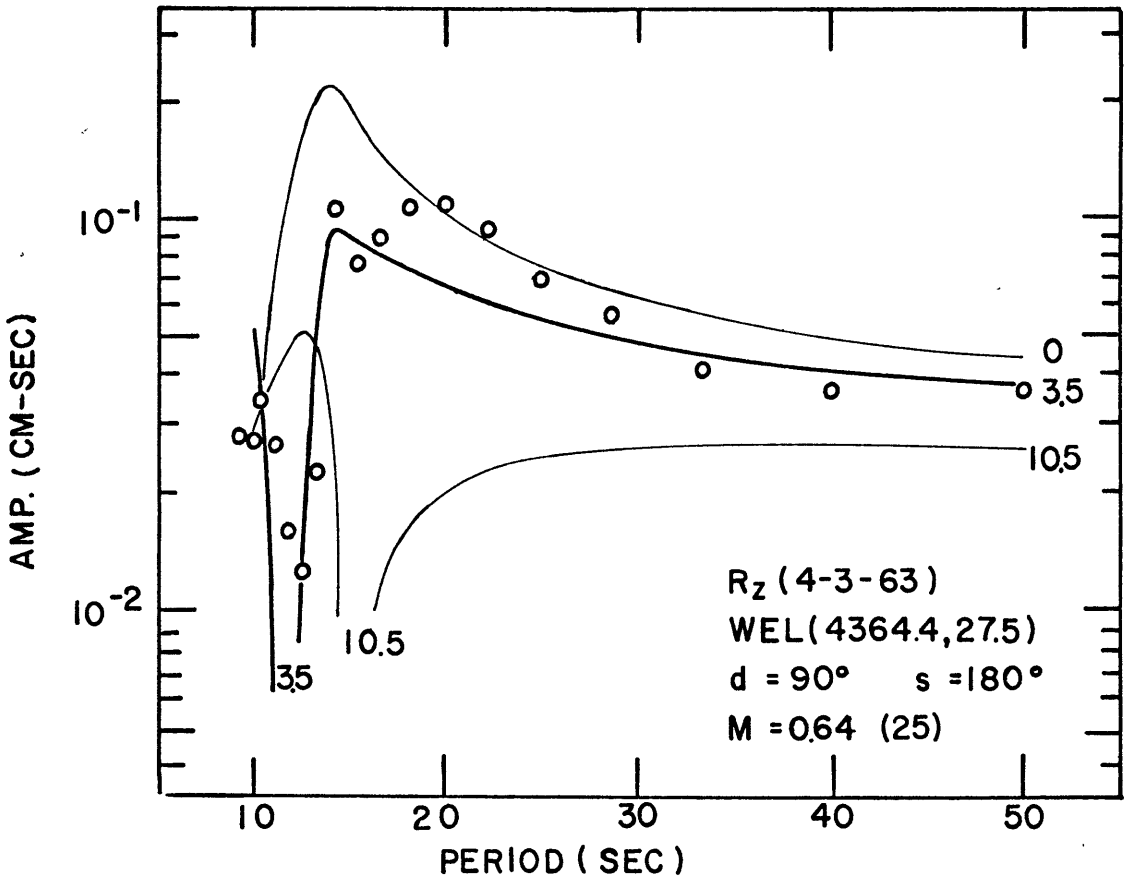

FIG. 34. Rz from event P2 observed at AFI.

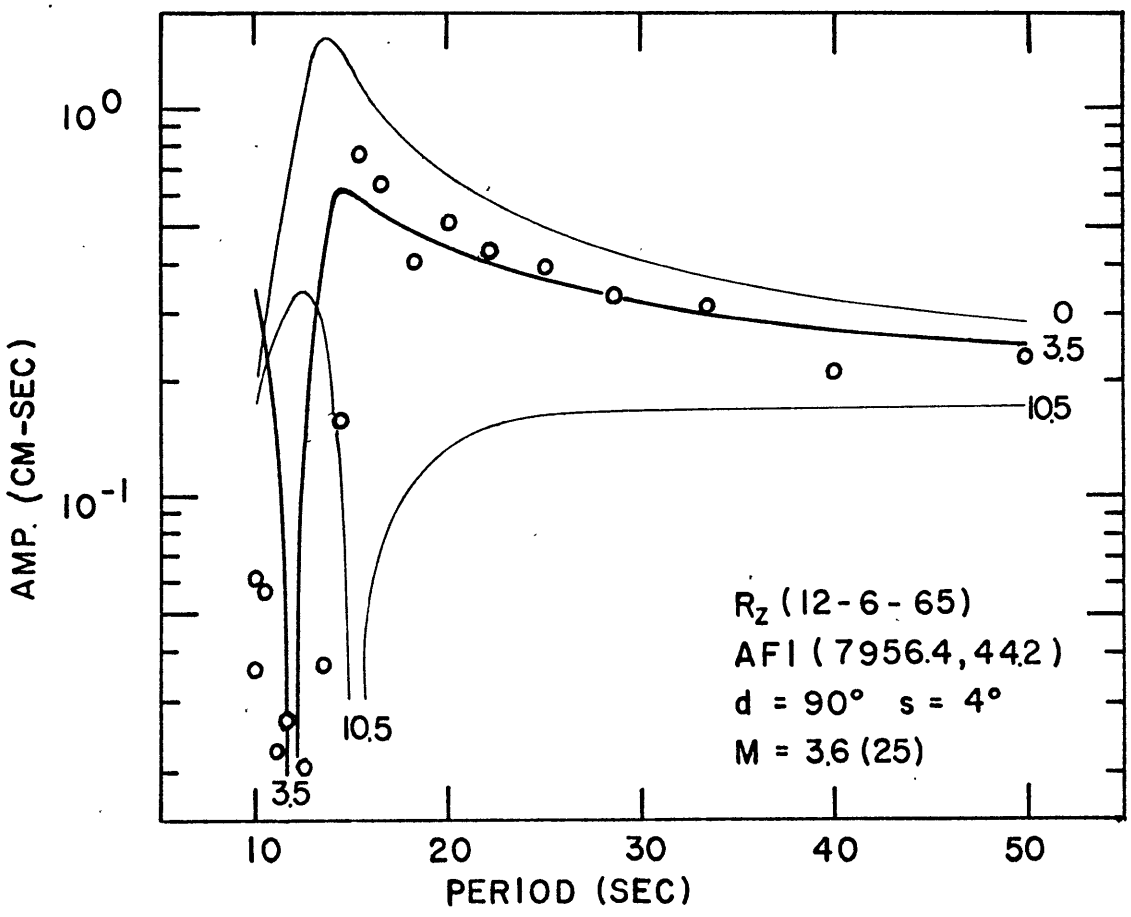

wave amplitude spectrum at three stations lying almost on the same continental path. These stations are ALQ (r=1520.4 km), GOL (r=2057.1 km) and RCD (r=2568.9 km). The spectra obtained at each station are shown in Figure 36a, Figure 36b and Figure 36c, respectively. All data indicate that the focal depth of this event is about 5 km, the same as that of event P3. The uncorrected seismic moment obtained from these three stations ranges from 0.20 to 0.26 x 10^{25} dyne-cm which show no systematic decrease with epicentral distance over about 1000 km segment.

From the above observations we must conclude that if the fault plane solutions obtained by Sykes (1968) are correct, the focal depths of event P3 and event P4 must be about 5 km. The USCGS reported that the depth of event P3 was 53 km and that of event P4 was 58 km. These values are too large to explain the observed Rayleigh wave amplitude spectra which contain strong short period components as shown in Figure 35a through Figure 36c. In order to resolve this large discrepancy between the focal depths determined by the surface wave method and those given by the USCGS, attempts were made to search for additional evidence such as the pP-P times. Unfornately, we were not able to find any useful data.

4. Events P5', P5, P6: These were the foreshock, the main shock and the largest aftershock of the Parkfield, California sequence of June 28, 1966. Details on these events have already been discussed in the preceding chapter.

5. Event P7: This earthquake occurred on November 16, 1964

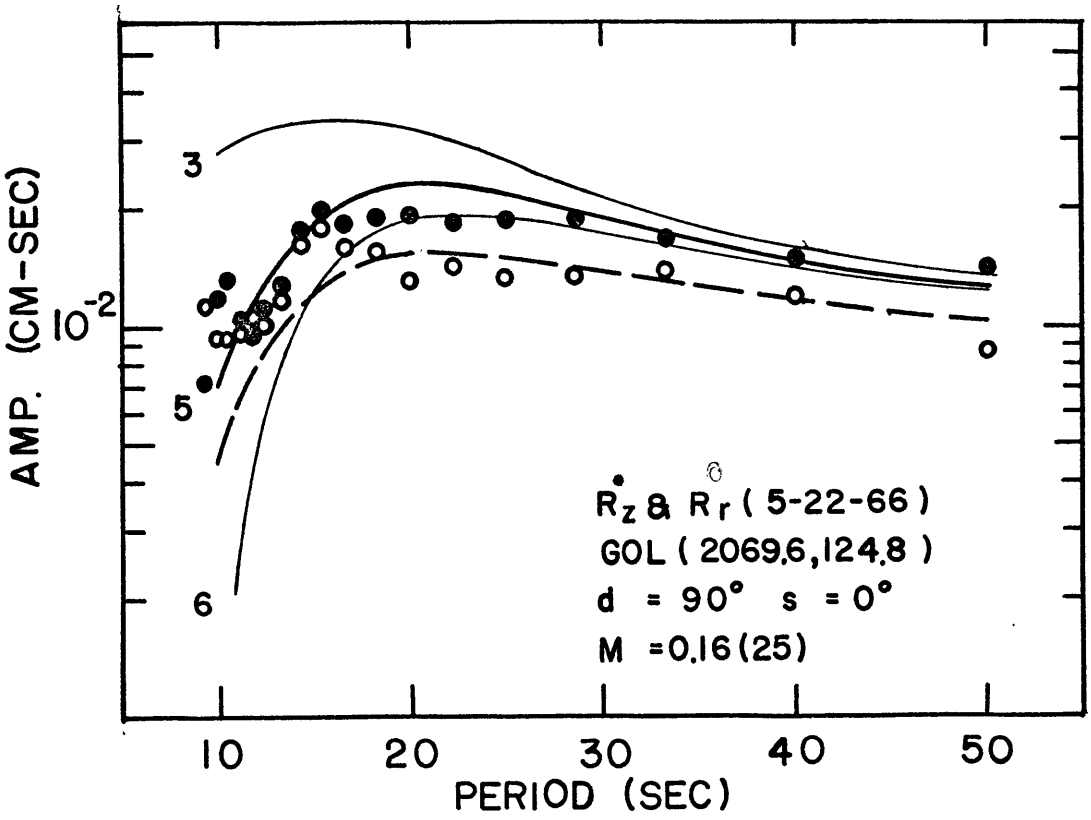

FIG. 35a. Rayleigh wave amplitude spectrum from event P3 observed at GOL.

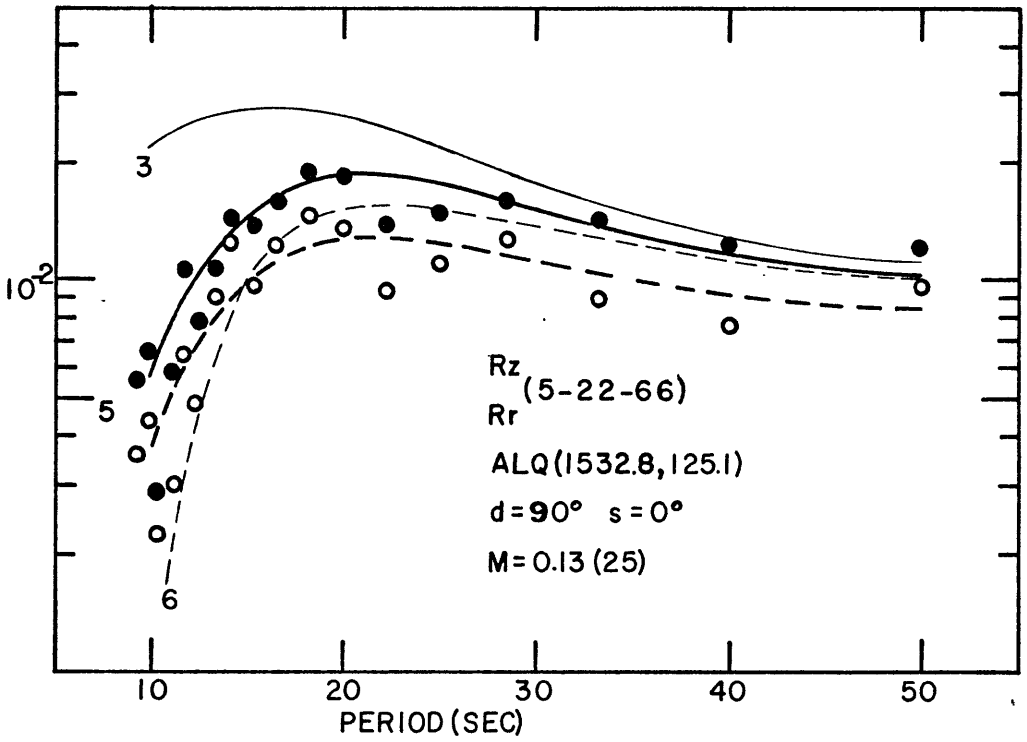

FIG. 35b. Rayleigh wave amplitude spectrum observed at ALQ from event P3.

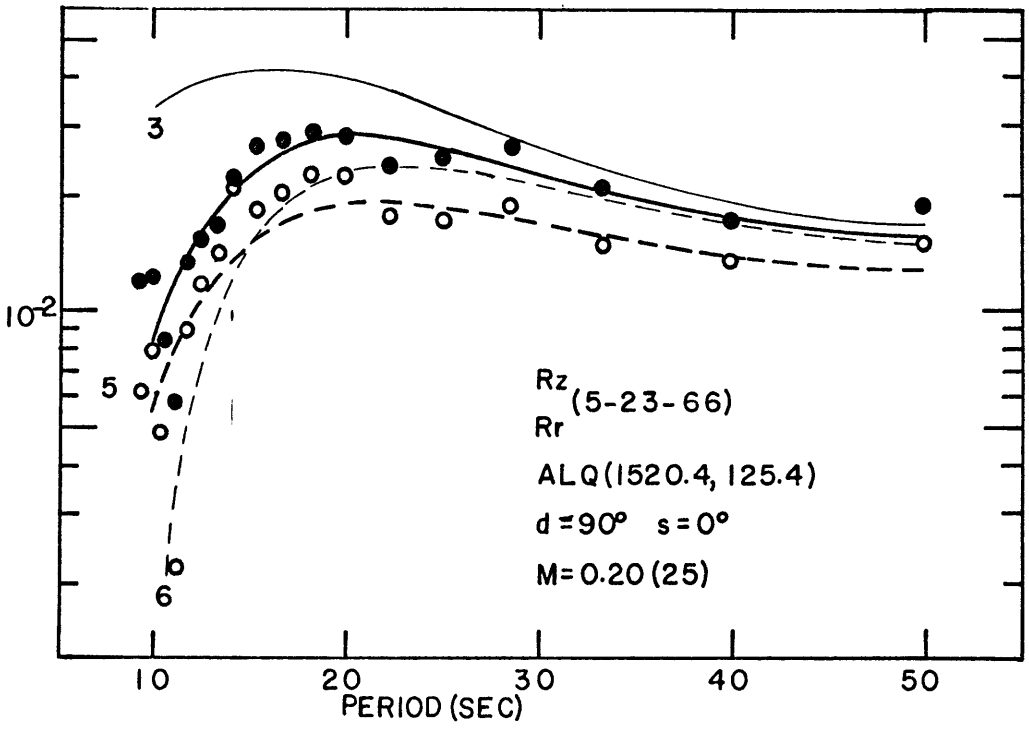

FIG. 36a. Rayleigh wave amplitude spectrum from event P4 observed at ALQ.

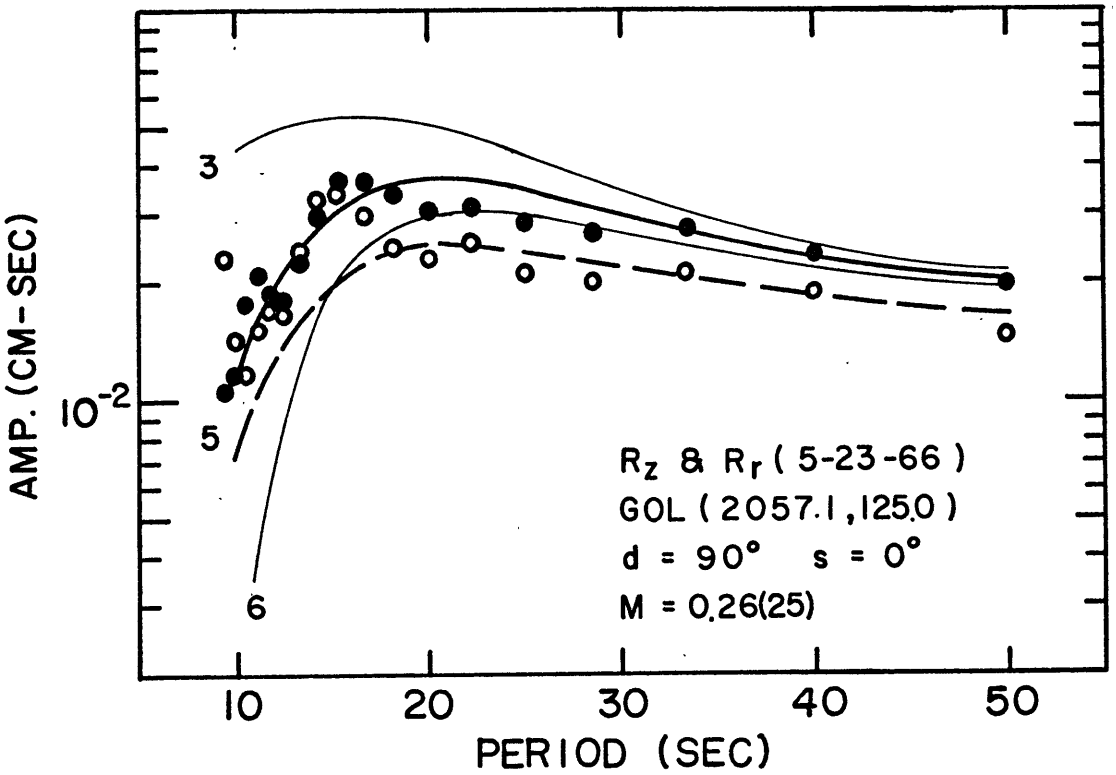

FIG. 36b. Rayleigh wave amplitude spectrum from event P4 observed at GOL.

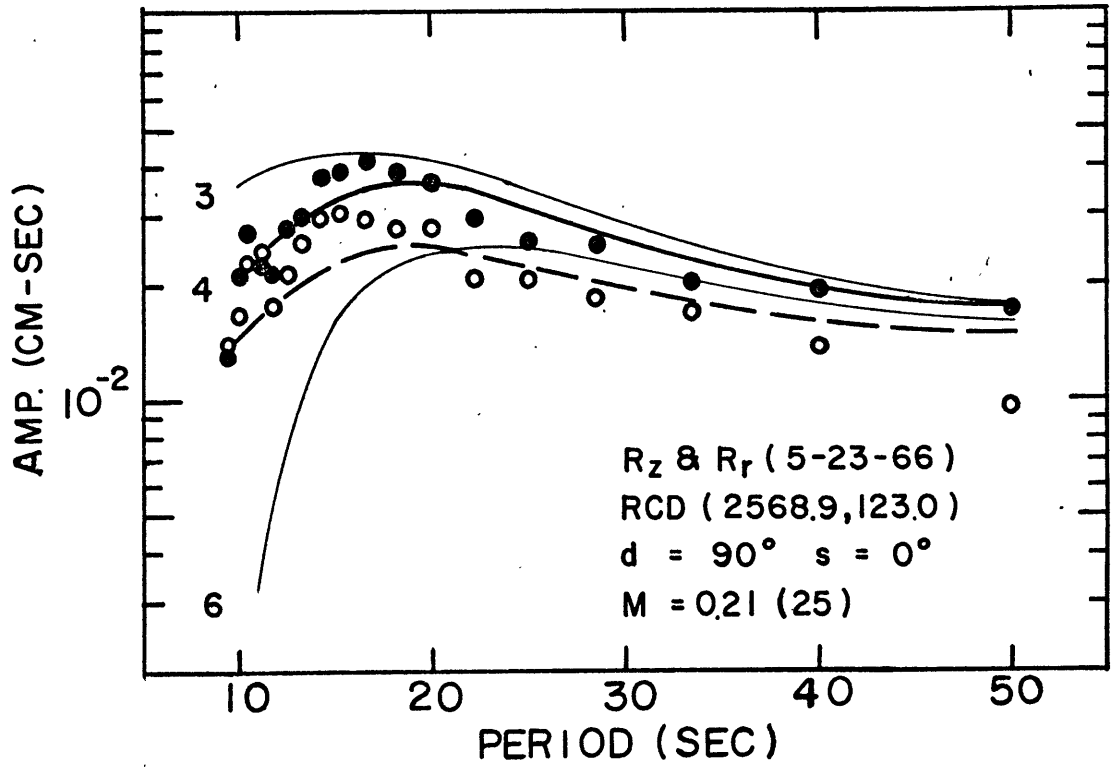

FIG. 36c. Rayleigh wave amplitude spectrum observed at RCD from event P4.

near the Sargent fault in Central California. The focal mechanism of this event was studied by McEvilly (1967). The pertinent source parameters derived from his fault-plane solution for the event are ϕ_o=126°, d=70°, s=0°. He also used three stations surrounding the epicenter at distances less than 40 km to obtain a focal depth of about 14 km for the earthquake with an uncertainty of a few kilometers.

The Rayleigh wave amplitude spectrum observed at GOL (r = 1450.3 km) is shown in Figure 37. The path is entirely continental from the source to GOL. The data are consistent with a focal depth of about 5 km and a seismic moment of 0.20×10^{24} dyne-cm.

The focal depth of 5km determined from the observed Rayleigh wave amplitude spectrum is shallower than that of 14 km determined by McEvilly (1967) or that of 13 km determined by ISC. Based upon the data shown in Figure 37, we believe that this discrepancy is significant. This discrepancy may be explained either by the finiteness effect in the dip direction or by some unknown biasing effect on P travel times.

6. Event P8: This was an event located on the western portion of the Gorda escarpment. Its fault plane solution as obtained by Bolt et. al. (1968) indicated that right-lateral motion with near-vertical nodal planes occurred. Accordingly we have ϕ_o=108°, d=90°and s=0° for this event.

Two measurements on Rayleigh waves from this event are made. The amplitude spectrum observed at BOZ (r =1294.9 km) is shown in Figure 38a and that at MDS (r =2991.1 km) in Figure

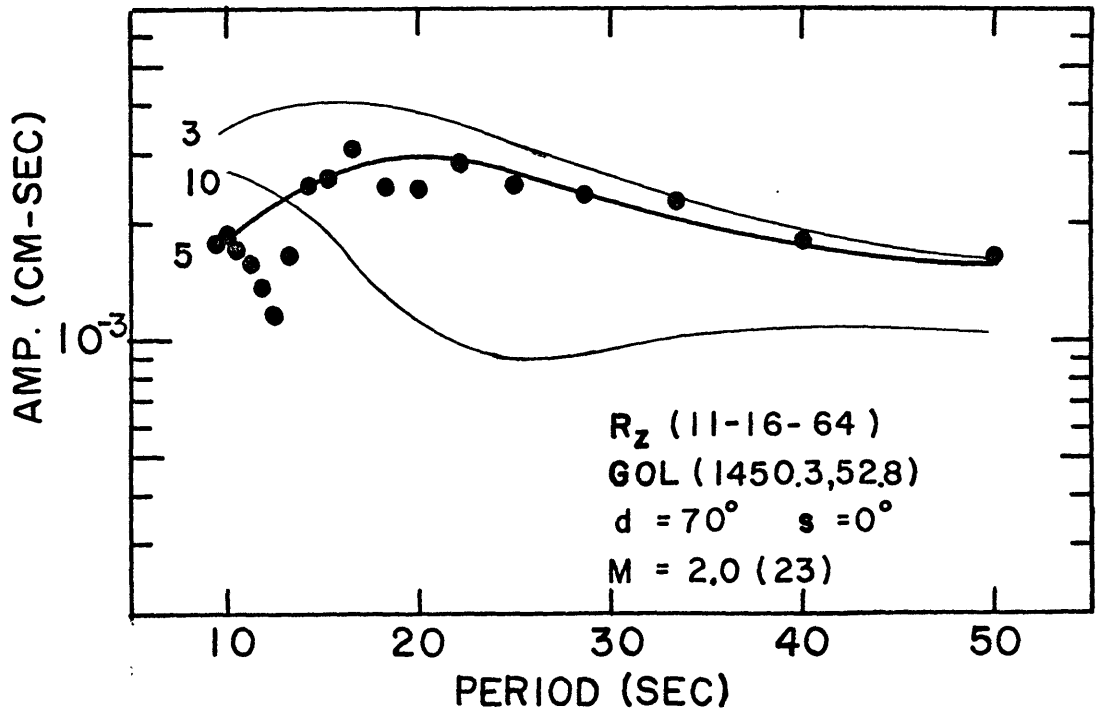

FIG. 37. Rz from event P7 observed at GOL.

38b. Both paths are continental. The one leading to BOZ was lying very near to the lobe direction of radiation. The data at BOZ are consistent with a focal depth of about 5 km and a seismic moment of about 0.46×10^{24} dyne-cm. The path to MDS was at another direction. The Rayleigh wave amplitude spectrum at MDS is also consistent with a focal depth of about 5 km and a seismic moment of 0.46×10^{24} dyne-cm. This close agreement of the focal depth and the seismic moment of the same event between observations from two stations at different distance and azimuth suggests that neglect of correction for attenuation, in fact, will not cause serious errors for path as long as 3000 km. The USCGS depth was 33 km for this event. CPO ($\Delta = 31.8^{\circ}$) reported a pP-P time of 7.9 seconds which would correspond to a depth of about 29 km.

7. Event P9: This event was located about midway along the Gorda ridge. Its focal mechanism was studied independently by Tobin and Sykes (1968) and by Bolt et. al. (1968). They all concluded that the earthquake was caused by a dip-slip fault, and the principal axis of tension was oriented essentially east west nearly perpendicular to the ridge. Following the solution of Bolt et. al. (1968), we have $\phi_o = 345^{\circ}$, $d = 70^{\circ}$, $s = 90^{\circ}$.

Two observations of Rayleigh waves are made, one at RCD (r=1978.3 km) and at BOZ (r=1336.8 km). The two paths were all continental and lay near to each other. The data observed at RCD are shown in Figure 39a and at BOZ in Figure 39b. The data from RCD are consistent with a focal depth of about 55 km and a seismic moment of 0.76×10^{25} dyne-cm. Unfortunately,

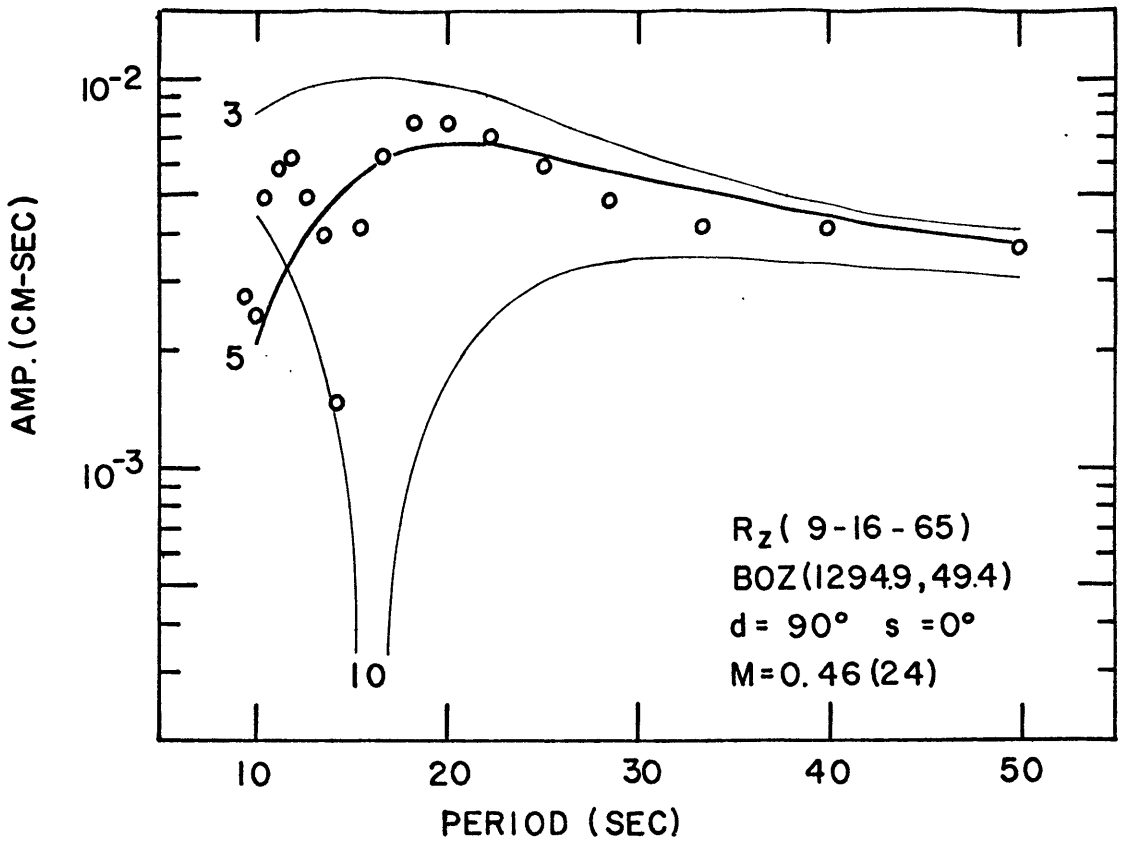

FIG. 38a. Rz from event P8 observed at BOZ.

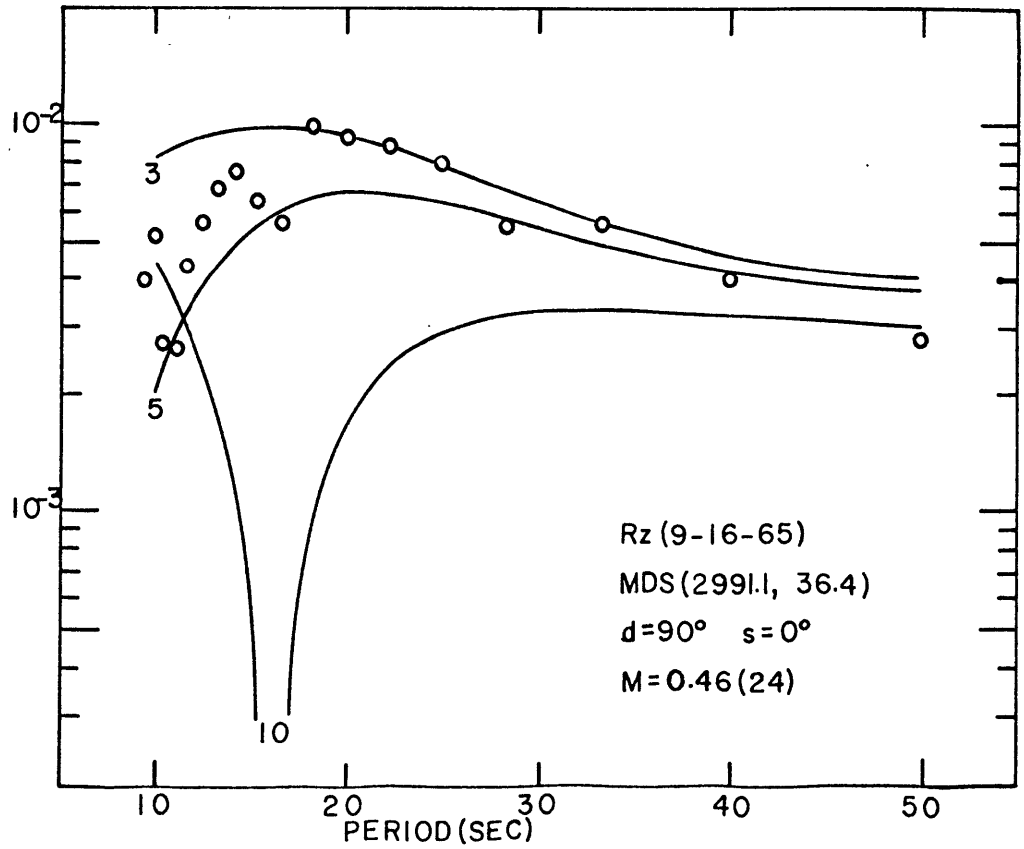

FIG. 38b. Rz from event P8 observed at MDS.

FIG. 39a. Rayleigh waves from event P9 observed at RCD.

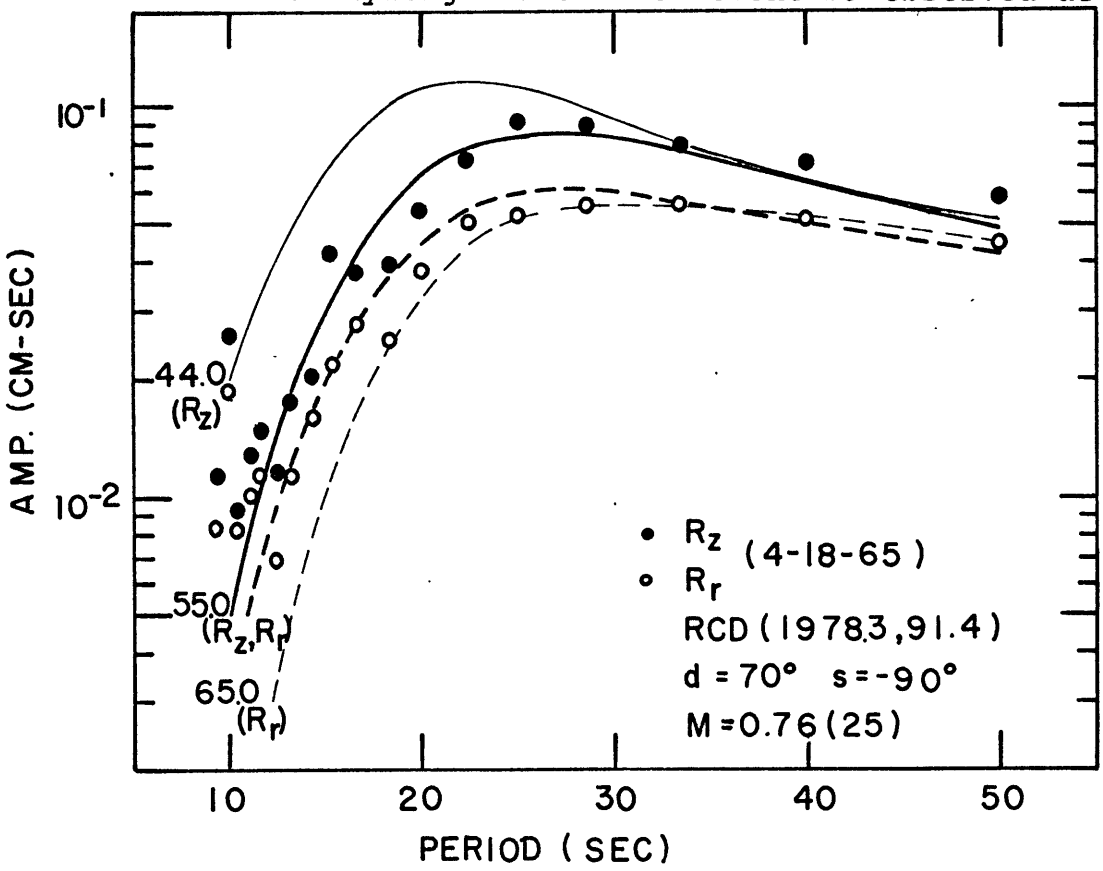

FIG. 39b. Rr from event P9 observed at BOZ.

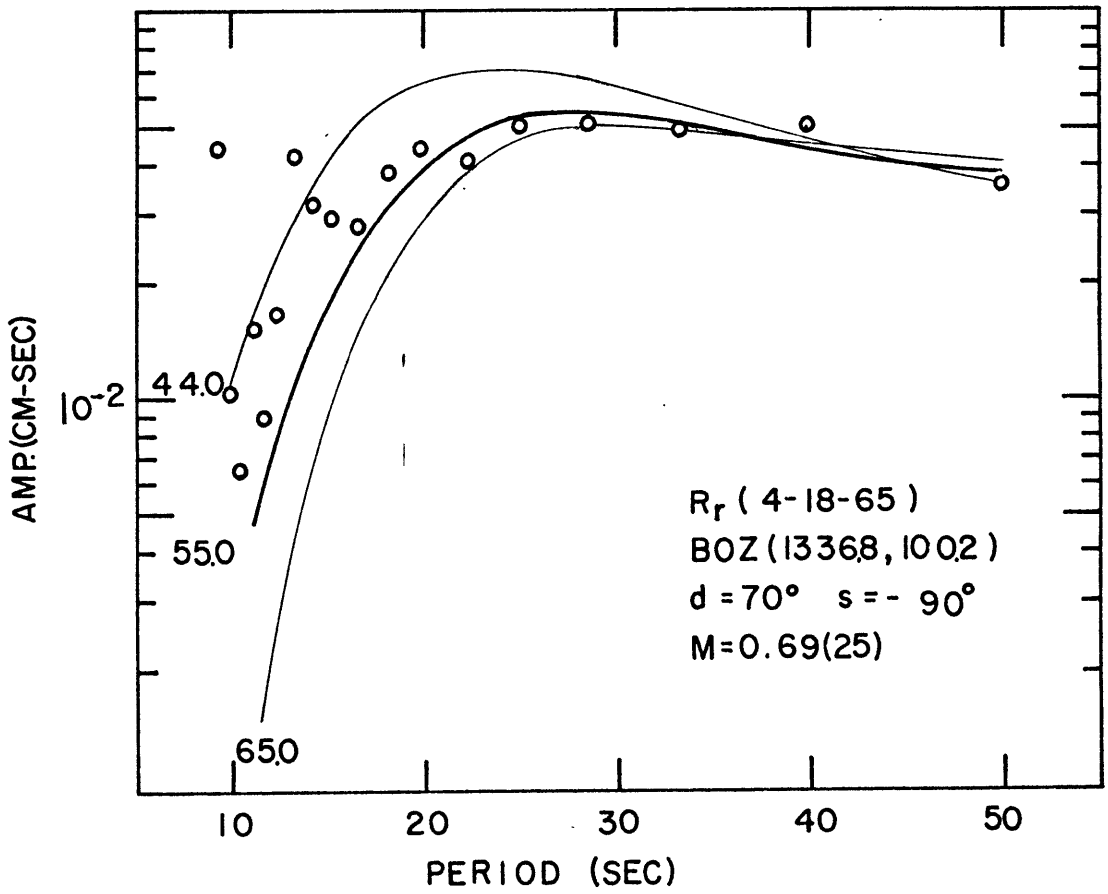

the LPZ record of this event was not available at BOZ. The spectrum of the radial component is consistent with a focal depth of about 55 km and a seismic moment of 0.69×10^{25} dyne-cm. Again the agreement between the results obtained at these two stations is quite good.

The USCGS depth for the event was 20 km. The ISC depth was essentially the same as the USCGS depth. The pP-P time reported by CPO ($\Delta = 32.8^{\circ}$) was 11.3 sec which corresponds to a focal depth of about 45mk. This value roughly agrees with our depth of 55 km.

8. Event P10: This was an event located near the intersection of the Blanco fracture zone and the Gorda ridge. According to the fault plane solution given by Tobin and Sykes (1968), the source parameters for this event are $\phi_o = 204^{\circ}$, $d = 80^{\circ}$ and $s = -30^{\circ}$.

We have observed Rayleigh wave amplitude spectrum at RCD (r=1865.0 km) and at BOZ (r=1205.5 km). The data from RCD are shown in Figure 40a and from BOZ in Figure 40b. Data from both stations all suggest the same focal depth of about 33 km and the same seismic moment of 0.15×10^{25} dyne-cm. The USCGS depth was 33 km. CPO ($\Delta = 32.2^{\circ}$) reported a pP-P time of 7.3 seconds for the event which corresponds to a depth of about 26 km.

9. Event P11: This event was located near the intersection of the Gorda ridge and the Blanco fracture zone. The fault plane solution obtained by Bolt et. al. is consistent with normal faulting due to a principal tension axis across the Gorda

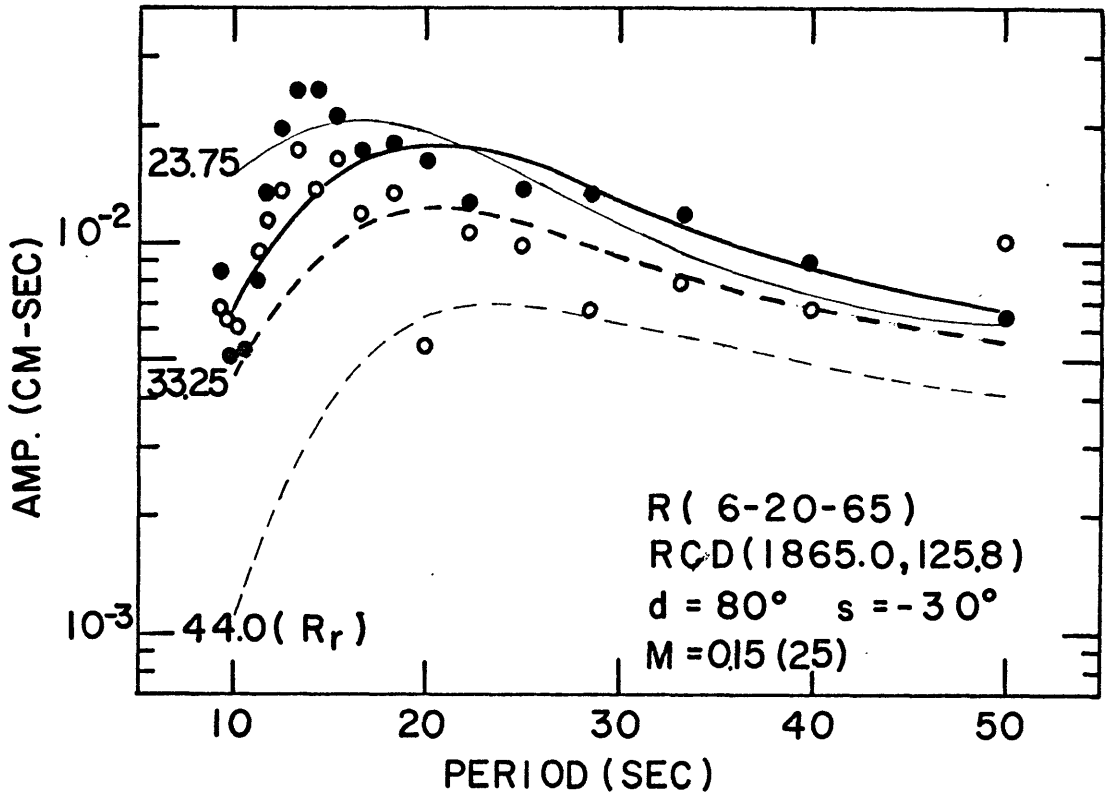

FIG. 4oa. Rayleigh waves from event P10 observed at RCD.

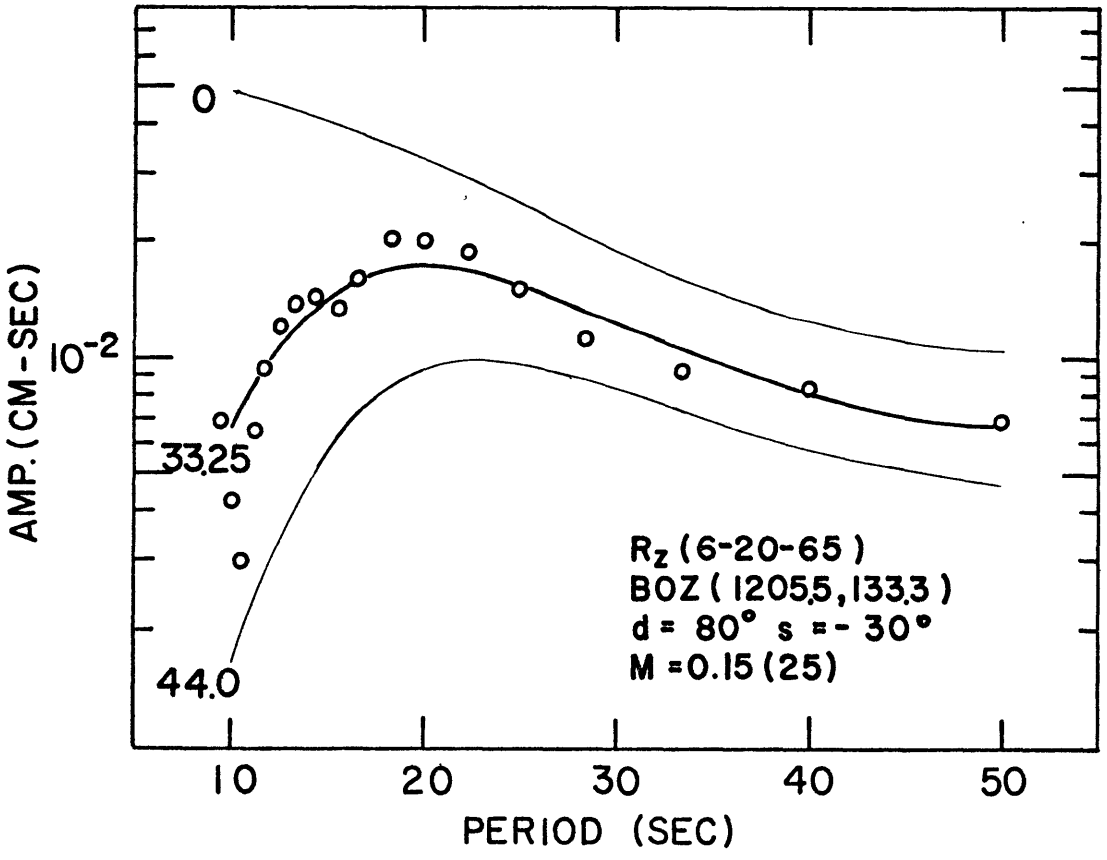

FIG. 40b. Rz from event P10 observed at BOZ.

ridge trend. The fault parameters derived from it are ϕ_o=170°, d=55° and s=-41.5°.

The Rayleigh wave amplitude spectrum from this event observed at BOZ (r=1228.8 km, continental) is shown in Figure 41a and the Love wave amplitude spectrum observed at GOL (r= 1812.9 km, continental) is shown in Figure 41b.

The Rayleigh wave data at BOZ are consistent with a focal depth of about 55 km and a seismic moment of 0.13 x 10^{25} dyne-cm. The Love wave data at GOL are consistent with a focal depth of about 44 km and a seismic moment of about 0.93 x 10^{24} dyne-cm. The seismic moment obtained at one station agree well with that obtained at another. The focal depth of this event is between 44 to 55 km from our observations. The USCGS depth was 33 km.

10. Event P12: This is an event located on the Blanco fracture zone. According to Tobin and Sykes (1968), it is a right-lateral strike-slip fault. The fault plane parameters are ϕ_o=123°, d=90° and s=0°.

A measurement of Rayleigh wave amplitude spectrum is made at BOZ (r=1261.4 km, continental). As shown in Figure 42, the data are consitent with a focal depth of 5 km and a seismic moment of 0.67 x 10^{24} dyne-cm. The USCGS depth was 7 km.

11. Event P13: This event was located on the Blanco fracture zone. According to the fault plane solution obtained by Bolt et. al. (1968), the event was a right-lateral strike-slip fault with ϕ_o =118°, d=90° and s=0°.

The Rayleigh wave amplitude spectrum observed at BOZ

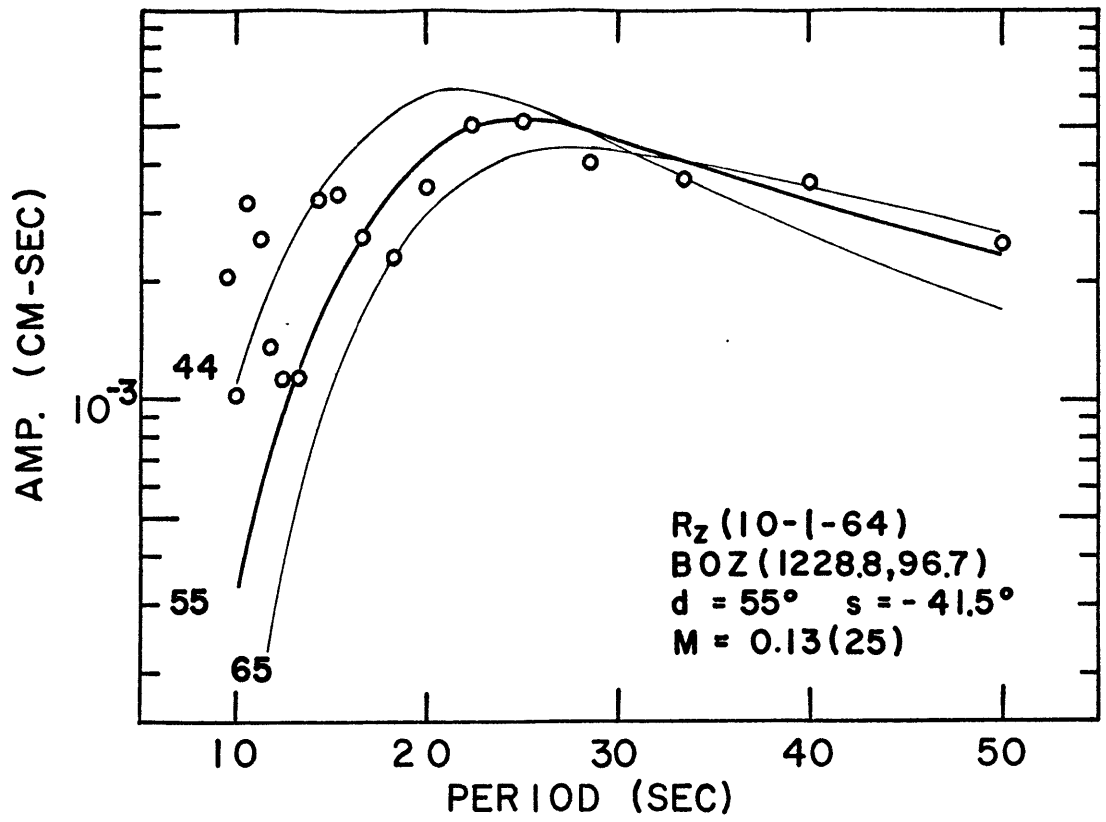

FIG. 41a. Rz from event P11 observed at BOZ.

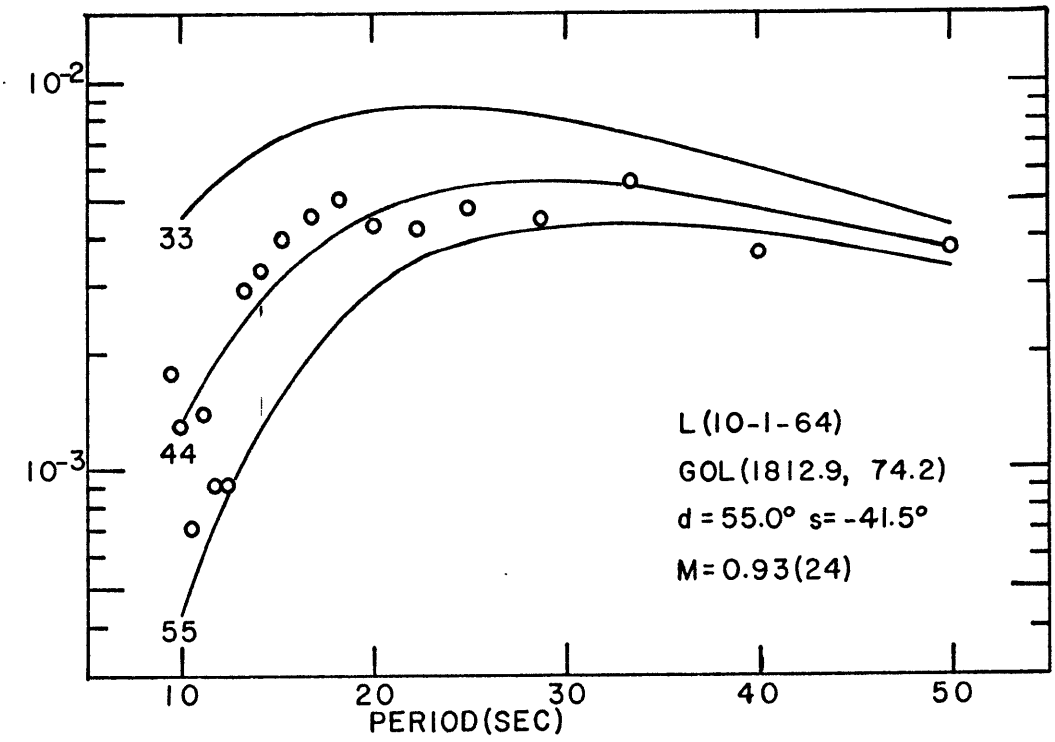

FIG. 41b. Love waves from event P11 observed at GOL.

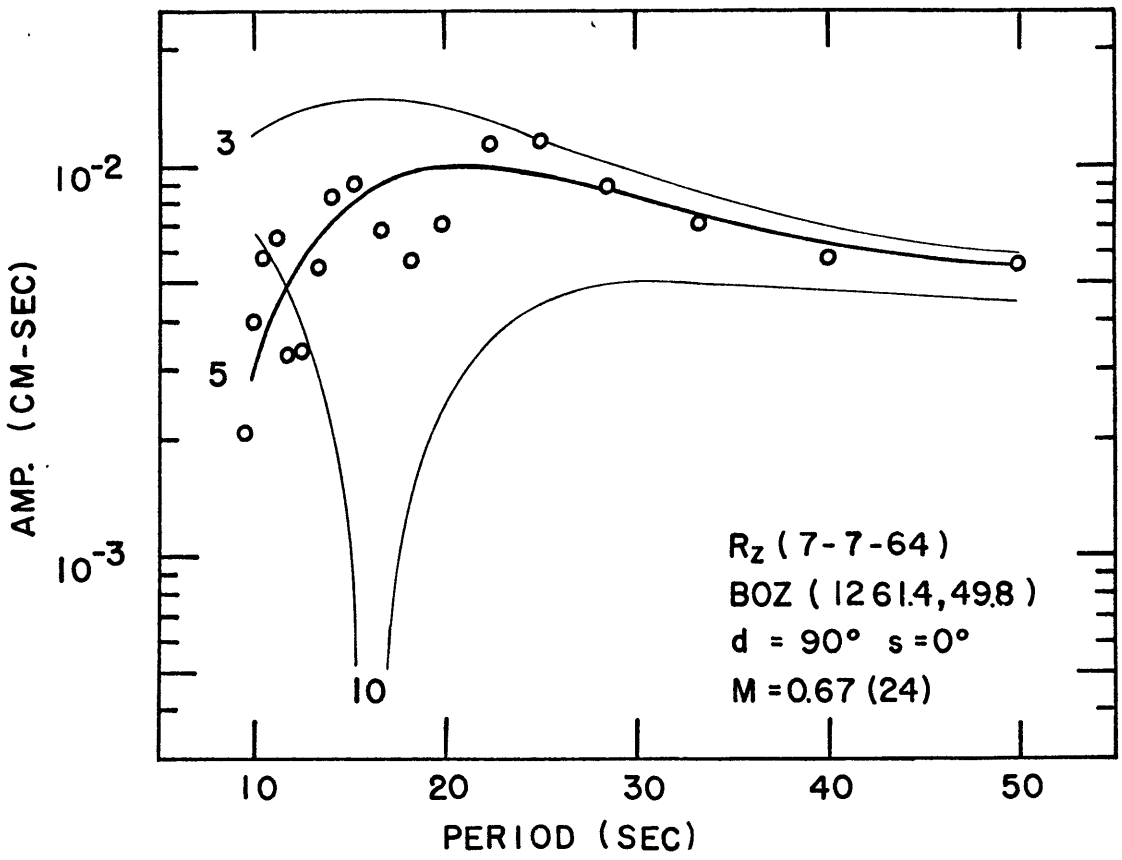

FIG. 42. Rz from event P12 observed at BOZ.

(r =1407.8 km,continental) is shown in Figure 43. The data are consistent with a focal depth of about 5 km and a seismic moment of 0.13 x 10^{15} dyne-cm. Both the USCGS depth and the ISC depth were 7 km for this event.

12. Event P14: This event was located on the Queen Charlotte Islands fault. According to the fault plane solution obtained by Tobin and Sykes (1968), the event was characterized by right-lateral strike-slip motion on a steeply dipping plane. The fault plane solution suggests that ϕ_o =165°, d=90° and s=0° for the event.

The Rayleigh wave amplitude spectrum observed at GDH (r = 4350.5 km) are shown in Figure 44. The data are consistent with a focal depth of about 4 km and a seismic moment of 0.86 x10^{25} dyne-cm. The USCGS depth was 15 km for the same event.

In summary, we have studied 15 events located on the east Pacific rise and its northward extension through the Gulf of California, San Andreas fault, Mendocino fracture zone, Gorda ridge, Blanco fracture zone up to Queen Charlotte Islands fault. As shown in Figure 32, our results indicate that the focal depths of 12 right-lateral strike-slip earthquakes in all segments of the system are, without exceptions, extremely shallow —— less than 10 km. On the contrary, the focal depths of the remaining three events on the Gorda ridge which were Characterized by dip-slip motion range from about 33 km to 55 km. These are noticeably deeper than the focal depths of those strike-slip earthquakes just mentioned.

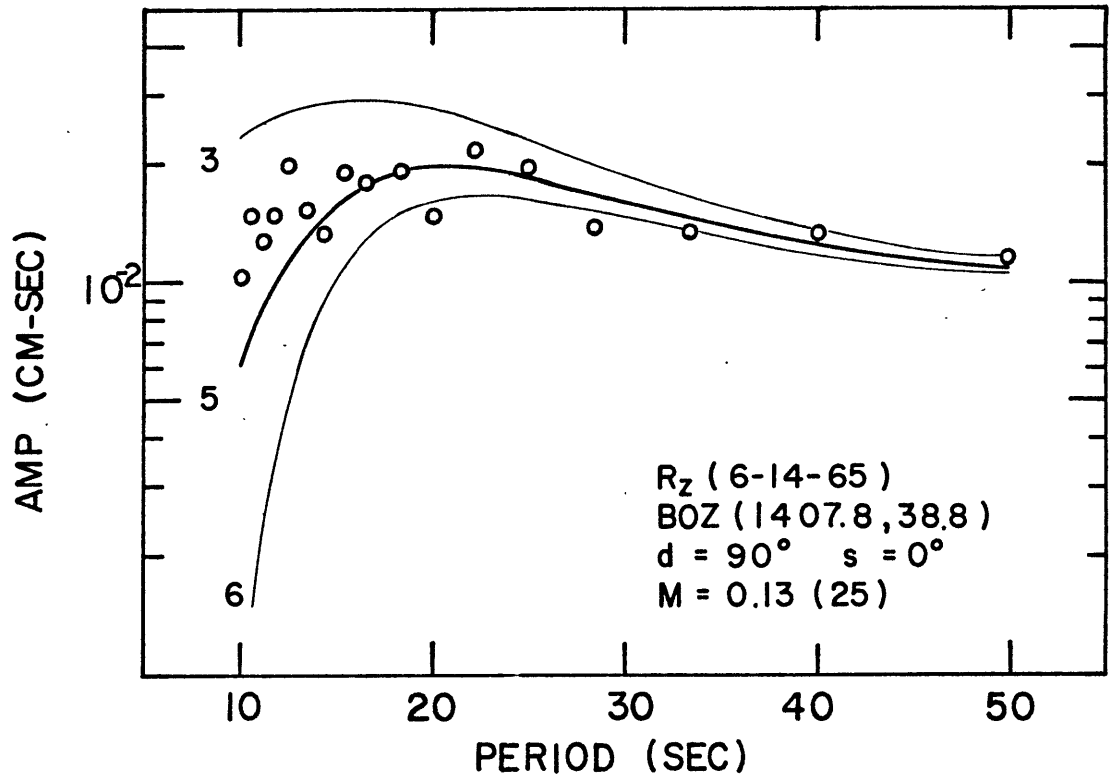

FIG. 43. Rz from event P13 observed at BOZ.

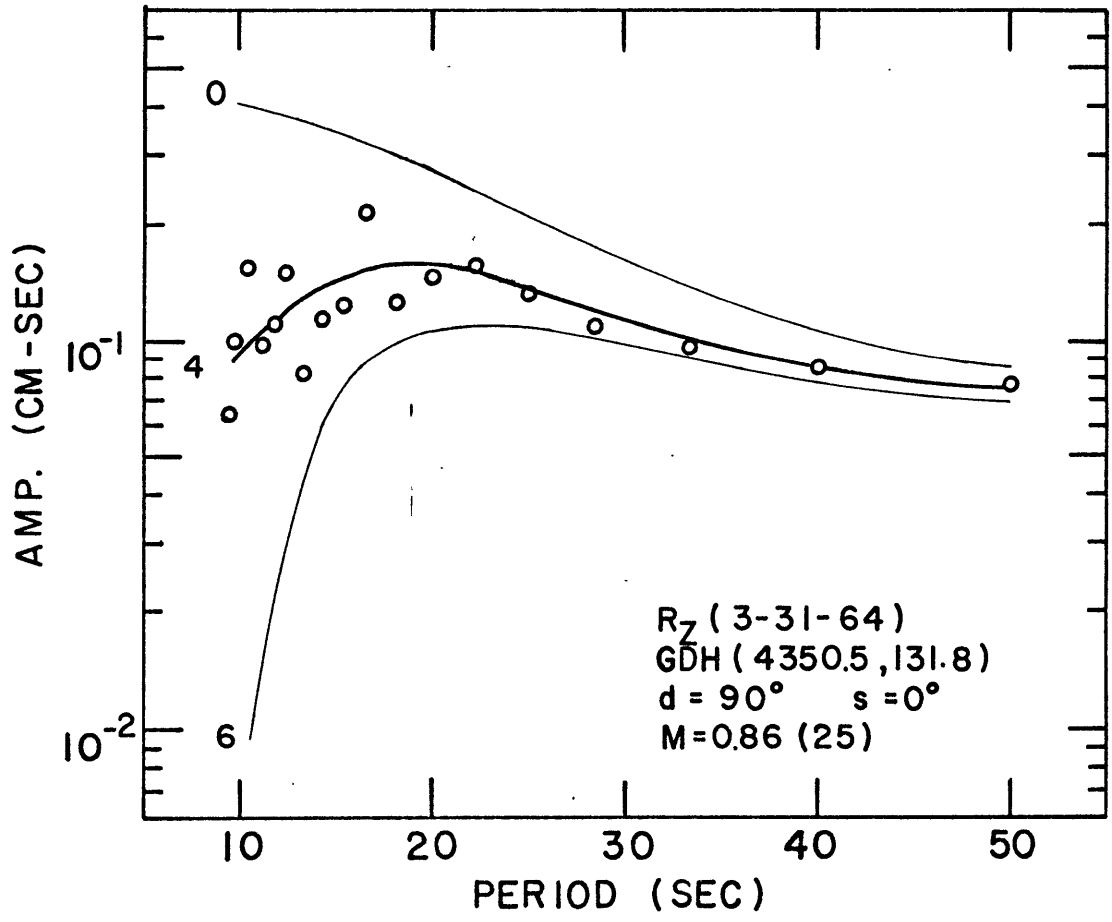

FIG. 44. Rz from event P14 observed at GDH.

The uniformity of depth distribution of the strike-slip earthquakes throughout the entire zone may be regarded as an evidence supporting Wilson's (1965a, 1965b) concept for the northern extension of the East Pacific rise to the Queen Charlotte Islands fault. The focal depth of 55 km of the earthquakes on the Gorda ridge suggests that the lithosphere there extends at least to that depth.

The seismic moment data of these earthquakes shall be treated later in this Chapter.

4.2 Earthquakes on the mid-Atlanic ridge

We have studied eight earthquakes located on the mid-Atlantic ridge from 38°N to 54°S. The fault plane solutions were obtained by Sykes (1967, 1968) and Banghar and Sykes (1969). Three of these eight events were characterized by predominantly strike-slip motion and the remaining five were characterized by predominantly dip-slip motion. The locations and other pertinent data of these earthquake are given in Table 4.

1. Event A1: This was an event located on the Azores-Gibraltar ridge. The fault plane solution by Banghar and Sykes (1969) indicated nearly equal components of dip-slip and strike-slip motion. The corresponding fault parameters are ϕ_o=112°, d=110°, and s=39°.

The Rayleigh wave amplitude spectrum observed at PTO (r =1451.6 km) is shown in Figure 45. The path was an oceanic one with about 5 km water. The data in Figure 45 are consistent with a focal depth of about 45 km. The seismic moment is obtained as 0.71 x 10^{25} dyne-cm. The USCGS depth was restricted at 33 km.

2. Event A2: This was an event on the mid-Atlantic ridge in the North Atlantic. The fault plane solution for the event (Sykes, 1967) is characterized by a large component of dip-slip motion on the plane that strikes approximately parallel to the axis of the ridge. The corresponding fault parameters are ϕ_o=49°, d=123° and s=50°.

TABLE 4 Earthquakes in the mid-Atlantic ridge

Event	Long.	Lat.	Date Day Mo Yr	Time Hr Min Sec	Strike	Dip	Slip	Figure number	Station code	Epidistance (km)	Focal depth (km)	M(uncorrected) (10^{25} dyne-cm)	M(corrected) (10^{25} dyne-cm)	Magnitude Ms	USCGS Depth (km)	USCGS m_b	ISC Depth (km)	ISC m_b	Reference
A1	24.8W	37.5N	04 07 66	12 15 28.1	112	110	39	45	PTO	1451.6	45	0.71	0.91	6.16	33	5.5			Banghar & Sykes (1969)
A2	41.0W	32.3N	06 08 62	01 35 27.7	49	123	50	46	BEC	2222.6	28	1.00	1.45	6.34	48	6.2			Sykes (1967)
A3	41.5W	31.0N	16 11 65	15 24 40.8	353	121	54	47	WES	2911.4	45	3.20	5.22	6.68	17	6.0			Sykes (1967)
A4	46.8W	16.0N	02 06 65	23 40 22.5	334	121	54	48	TRN	1687.9	65	2.10	2.79	6.52	33	5.8	27 ± 2.3	5.8	Sykes (1968)
A5	37.4W	7.8N	17 11 63	00 47 58.8	98	86	0	49	PDA	3519.8	4	10.00	18.00	6.94	33	5.9			Sykes (1967)
A6	20.0W	0.5S	16 08 65	12 36 24.3	263	70	6	50	SDB	4017.8	4	1.40	2.76	6.52	35	6.2			Sykes (1968)
A7	18.7W	0.2S	15 11 65	11 18 46.8	267	70	6	51	WIN	4601.1	4	0.94	2.03	6.43	26	5.8			Sykes (1967)
A8	2.4W	54.3S	14 12 64	01 59 05.6	82	110	15	52	LPA	4751.7	28	3.60	7.99	6.77	33	6.0	33	5.7	Banghar & Sykes (1969)

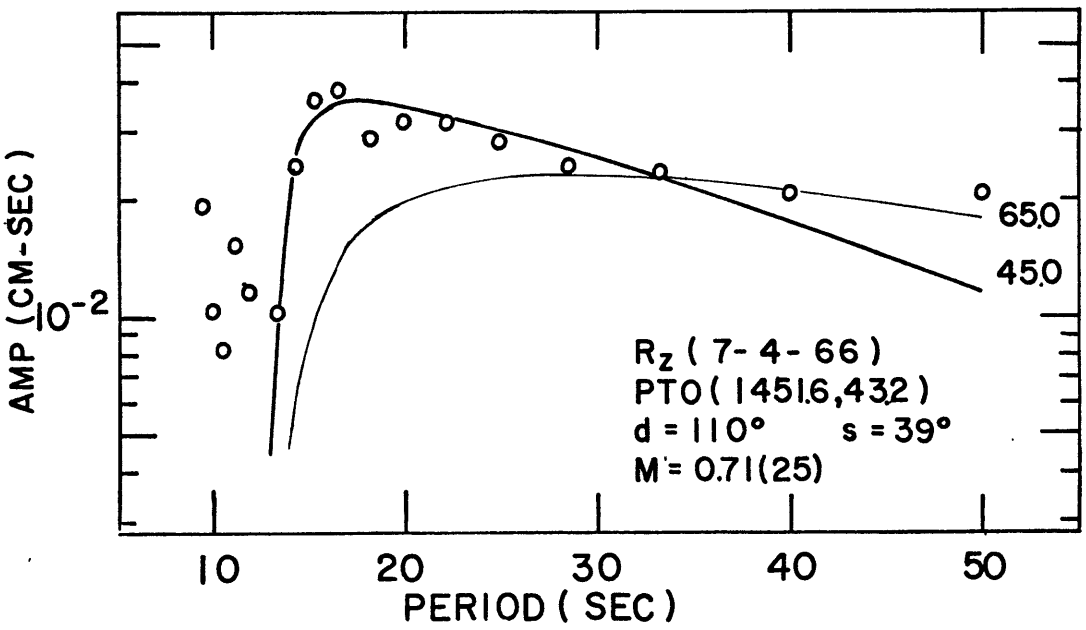

FIG. 45. Rz from event A1 observed at PTO.

The Rayleigh wave amplitude spectrum observed at BEC (r=2222.6 km) is shown in Figure 46. The path was entirely oceanic. The focal depth of 27.5 km gives a satisficatory agreement between observed and theoretical spectra. The seismic moment is obtained as 1.0×10^{25} dyne-cm.

The USCGS reported 48 km for the focal depth of this event.

3. Event A3: This was also an event located on the mid-Atlantic ridge about 1.3 degree south of event A2. The fault plane solution given by Sykes (1967) was also characterized by a large component of dip-slip motion on the nodal plane striking approximately parallel to the axis of the ridge.

The amplitude spectrum of Rayleigh waves observed at WES (r=2911.4 km) is shown in Figure 47. The path lies in the western Atlantic basin covered by 5 km water. Only a small portion of the path near the station was continental. A focal depth of about 45 km and a seismic moment of about 3.2×10^{25} dyne-cm give a good agreement between observed and theoretical spectra. The USCGS reported a focal depth of 17 km for this event.

4. Event A4: This was an event located on the mid-Atlantic ridge at about 16°N. Focal mechanism study by Sykes (1968) revealed that the earthquake was characterized by a large component of dip-slip motion. The details of the fault plane solution were not given. Since it was similar to that of event A3, its fault parameters should not differ much from those for event A3. Thus, we adopted the dip and the slip angles

FIG. 46. Rz from event A2 observed at BEC.

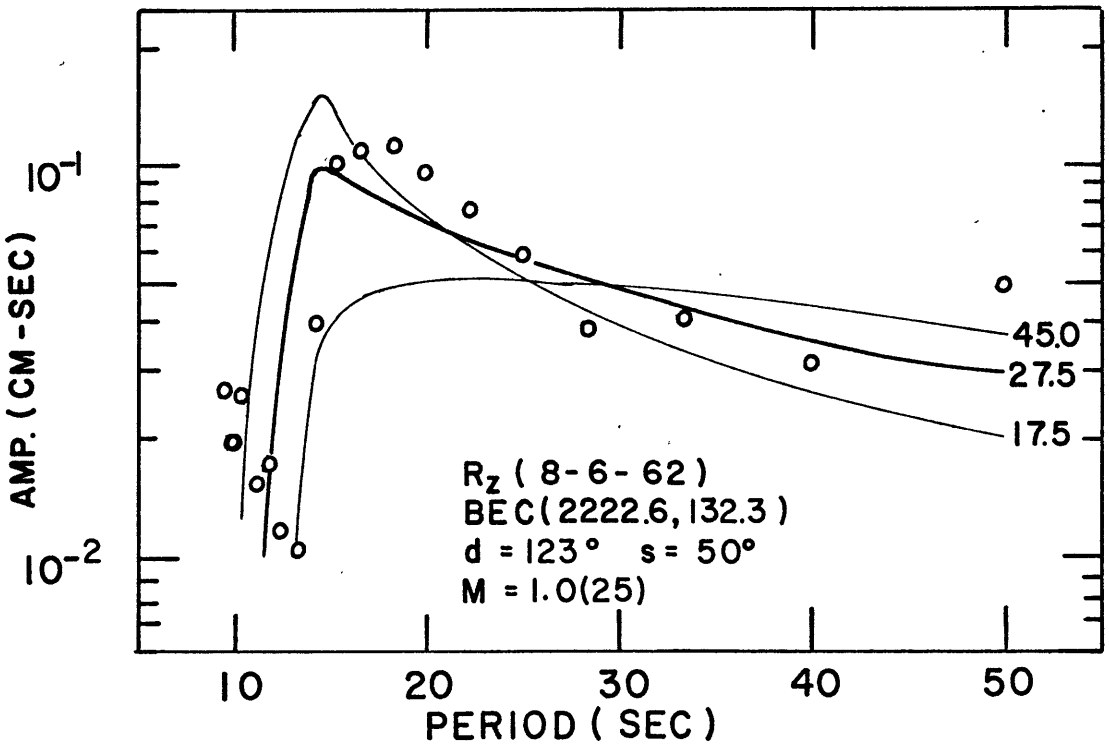

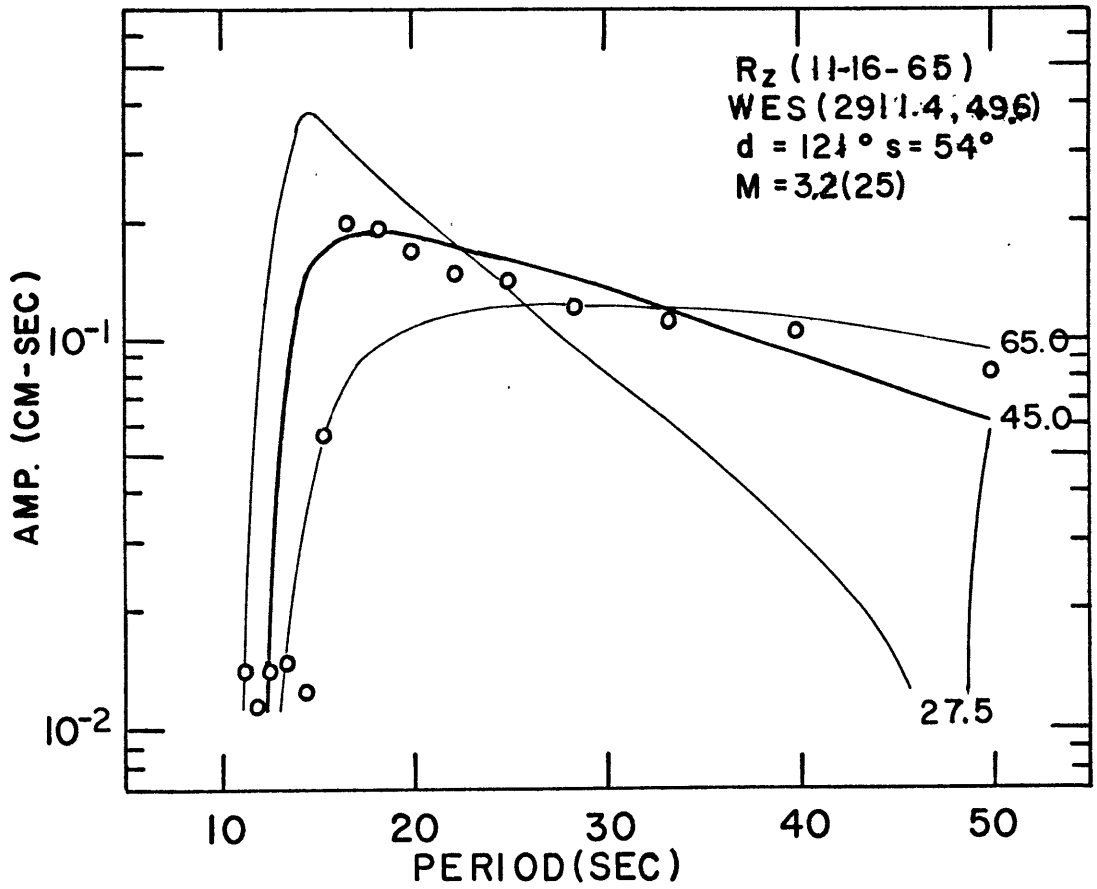

FIG. 47. Rz from event A3 observed at WES.

of event A3 for this event, i.e. d=121° and s=53.5°. As shown in Chapter 2, if the difference between the true solution and this adopted one is within 15° in the dip or the slip or both, our results here shall not be seriously affected. The strike is taken as ϕ_o=334° as indicated by Sykes (1968).

Figure 48 shows the Rayleigh wave amplitude spectrum observed at TRN (r=1687.9 km). Although the spectrum varys considerably, it is still consistent with a focal depth of about 65 km. The seismic moment is determined as 0.21 x 10^{26} dyne-cm. The USCGS depth for this event was 33 km.

5. Event A5: This event was located on a large fracture zone associated with the mid-Atlantic ridge near 8°N. According to Sykes (1967), its fault plane solution was characterized by predominantly strike-slip motion on a steeply dipping plane. The fault parameters are ϕ_o=98°, d=86° and s=0°.

The Rayleigh wave amplitude spectrum observed at PDA (r=3519.8 km) is shown in Figure 49. The path was relatively long, and oceanic and lies in the nodal direction of radiation. We choose such a marginal station because of the small number of records available for this event. It is seen from the data that the focal depth is about 3.5 km. The seismic moment is determined as 1.00 x 10^{26} dyne-cm which may have a large uncertainty due to the proximity of the path to the nodal direction. The USCGS depth was 33 km for this event.

6. Events A6 and A7: These were two events located on the Romanche fracture zone in the equatorial Atlantic. According

FIG. 48. Rz from event A4 observed at TRN.

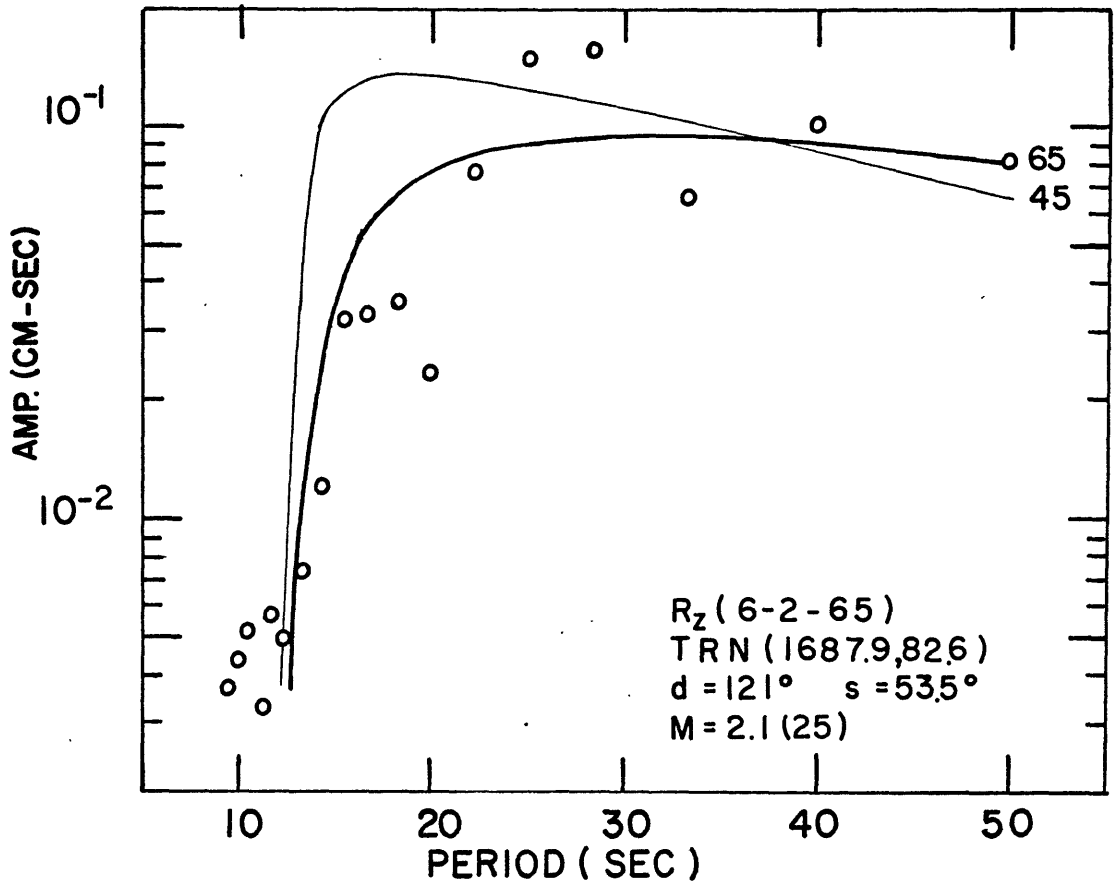

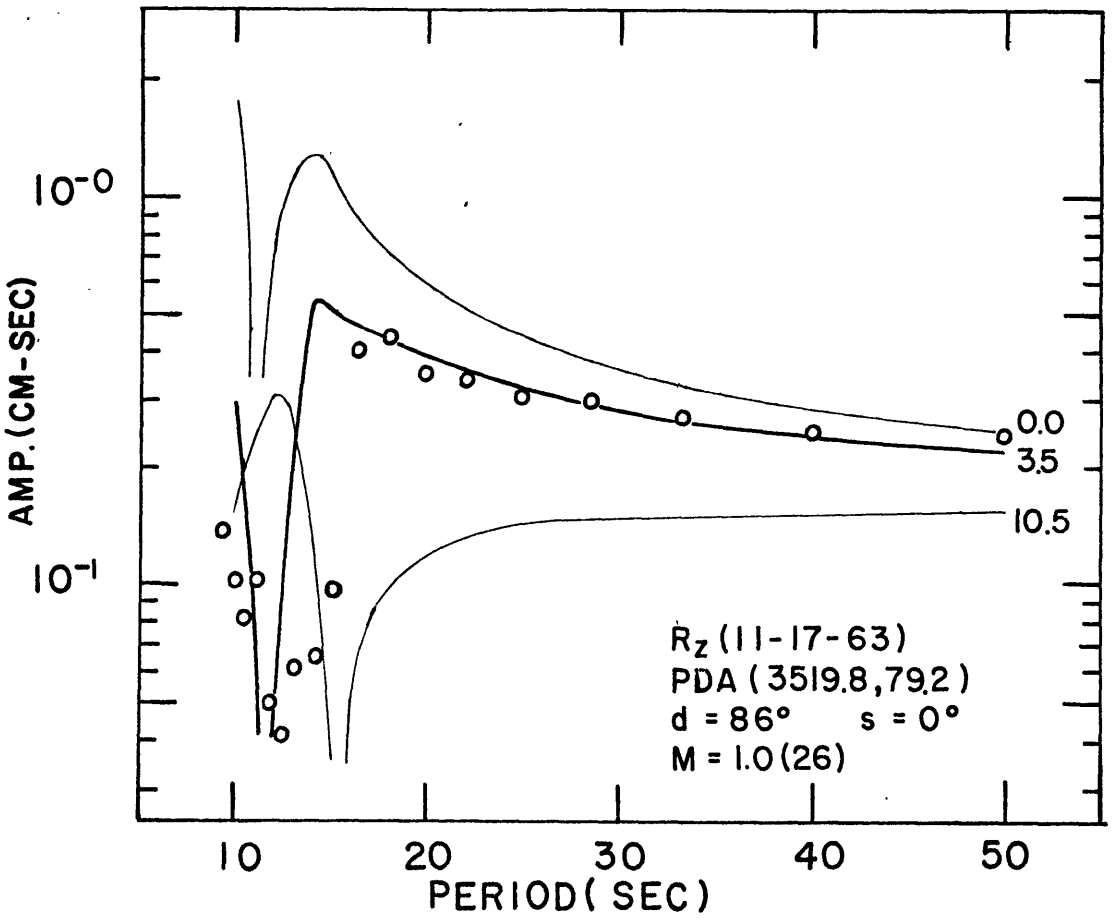

FIG. 49. Rz from event A5 observed at PDA.

to Sykes (1967, 1968) the fault plane solutions for both events were characterized by predominantly strike-slip motion on a steeply dipping plane. The corresponding dip and slip angles are $d=70^{\circ}$ and $s=6^{\circ}$, respectively. For event A6, $\phi_o=263^{\circ}$ and for event A7, $\phi_o=267^{\circ}$.

The Rayleigh wave amplitude spectrum from event A6 observed at SDB ($r=4017.8$ km) is shown in Figure 50. The spectrum for event A7 observed at WIN ($r=4601.1$ km) is shown in Figure 51. Both these two paths were predominantly oceanic.

The data in Figure 50 suggests that the focal depth of event A6 was shallow, probably 3.5 km. The seismic moment is determined as 0.14×10^{26} dyne-cm which may contain a large uncertainty due to the proximity of the path to the nodes of the radiation pattern. The USCGS depth was reported as 35 km.

The data in Figure 51 are consistent with a focal depth of 3.5 km and a seismic moment of 0.94×10^{25} dyne-cm for event A7. Although the observed spectra at this station have rather large fluctuations, they roughly agree with the theoretical curve with a focal depth of 3.5 km. The USCGS depth was 26 km. UPP reported a focal depth of 30 km for this event using pP-P times.

7. Event A8: This was an event located in the South Atlantic ridge near Bouvet Island which is a complex region. According to Banghar and Sykes (1969), the fault plane solution for this event was characterized by a large component of strike-slip motion. The corresponding fault parameters are

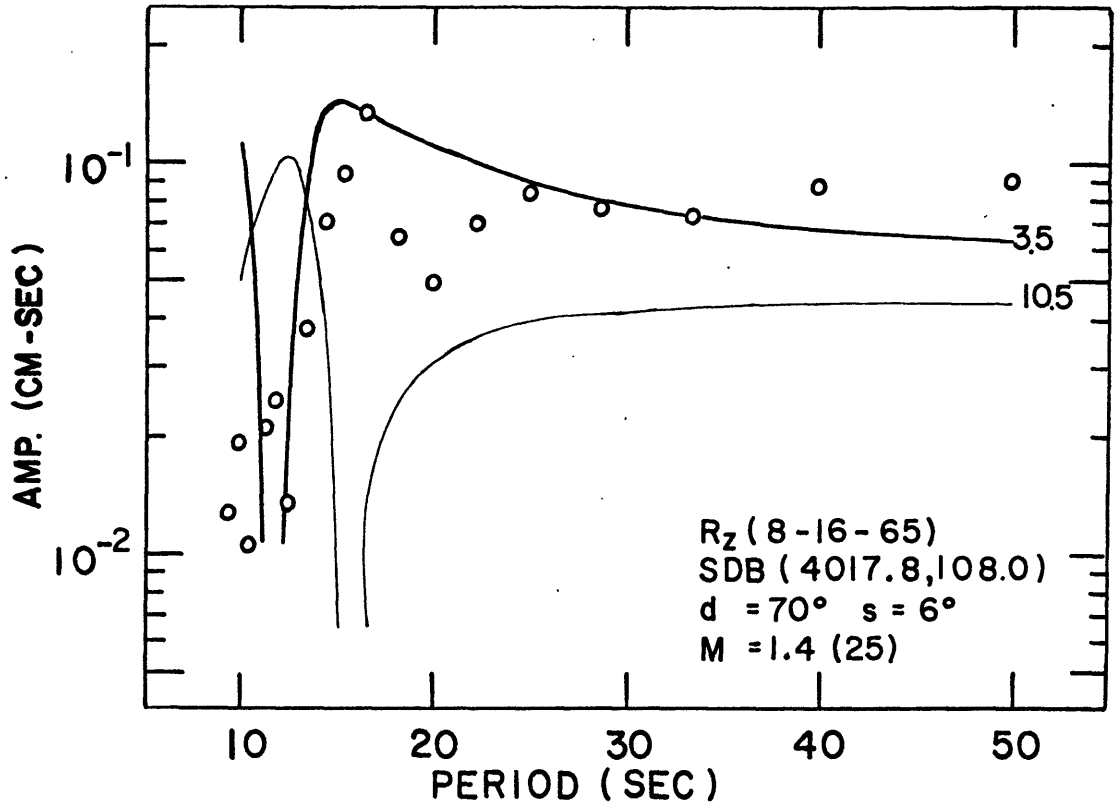

FIG. 5o. Rz from event A6 observed at SDB.

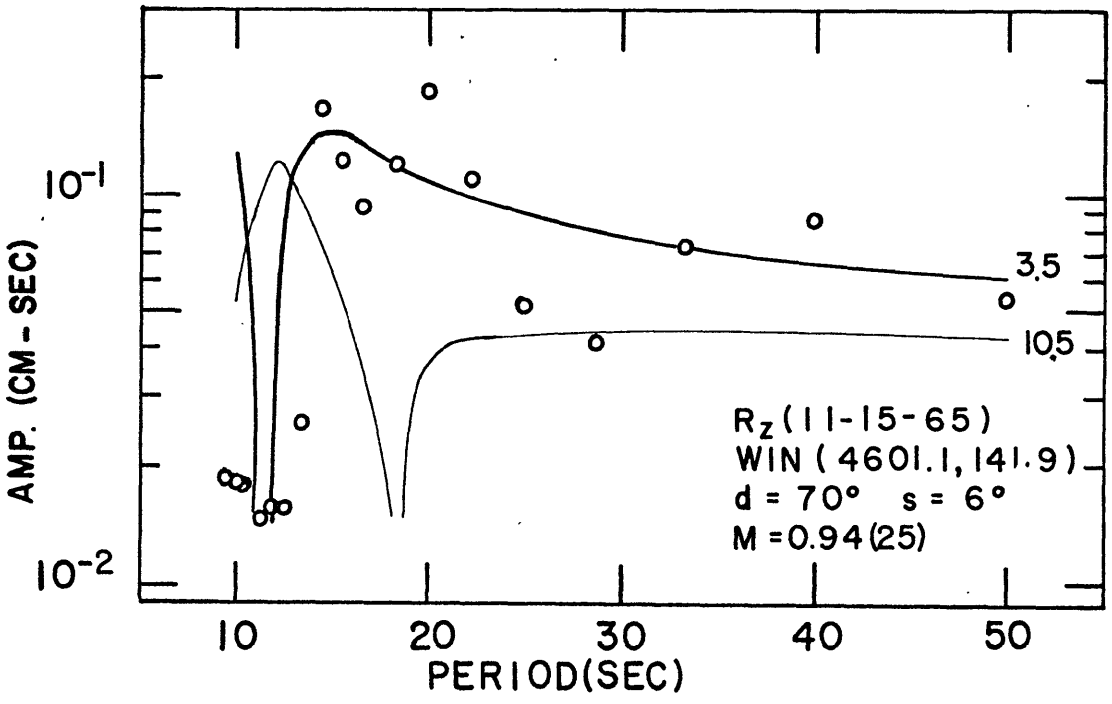

FIG. 51. Rz from event A7 observed at WIN.

$\phi_o = 82^o$, d=110^o and s=15^o.

The Rayleigh wave amplitude spectrum from this event observed at LPA (r=4751.7 km) is shown in Figure 52. LPA was the nearest station with available records. The whole path was oceanic.

The data in Figure 52 are roughly consistent with a focal depth of about 27.5 km and a seismic moment of 0.36 x 10^{26} dyne-cm. Both the USCGS and the ISC gave 33 km for the focal depth of this event A8.

In total we have studied eight earthquakes on the mid-Atlantic Ridge from Azores-Gibraltar ridge to the south Altantic. Three of the eight events were characterized by predominantly strike-slip motion. Their focal depths are found to be very shallow-about 3 to 4 km below the ocean floor. On the contrary, the remaining five events were characterized by predominantly dip-slip motion. And their focal depths are found to range from about 28 km to 65 km. As pointed out in the preceding section, the same pattern of focal depth distribution was also found for earthquakes in the east Pacific rise and its northward extensions.

The results of our study on the focal depths of earthquakes on the mid-Atlantic ridge are summarized in Table 4 and Figure 32.

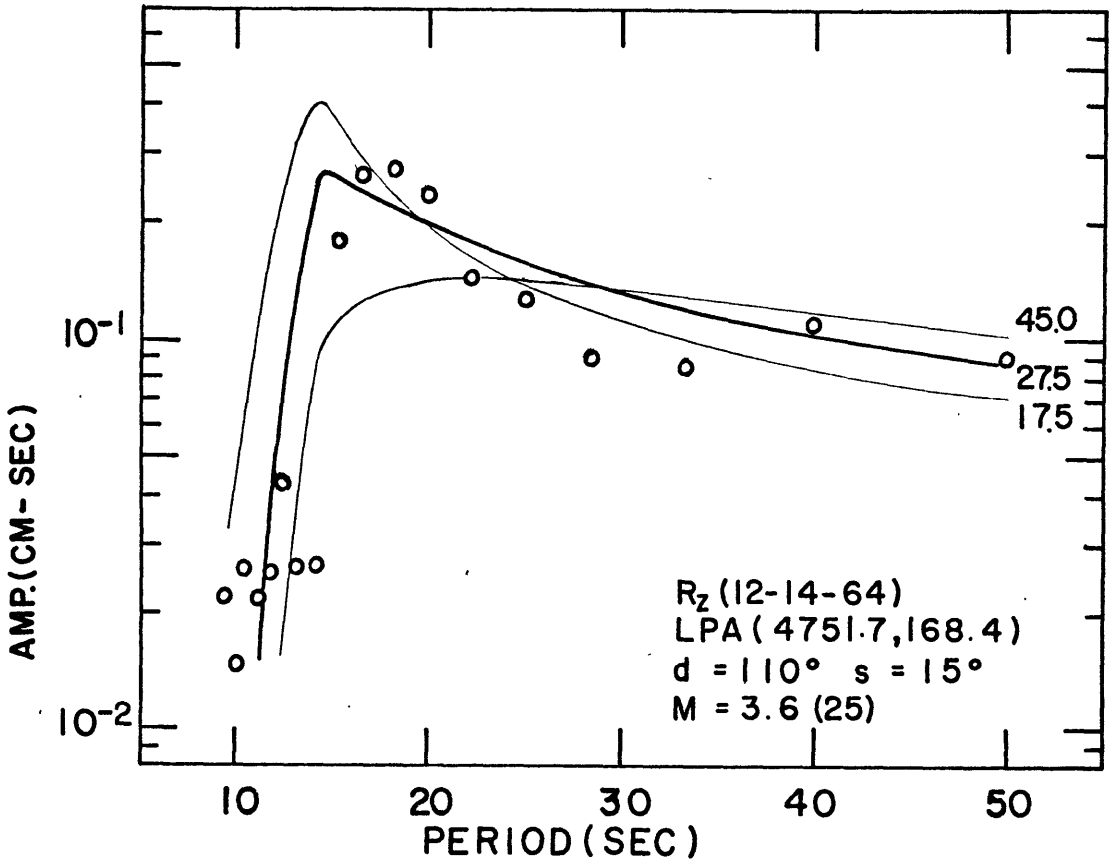

FIG. 52. Rz from event A8 observed at LPA.

4.3 Earthquakes on the mid-Indian ocean ridge:

Nine earthquakes on the Indian ocean ridge are studied in this paper. All the fault plane solutions of these earthquakes were given by Banghar and Sykes (1969). Eight of the nine earthquakes were characterized by a large dip-slip component. For some of the earthquakes it has been possible to use records from more than one station. Repeatability of the observational result from one station to another for a given event will be demonstrated in order to show the dependability of our method.

The locations and other pertinent data of these earthquakes are given in Table 5. Their locations are also shown in Figure 53.

1. Event N1: This event was located on the northern extension of the Owen fracture zone in the Arabian sea. According to Banghar and Sykes (1969), the fault plane solution of this event was characterized by a large component of dip-slip motion. The corresponding fault plane parameters are $\phi_o = 26^o$, $d = 56^o$ and $s = 37.5^o$.

The Rayleigh wave amplitude spectrum from this event observed at NDI ($r = 1686.2$ km) is shown in Figure 54a and that at LAH ($r = 1611.3$ km) is shown in Figure 54b. Both paths were largely continental. Thus we use the Gutenberg continental model in the interpretation. The same focal depth of about 55 km and the same seismic moment of about 0.50×10^{25} dyne-cm for this event. The USCGS reported 33 km as the focal depth of the same event.

TABLE 5 Earthquakes in the mid-Indian ridge

Event	Long.	Lat.	Date Day	Mo	Yr	Time Hr	Min	Sec	Strike	Dip	Slip	Figure number	Station code	Epidistance (km)	Focal depth (km)	M(uncorrected) (10^{25} dyne-cm)	M(corrected) (10^{25} dyne-cm)	Magnitude Ms	USCGS Depth (km)	m_b	ISC Depth (km)	m_b	Reference
N1	62.2E	21.8N	30	03	66	04	18	38.1	26	56	38	54a	NDI	1686.2	55	0.50	0.66	6.03	33	5.5			Banghar & Sykes (1969)
N1	"	"	"	"	"	"	"	"	"	"	"	54b	LAH	1611.3	55	0.50	0.64	6.02					
N2	64.0E	3.8N	15	08	66	10	20	42.2	92	62	-90	55	NAI	3077.5	45	0.75	1.26	6.28	37	5.6			Banghar & Sykes (1969)
N3	65.8E	2.9N	18	10	64	09	06	26.0	160	70	-36	56a	NAI	3258.7	45	1.00	1.73	6.38	33	6.3	50±19	5.9	Banghar & Sykes (1969)
N3	"	"	"	"	"	"	"	"	"	"	"	56b	QUE	3022.8	45	1.60	2.66	6.51					
N3	"	"	"	"	"	"	"	"	"	"	"	56c	NDI	3100.0	45	1.00	1.68	6.37					
N4	70.8E	6.4S	12	09	65	22	02	34.3	90	54	-52	57	NAI	3816.9	28	2.00	3.80	6.60	34	6.2			Banghar & Sykes (1969)
N6	66.8E	15.0S	03	12	64	03	50	01.2	134	60	-33	58a	AAE	4078.2	65	1.38	2.73	6.52	46	6.1	50±21	5.7	Banghar & Sykes (1969)
N6	"	"	"	"	"	"	"	"	"	"	"	58b	LEM	4545.0	65	1.87	4.00	6.62					
N7	78.8E	32.2S	19	12	65	22	06	32.7	104	66	-90	59a	MUN	3513.3	45	0.70	1.26	6.28	33	5.7			Banghar & Sykes (1969)
N7	"	"	"	"	"	"	"	"	"	"	"	59b	LEM	4099.6	45	0.83	1.65	6.37					
N8	78.9E	32.2S	17	02	66	11	48	00.8	95	64	-90	60a	LEM	4092.1	65	4.00	7.96	6.77	33	6.4			Banghar & Sykes (1969)
N8	"	"	"	"	"	"	"	"	"	"	"	60b	MUN	3504.0	65	5.40	9.72	6.81					
N9	96.1E	45.8S	06	04	66	02	59	01.7	108	82	-8	61	ADE	3762.3	4	2.00	3.76	6.60	33	5.8			Banghar & Sykes (1969)
N10	163.7E	49.0S	08	11	64	02	43	57.2	326	78	90	62	TAU	1434.8	28	1.20	1.52	6.34	33	5.6	33	5.6	Banghar & Sykes (1969)

FIG. 53. Locations and focal depths of earthquakes in the mid-Indian ocean ridge studied in this paper.

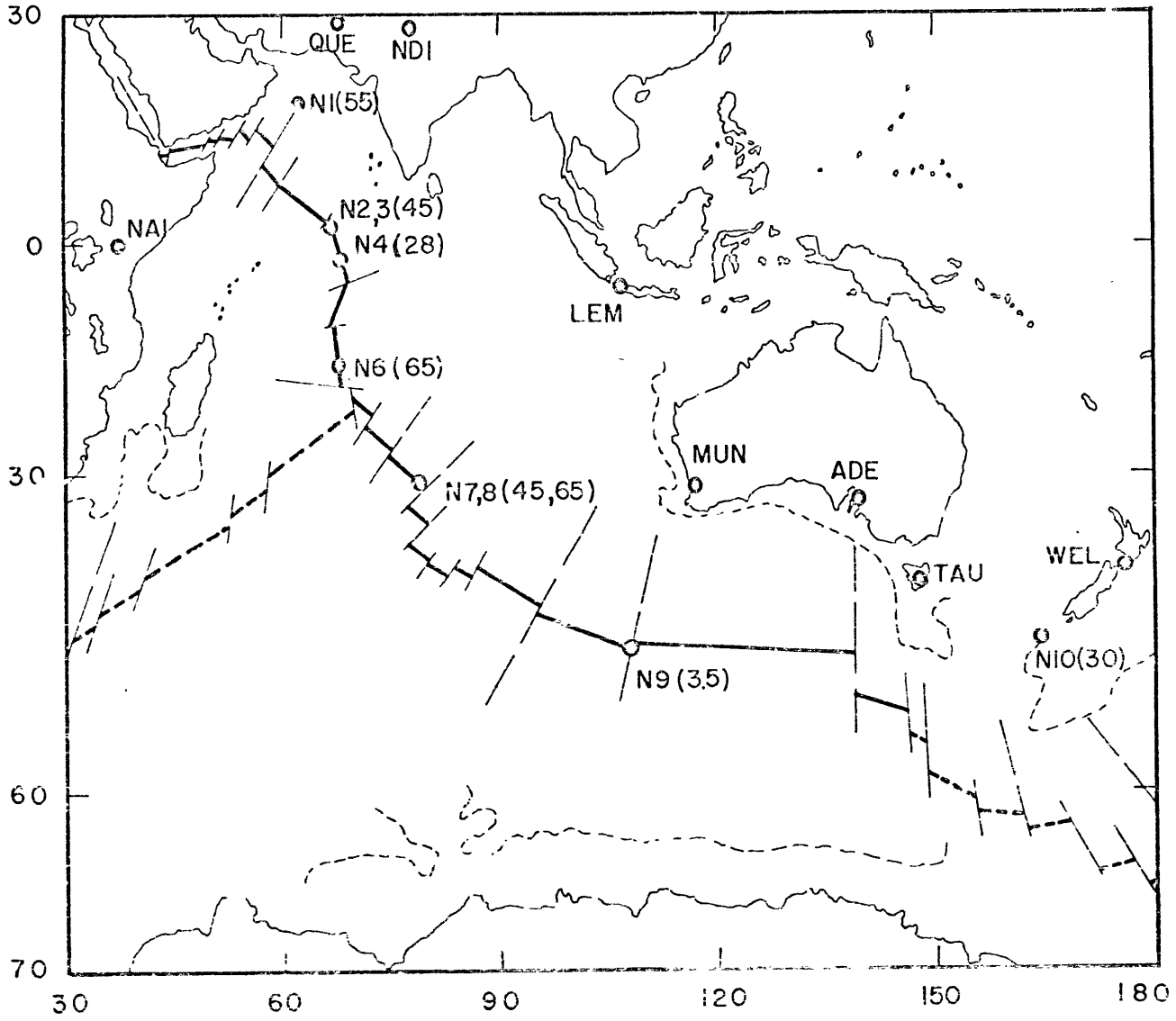

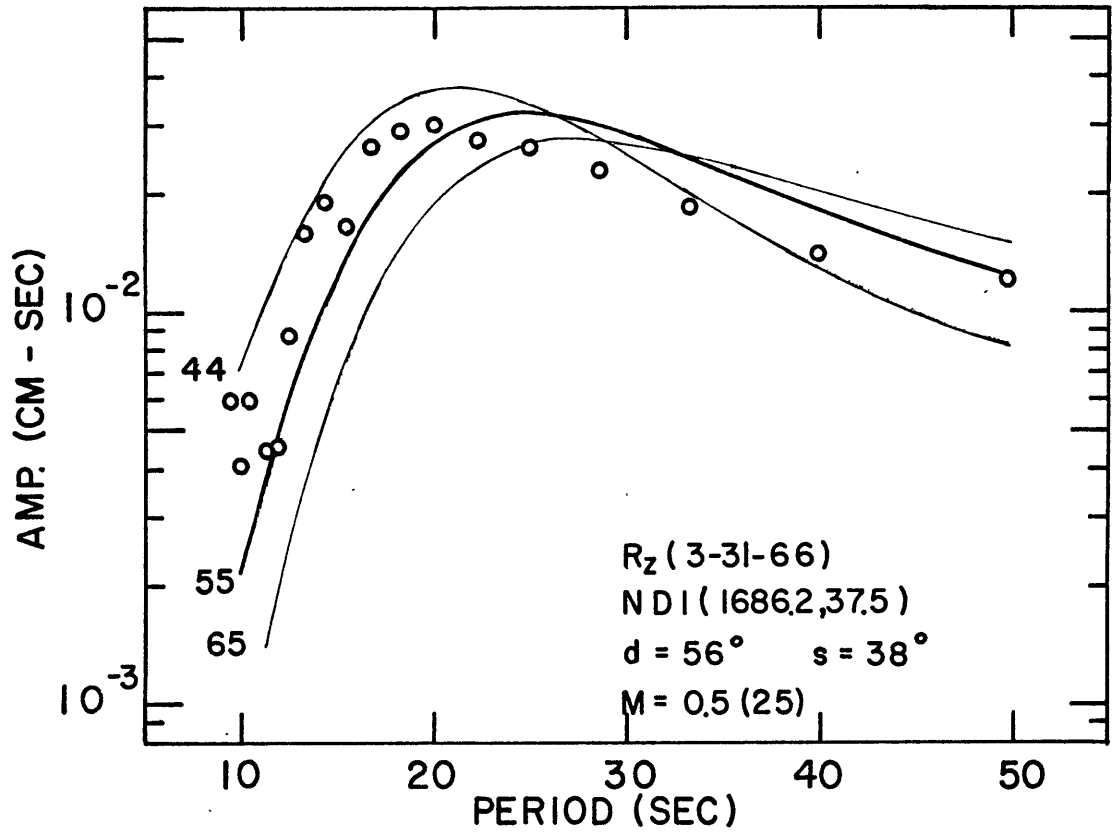

FIG. 54a. Rz from event N1 observed at NDI.

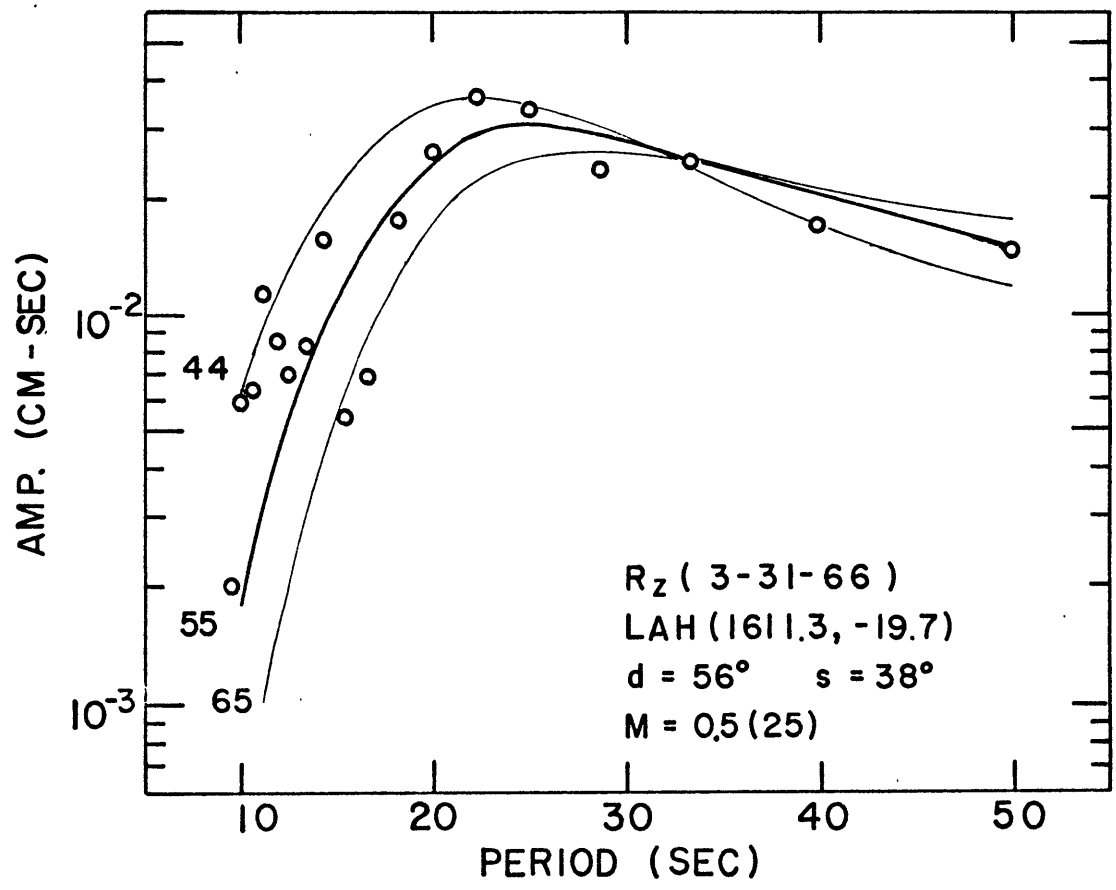

FIG. 54b. Rz from event N1 observed at LAH.

2. Events N2 and N3: These were two events located about one degree apart from each other on the Carlsberg ridge in the Indian Ocean. According to Banghar and Sykes (1969), the fault plane solutions for these two events were characterized by predominantly dip-slip motion. The corresponding fault plane parameters are $\phi_o = 92^o$, $d = 62^o$ and $s = -90^o$ for event N2 and $\phi_o = 160^o$, $d = 70^o$ and $s = -36^o$ for event N3.

The Rayleigh wave amplitude spectrum from event N2 observed at NAI ($r = 3077.5$ km) is shown in Figure 55. The path was mostly oceanic. The data are consistent with a focal depth of about 45 km and a seismic moment of 0.75×10^{25} dyne-cm. The USCGS reported 37 km as the focal depth of event N2. UPP determined a focal depth of 25 km for the event by using the pP-P times at two Stations.

As for event N3 the Rayleigh wave amplitude spectrum observed at NAI ($r = 3258.7$ km), QUE ($r = 3022.8$ km) and NDI ($r = 3100.0$ km) is shown in Figure 56a, Figure 56b and Figure 56c, respectively. All these three paths are oceanic in the main. The data from all of these stations suggest the same focal depth of about 45 km. The seismic moment is determined as 0.10×10^{26} dyne-cm at NAI and NDI and as 0.16×10^{26} dyne-cm at QUE. The agreement among these three observations is indeed remarkable. The USCGS determined the focal depth of event N3 as 33 km. The ISC reported a focal depth of 50 ± 19 km for event N3. The latter value is in agreement with our focal depth determination of 45 km.

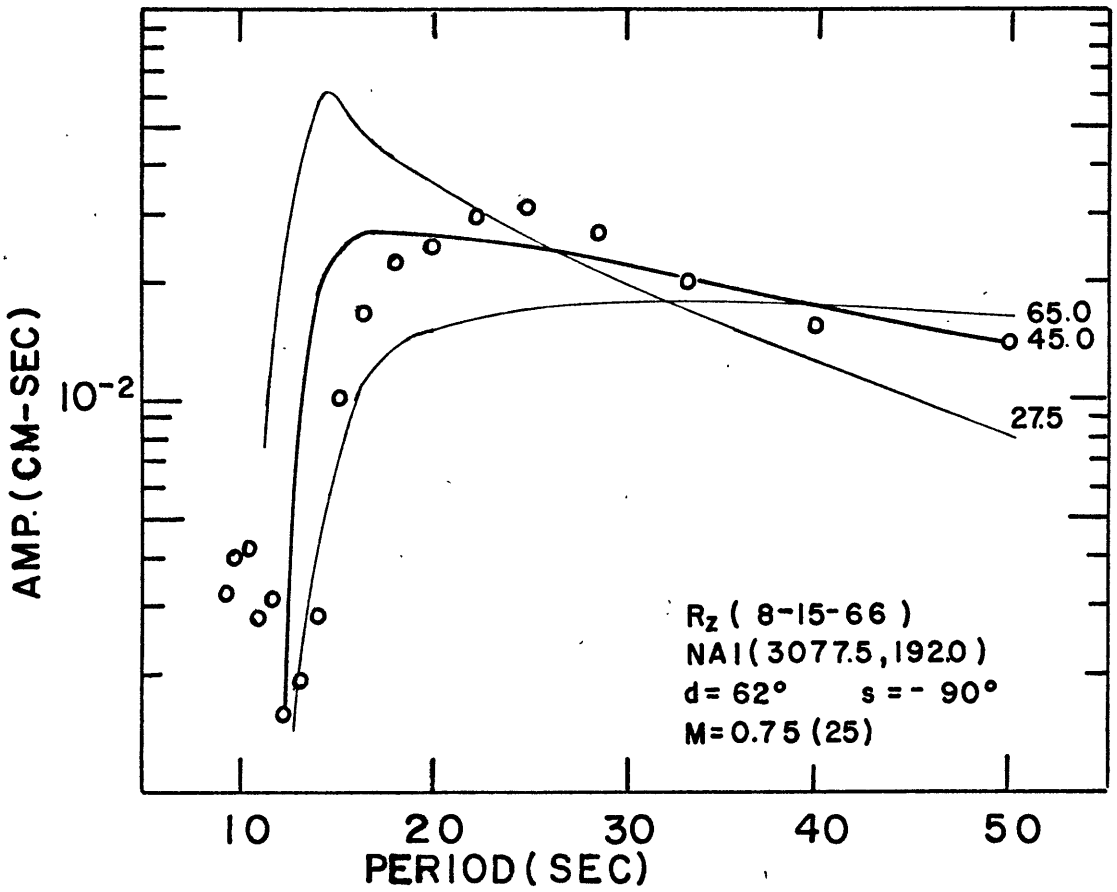

FIG. 55. Rz from event N2 observed at NAI.

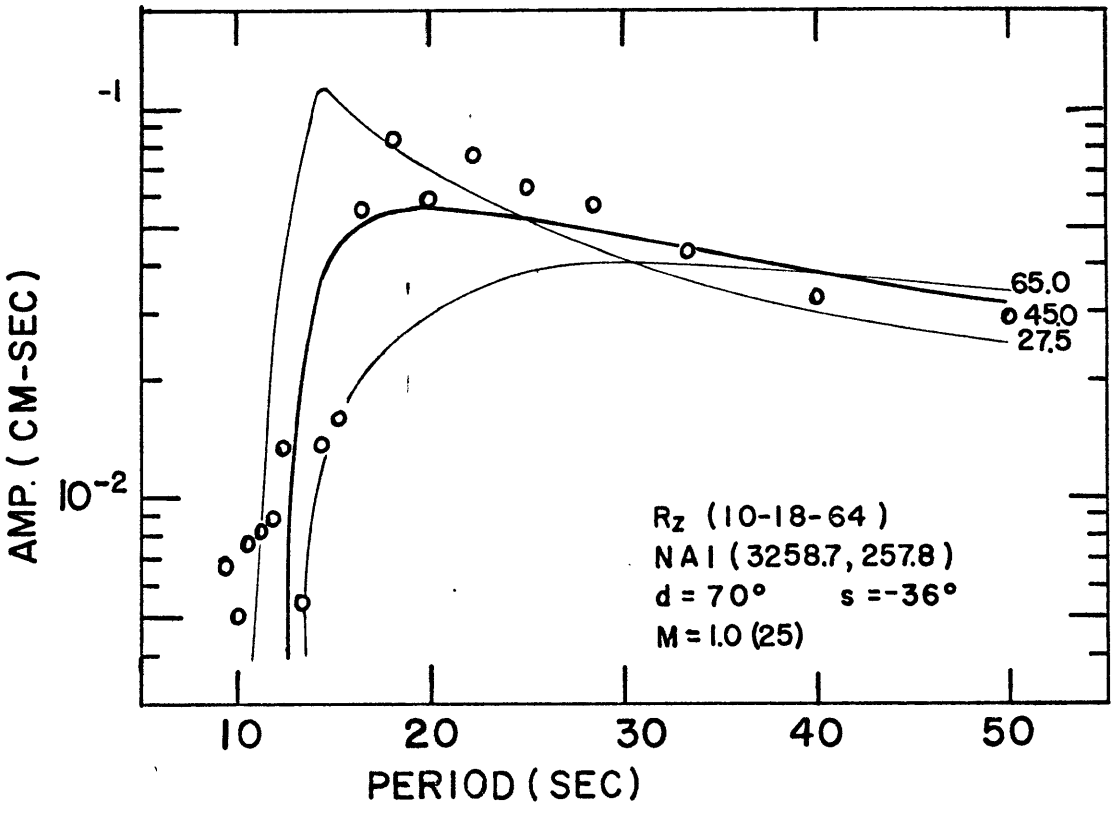

FIG. 56a. Rz from event N3 observed at NAI.

FIG. 56b. Rz from event N3 observed at QUE.

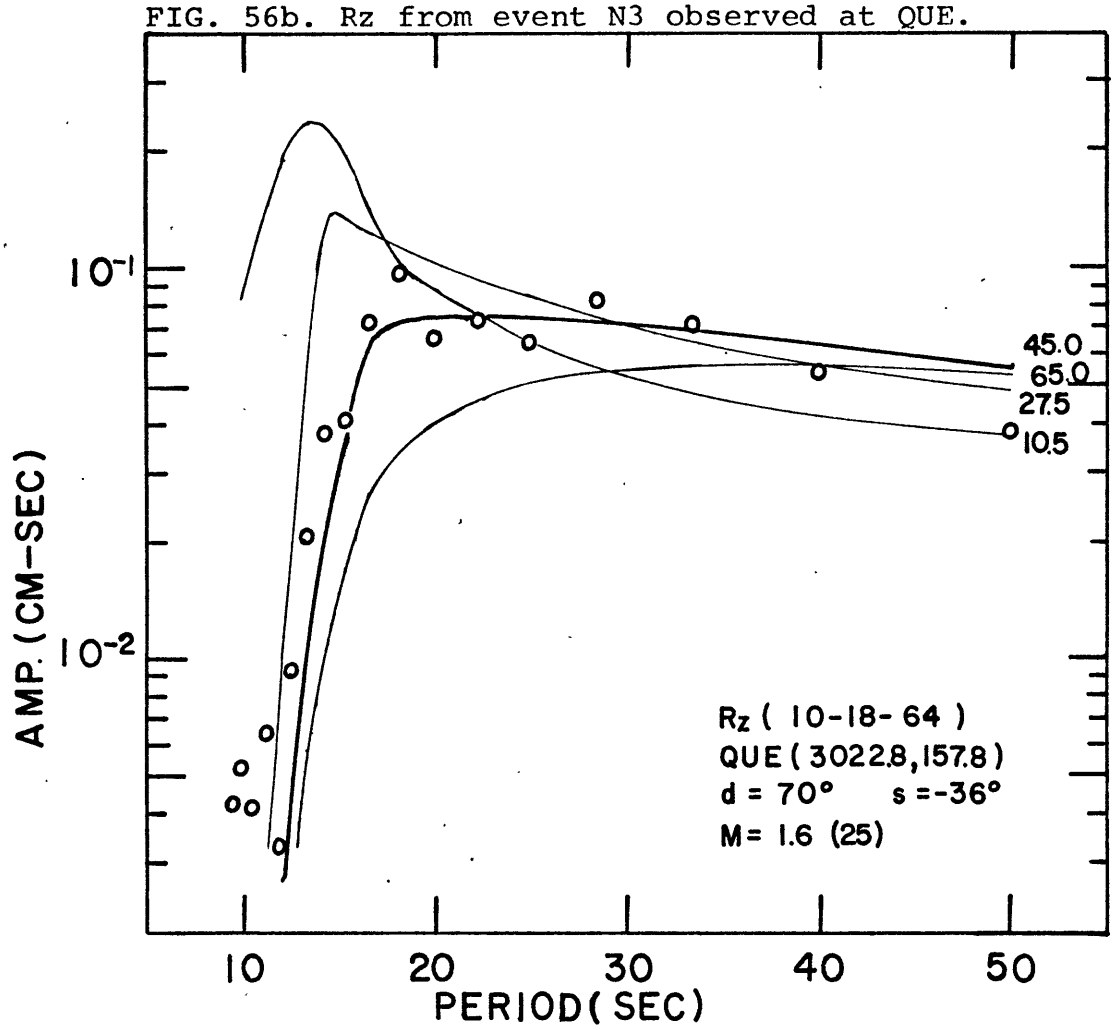

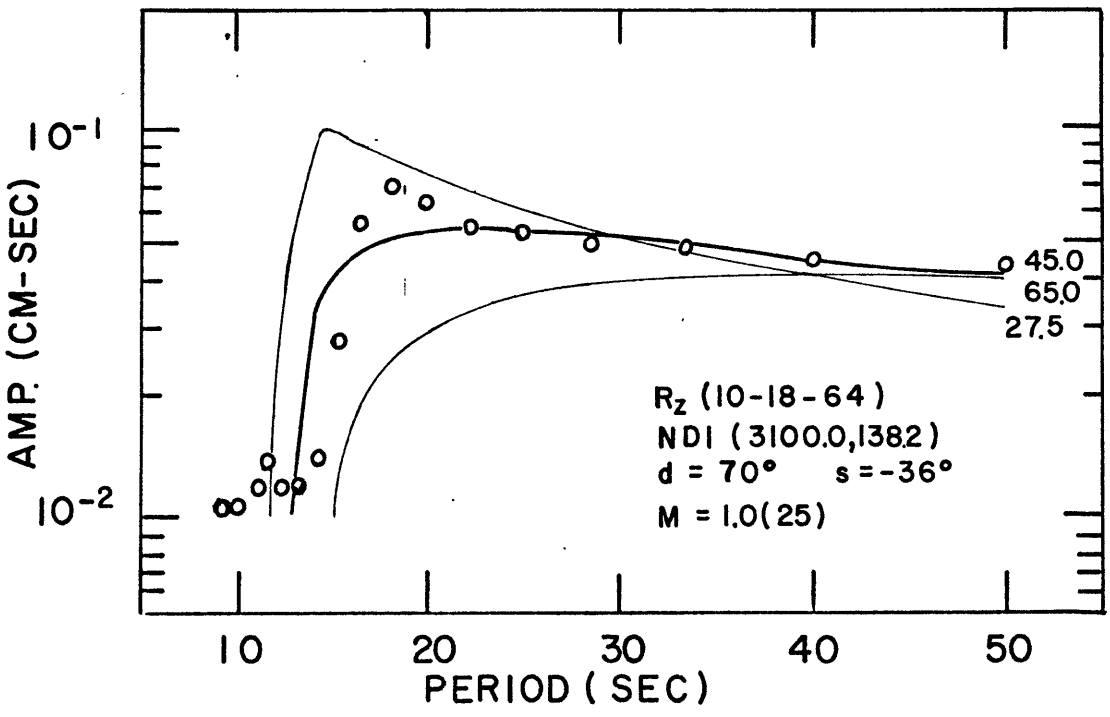

FIG. 56c. Rz from event N3 observed at NDI.

3. Event N4: This was an event located on the Carlsberg ridge about 9° south of event N3. Quite similar to events N2 and N3 above, this event was also characterized by predominantly dip-slip motion. According to Banghar and Sykes (1969) the pertinent fault plane parameters are ϕ_o =90°, d=54° and s=52°.

The Rayleigh wave amplitude spectrum observed at NAI (r=3816.9 km) is shown in Figure 57. The path was essentially oceanic. The data are consistent with a focal depth of about 28 km and a seismic moment of about 0.20 x 10^{26} dyne-cm. The USCGS reported depth was 34 km. UPP determined the focal depth as 25 km by using pP-P times recorded at four stations.

4. Event N6: This was another event on the Carlsberg ridge in the Indian ocean. According to Banghar and Sykes (1969), the fault-plane solution for the event was characterized by a large component of dip-slip motion. The correspondinf fault plane parameters are ϕ_o=134° , d=60° and s=32.5°.

Because of its remoteness, event N6 is studied here by using two rather distant stations. Figure 58a and Figure 58b show the Rayleigh wave amplitude spectrum observed at AAE (r =4078.2 km) and at LEM (r =4545.0 km), respectively. Both paths were essentially oceanic. The data from both stations are consistent with a focal depth of about 65 km. The seismic moment is determined as 1.38 x 10^{25} dyne-cm at AAE and as 1.87 x 10^{25} dyne-cm at LEM.

The USCGS focal depth was 46 km for the event and the ISC

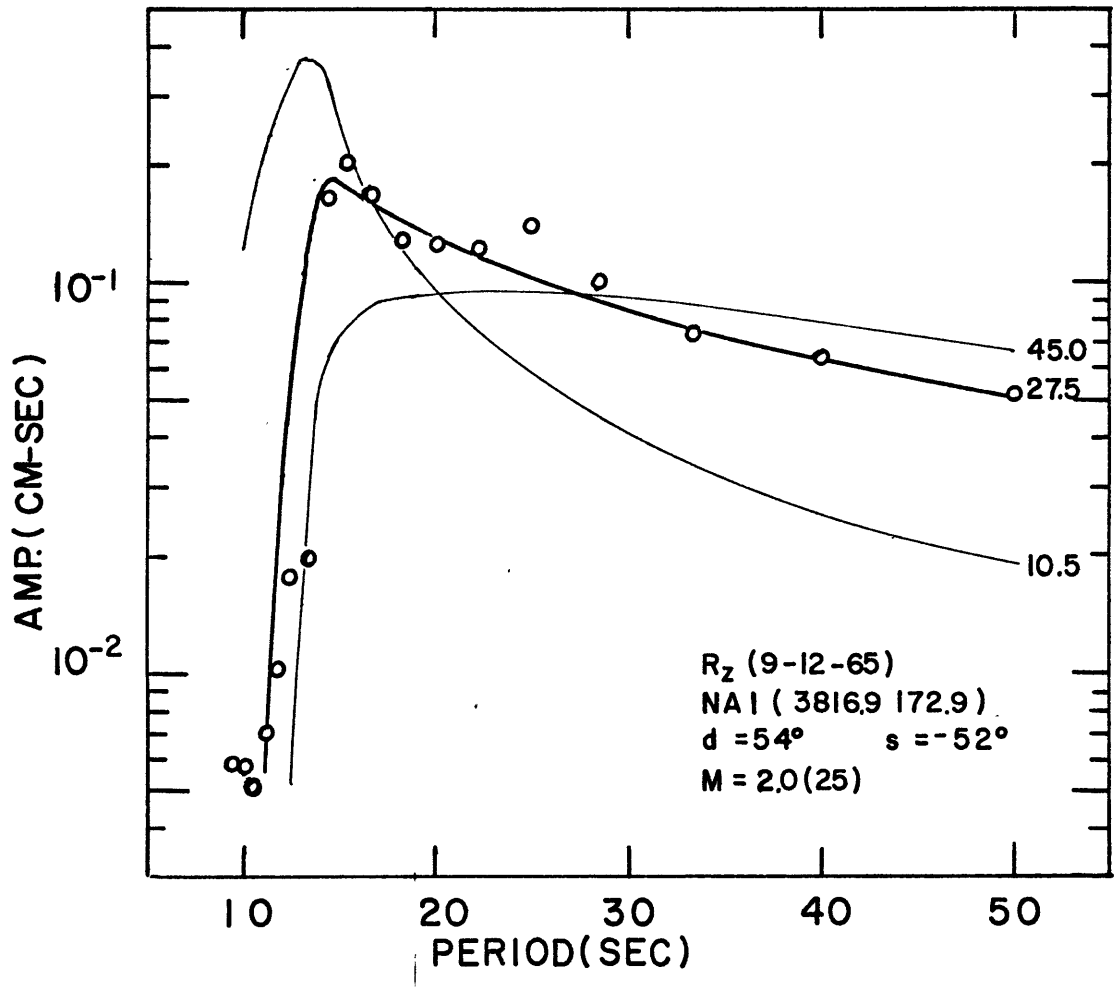

FIG. 57. Rz from event N4 observed at NAI.

FIG. 58a. Rz from event N6 observed at AAE.

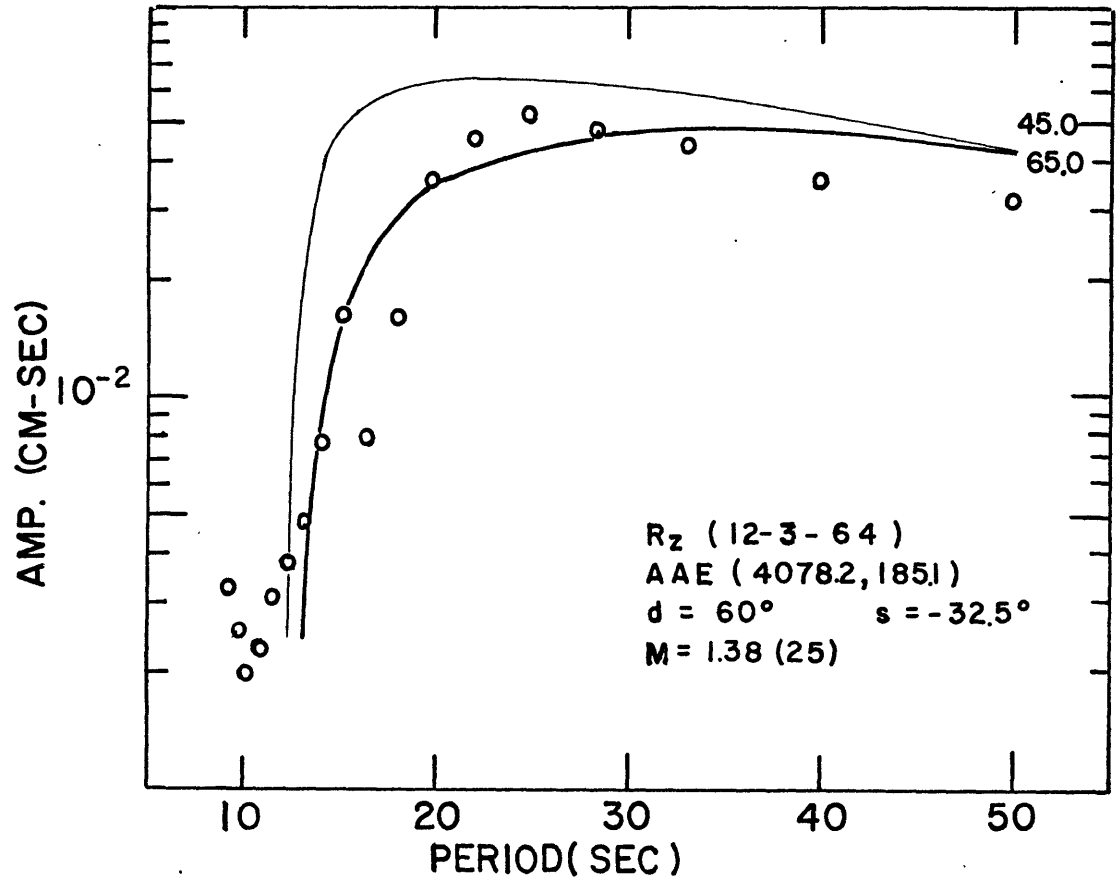

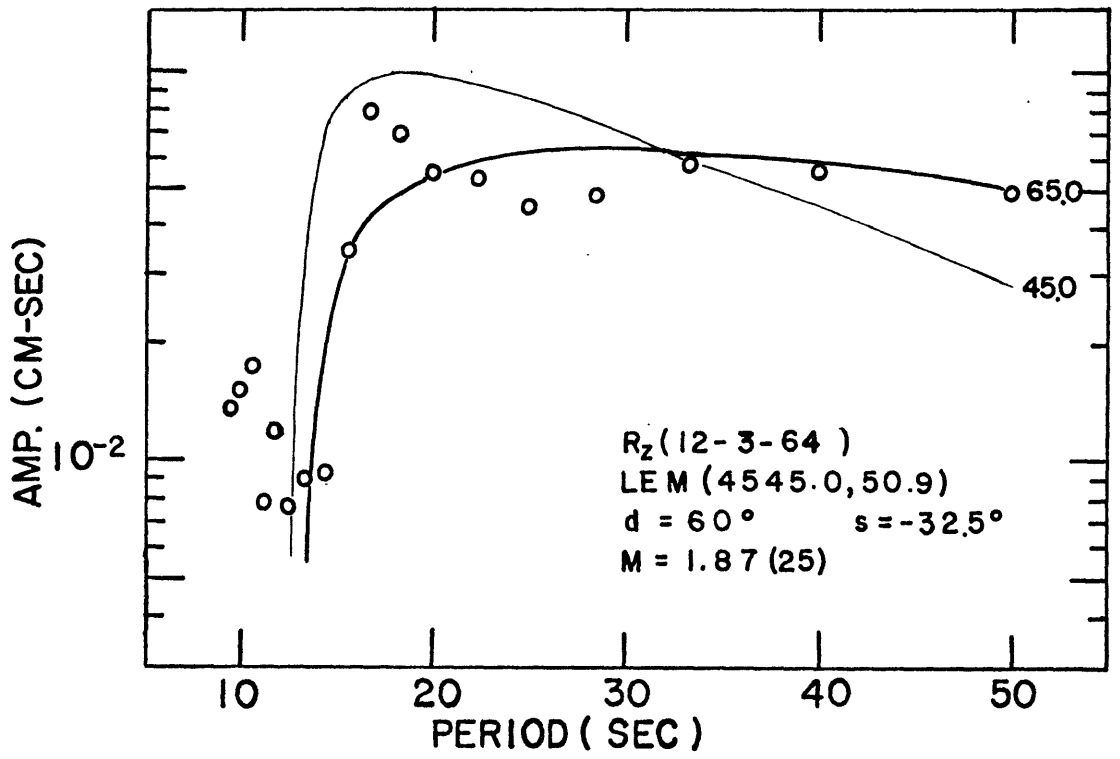

FIG. 58b. Rz observed at LEM from event N6.

reported 50 $\pm$ 21 km for the same event.

5. Events N7 and N8: These were two events located at the same segment of the south Indian ocean ridge. According to Banghar and Sykes (1969), the fault plane solutions for both earthquakes were characterized by a large component of dip-slip motion. The corresponding fault plane parameters are $\phi_o = 104^o$, $d = 66^o$ and $s = -90^o$ for event N7 and $\phi_o = 95^o$, $d = 64^o$ and $s = -90^o$ for event N8.

For event N7, the Rayleigh wave amplitude spectrum observed at MUN ($r = 3513.3$ km) is shown in Figure 59a and that observed at LEM ($r = 4099.6$ km) in Figure 59b. Both paths were oceanic. The data from both stations are consistent with the same focal depth of about 45 km. The seismic moment of event N7 is determined as 0.70×10^{25} dyne-cm from MUN and 0.83×10^{25} from LEM.

As for event N8, the Rayleigh wave amplitude spectrum observed at LEM ($r = 4092.1$ km) is shown in Figure 60a and that observed at MUN ($r = 3504.0$ km) in Figure 60b. The data are consistent with a focal depth of about 65 km. The seismic moment is determined as 0.40×10^{26} dyne-cm from LEM and 0.54×10^{26} dyne-cm from MUN. The USCGS reported 33 km for both events.

The observed difference of 20 km between the focal depths of events N7 and N8 is probably real because both events were located quite close to each other and had quite similar fault plane solutions and are observed at the same set of stations. However, it should also be pointed out that the neglected

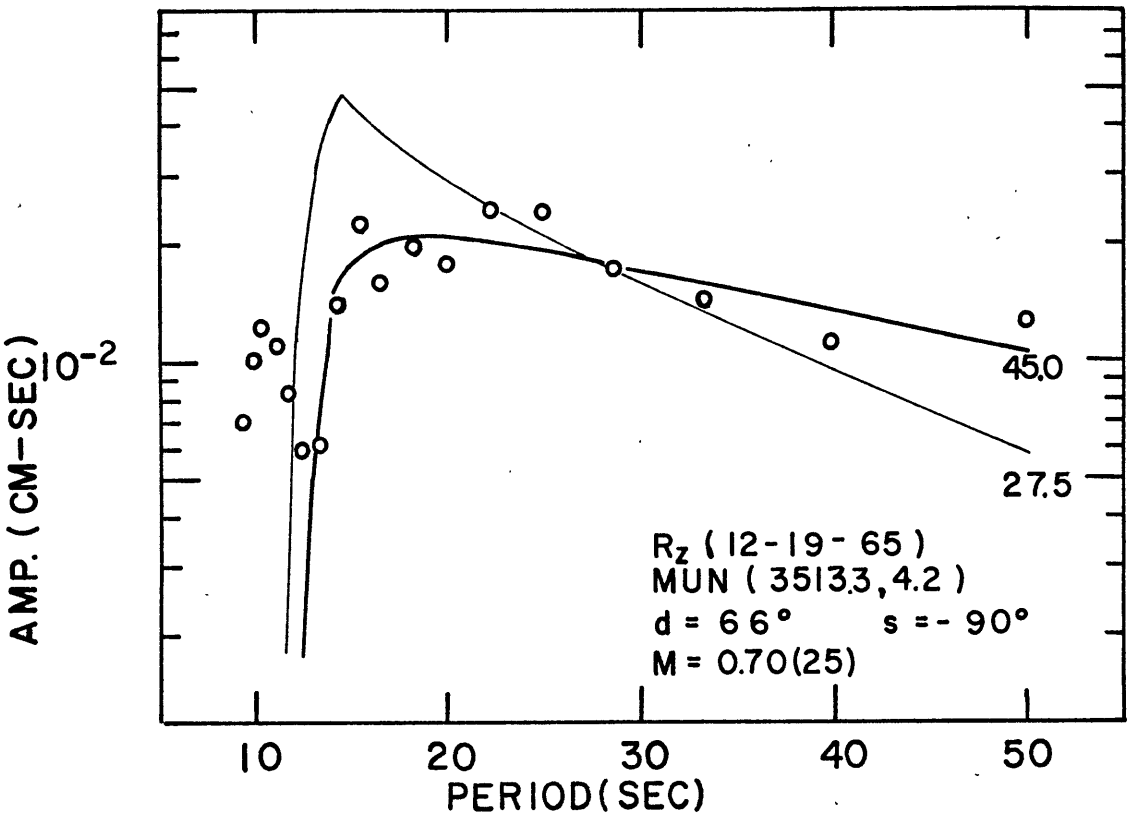

FIG. 59a. Rz from event N7 observed at MUN.

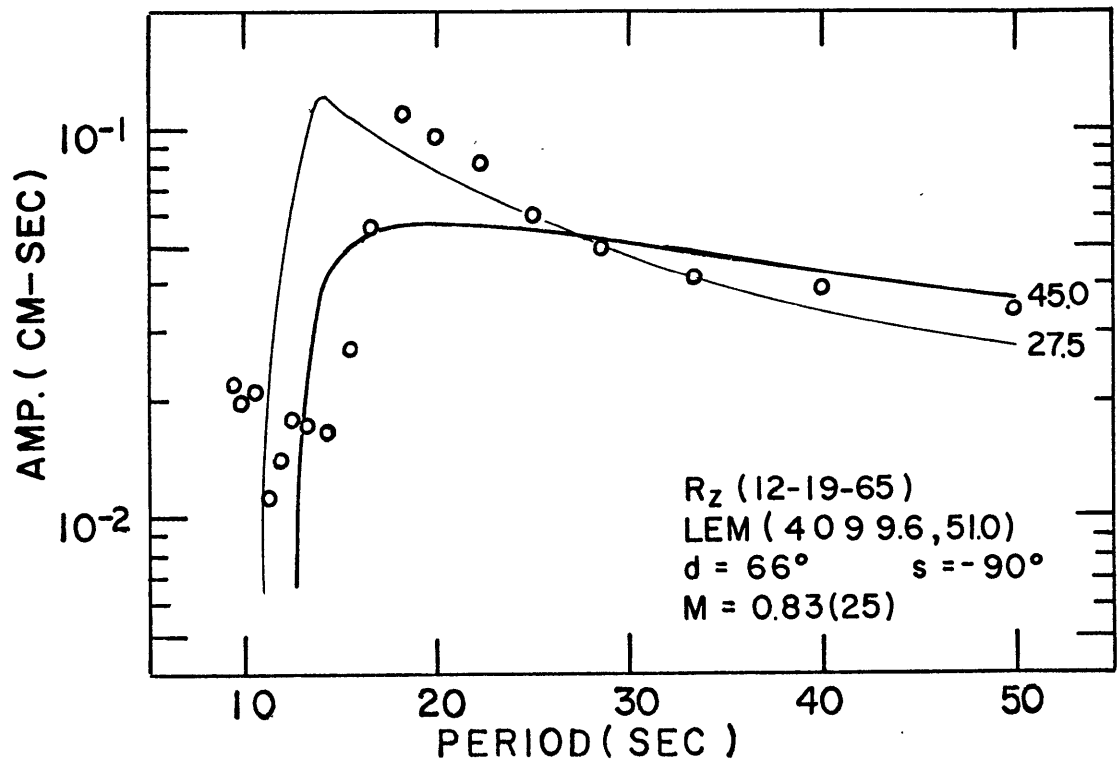

FIG. 59b. Rz from event N7 observed at LEM.

FIG. 60a. Rz from event N8 observed at LEM.

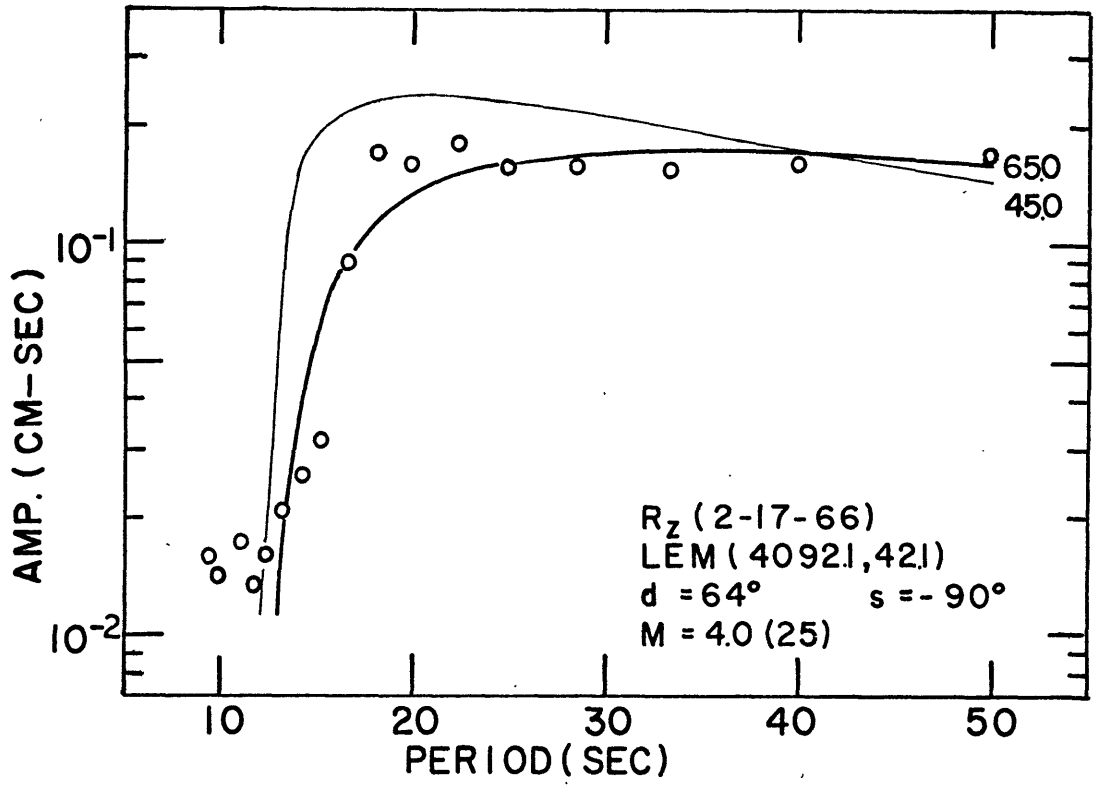

FIG. 60b. Rz from event N8 observed at MUN.

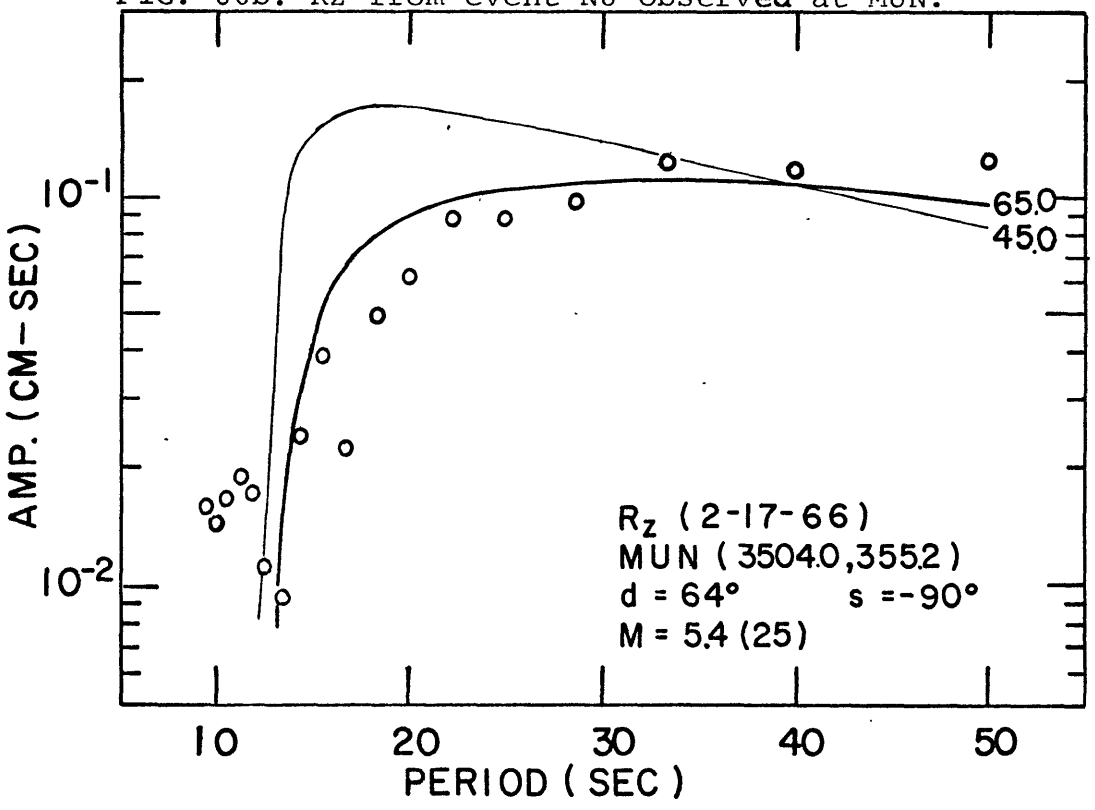

finiteness factor may have contributed to some extent to the apparent deepending of the focal depth of event N8 which had a magnitude of 6.4. We believe that this is not so, because we have found no systematic relation between the seismic moment and focal depth among earthquakes studied in this paper.

6. Event N9: This event was located on the southeast Indian ocean ridge. According to Banghar and Sykes (1969), the fault plane solution was characterized by a large component of strike-slips motion on a steeply dipping plane. The corresponding fault plane parameters are ϕ_o=107.5°, d=82° and s=7.5°.

The Rayleigh wave amplitude spectrum observed at ADE (r=3762.3 km) is shown in Figure 61. The path was essentially oceanic. The data are consistent with a focal depth of about 3.5 km. The seismic moment is determined as 0.20×10^{26} dyne-cm. The USCGS reported a depth of 33 km for the event.

8. Event N10: This event was located on the Macquarie ridge between the South Island of New Zealand and the mid-Indian Ocean ridge. The fault plane solution was characterized by purely dip-slip motion on a steeply deeping plane, as shown by Nanghar and Sykes (1969). The corresponding fault plane parameters are ϕ_o=326° d=78° and s=90°.

The Rayleigh wave amplitude spectrum observed at TAU (r=1434.8 km) is shown in Figure 62. The path was entirely oceanic. The data are consistent with a focal depth of about

FIG. 61. Rz from event N9 observed at ADE.

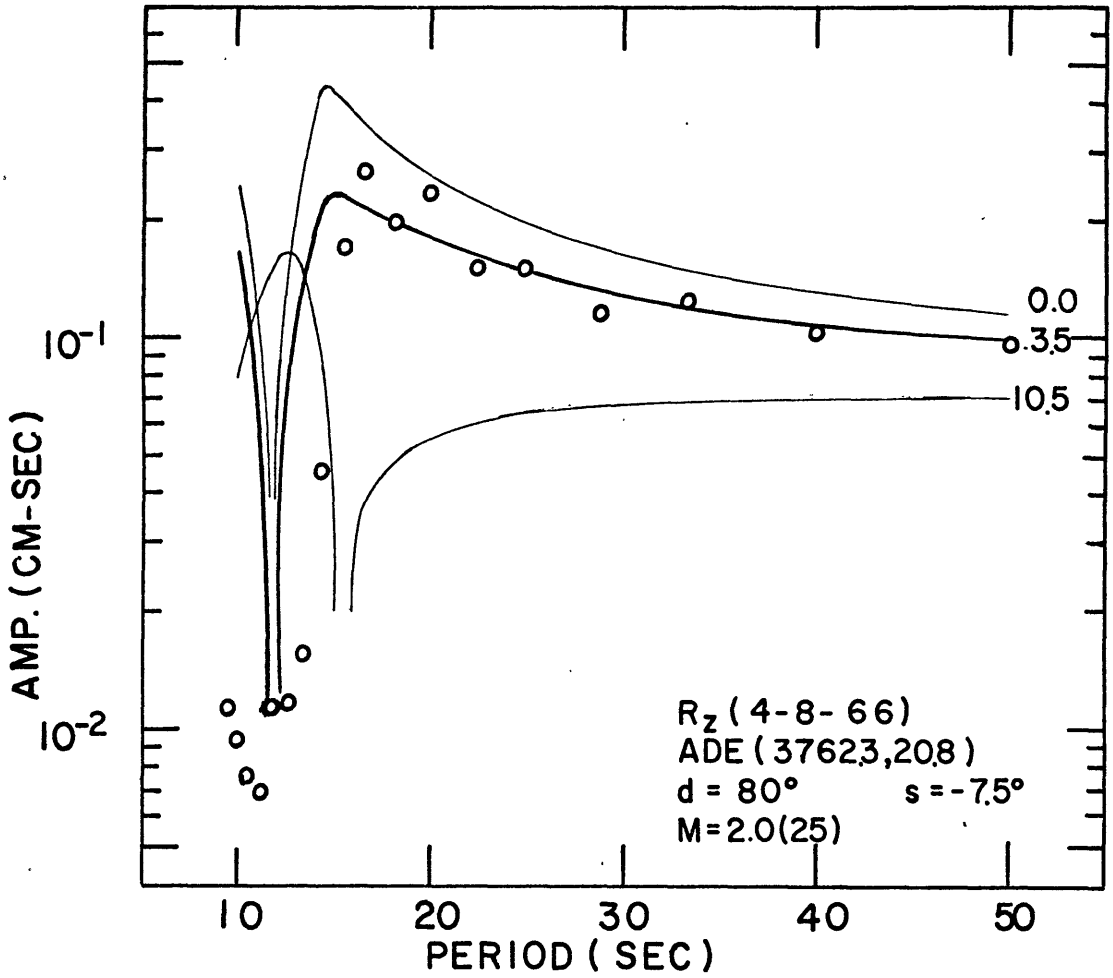

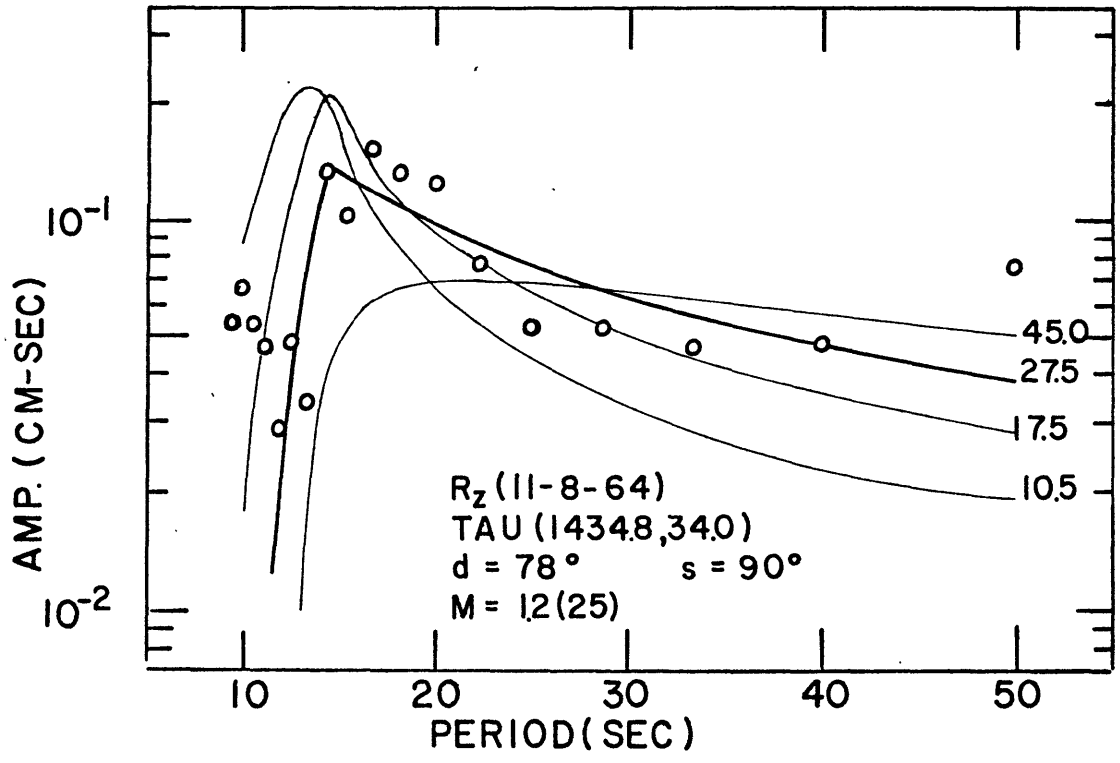

FIG. 62 Rz from event N10 observed at TAU.

27.5 km. The seismic moment is determined as 0.12×10^{26} dyne-cm. The USCGS reported 33 km for the focal depth of event N9.

Our results of focal depth determination of the nine earthquakes on the mid-Indian ocean ridge are summarized in Table 5 and also shown in Figure 53.

In summary, eight of the nine events on the mid-Indian ocean ridge which we have studied were characterized by a large component of dip-slip motion. The focal depths of these events are found to range from about 30 km to about 65 km. The remaining one earthquake was characterized by predominantly strike-slip motion. The focal depth of this event is only about 3.5 km below the ocean floor. Thus, the focal depth distribution of earthquakes on the mid-Indian ocean ridge appears to follow the same pattern as these on the mid-Atlantic ridge and on the east Pacific rise including its northern extensions, as described in the preceding two sections.

4.4 The focal depths of earthquakes on the mid-oceanic ridges

From the individual study of 32 earthquakes on the three major ridge systems of the world, we have found a surprisingly systematic pattern of the focal depth distribution. Half of the 32 events which were located on the fracture zones and characterized by strike-slip faulting occurred at extremely shallow depths —— all less than 10 km (excluding the water depth); the remaining 16 earthquakes which were located on the central ridges and characterized by dip-slip faulting occurred at greater depths —— ranging from about 30 km down to about 65 km.

The locations and the focal depth of all these earthquakes are shown in Figures 32 and 53. They are also given in Tables 3, 4 and 5. In these tables the USCGS focal depths for all events and the ISC focal depths are also included whenever available. About two-third of the earthquakes were assigned by the USCGS with a restrained depth of 33 km. The ISC focal depths are compared with our determination in Figure 63 which also includes the three Parkfield events.

Figure 63 shows that our finding of two distinct groups of focal depths corresponding to two different types of focal mechanism appears to be substantiated by the ISC data.

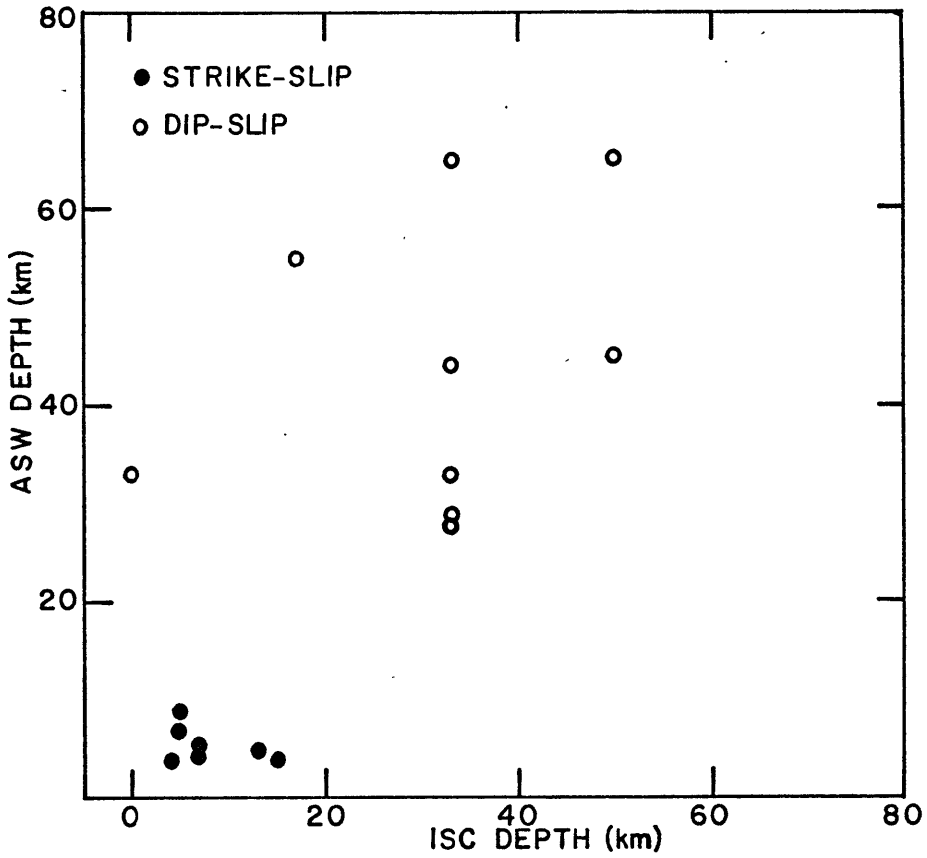

FIG. 63 Comparison of the focal depths obtained in the present paper with available ISC focal depths.

4.5 Interpretation of the seismic moment data

In the course of determining the focal depth we have also obtained the seismic moment of each earthquake. The results are shown in Tables 3, 4 and 5. As mentioned before, these values are not corrected for attenuation. As shown in Chapter 3, the attenuation coefficient $\eta(\omega)$ of Rayleigh waves is approximately independent of frequency in the range between 10 and 50 seconds. Therefore, the correction factor $e^{\eta(\omega)r}$ (where r is the epicentral distance) is a constant independent of frequency within this range. We used $\eta(\omega) = 168 \times 10^{-6}$ km^{-1} for the oceanic paths and $\eta(\omega) = 157 \times 10^{-6}$km^{-1} for the continental paths. The corrected values for the seismic moment are also shown in Tables 3, 4 and 5.

Recently, Liebermann and Pomeroy (1969) made a comparative study of the Ms versus m_b relationships for earthquakes in different regions of the world. Their results showed that earthquakes from the Aleution-Kamchatka island . . follow closely the Gutenberg-Richter's empirical formula, that is, Ms=1.59 X m_b-3.97. They have also found that earthquakes from western United States all have a remarkably larger Ms for a given m_b than that predicted by the Gutenberg-Richter's empirical formula. On the other hand, underground explosions throughout the world are characterized by a smaller Ms for a given m_b than that expected from the Gutenberg-Richter's curve.

Liebermann and Pomeroy's (1969) data and the theoretical curve derived on their ω^2-model are shown in Figure 64.

It is interesting to compare the Ms-versus-m_b relationship for the earthquakes of mid-oceanic ridges with those for the earthquakes of other regions.

Aki (1967) showed that the seismic moment can be related to the surface wave magnitude Ms of an earthquake on the assumption of similarity which implies a constant stress drop independent of source size. Using his ω-square model and calibrating the absolute value by the result on the Niigata and the Parkfield earthquakes, the relation between the seismic moment and Ms is obtained and shown below:

Ms	4.5	5.0	5.5	6.0	6.5	7.0
Seismic moment (dyne-cm)	1.35×10^{23}	4.75×10^{23}	1.70×10^{24}	6.00×10^{24}	2.55×10^{25}	2.50×10^{26}

Using the above table, we obtain the magnitude Ms from the observed seismic moment and compare it with m_b for each event. Because of the considerable scatter of the USCGS magnitude values, we use the ISC determinations for m_b. The results are shown in Figure 64. Our data clearly indicate that the Ms-versus-m_b relationship for earthquakes of the mid-oceanic ridges is essentially the same as the one for earthquakes in the western United States. Liebermann and Pomeroy's theoretical curve which is obtained by modifying the ω-square model proposed by Aki (1967) fits surprisingly well with our data. This similarity of the Ms-versus-m_b relationship for earthquakes from western United States and from the mid-oceanic ridges is another evidence for Wilson's (1965a,1965b)

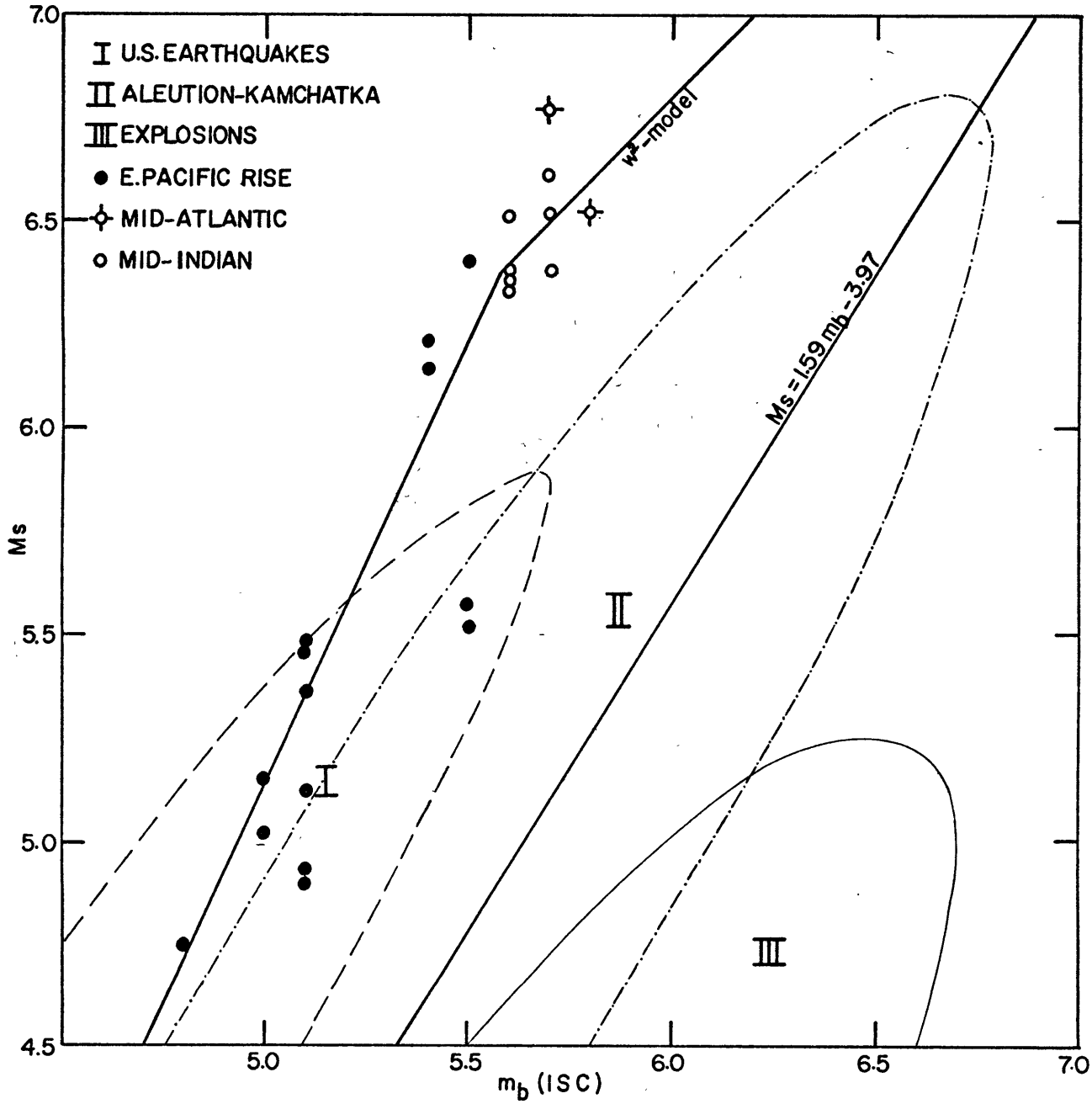

FIG. 64. The Ms-versus-m_b relationship for earthquakes in the mid-oceanic ridges.

idea that the east Pacific rise extends northward through San Andreas fault up to the Queen Charlotte Island fault. This similarity suggests that the low stress drop observed with earthquakes on San Andreas fault may also apply to those earthquakes on the mid-oceanic ridges.

CHAPTER 5

Summary and discussions

5.1 On the method

A method for determining the focal depths of remote earthquakes with known fault plane solutions is successfully developed. In this method the normal mode theory for surface waves excited by a slip-dislocation in a realistic, multilayered earth model is used to interpret the observed amplitude spectrum. For an earthquake with magnitude 6.0 or less the finiteness and the temporal factors of the source appear to have negligible effect on the spectral shape of surface waves in the period range from 10 to 50 seconds. In this period range the dominant source parameters which determine the surface wave amplitude spectral shape are the geometry of fault motion and the focal depth. Therefore, if the fault plane solution is know, the focal depth can be determined from the amplitude spectral shape. The method is tested by applying it to several earthquakes with known fault plane solutions and known focal depths. The results from these tests show that our method is capable of determining focal depths with an accuracy of a few kilometers.

For earthquakes with magnitudes considerably larger than 6.0 the applicability of the method is limited by the growing contribution to the Fourier spectrum from the finiteness and the temporal factors of the source. On the other hand, the method can bot be applied to earthquakes with magnitudes

smaller than about 4.5 because the surface waves from those earthquakes are not well recorded by most standard seismograph stations currently in operation.

By using the amplitude spectrum of surface waves, not only the focal depth but also the seismic moment of the equivalent double couple force system of an earthquake can be obtained.

5.2 On the results

We have applied this method to 32 earthquakes on the mid-oceanic ridges. Our results (see Tables 3,4,5) can be summarized as the following:

(1) The focal depths of sixteen earthquakes located on the fracture zones were all extremely shallow —— less than 10 km excluding the water depth (see Figures 32, 53). These earthquakes were characterized by strike-slip motion on a steeply dipping fault plane. The similarity in the focal depth distribution of the strike-slip earthquakes from the east Pacific rise and from the Gulf of California, the San Andreas fault, the Mendocino fracture zone, the Blanco fracture zone and the Queen Charlotte Island fault strongly supports Wilson's (1965a,b) idea that the east Pacific rise extends northwards through all the above mentioned tectonic features up to the Queen Charlotte Island fault, and that the San Andreas fault is a transform fault.

Brune (1968) compared the rates of motion obtained from the cummulative seismic moments of earthquakes in the fracture zone with the sea-flooring spreading rates determined from magnetic data, and found that reasonable agreement between them could be achieved if the depths of fault in the fracture zone were of the order of 5 km. His conclusion is consistent with our results of focal depth determination. He suggested that creep motion at a relatively shallow depth might be responsible for confining the seismic zone within the top few kilometers beneath the ocean floor.

(2) The remaining sixteen earthquakes which were located on the central ridges and characterized by predominantly dip-slip motion occurred systematically at greater depths —— ranging from about 30 km to about 65 km (See Figures 32,53). This suggests that the thickness of the lithosphere beneath the central ridges is at least 65 km. This evidence would reject the idea that lithosphere is quite thin (10 km) at the ridge axis (Sleep, 1969).

(3) The Ms-versus-m_b relationship for these earthquakes is investigated. The observed seismic moment is translated to the surface wave magnitude Ms and compared with the body wave magnitude m_b. Our results show that all earthquakes from the three major mid-oceanic ridge system,whether they are dip-slip or strike slip, follow the same Ms-versus-m_b relationship which also applies to earthquakes in the western United States (See Figure 64). This similarity of the Ms-versus-m_b relationship again supports the idea that the seismicity in the western United States is closely related to the east Pacific rise. The similarity also implies that the low stress drop observed for earthquakes on the San Andreas fault may be characteristic of those earthquakes on the mid-oceanic ridges.

It should be emphasized that the foregoing results are derived from studying earthquakes from all three major mid-oceanic ridge systems. The surprisingly uniform pattern of focal depth distribution and the unique Ms-versus-m_b relationship for these earthquakes strongly support the concept of new global tectonics (Isacks, et. al., 1968).

5.3 Future studies

(1) Once the focal depth of an earthquake with known fault plane solutions is determined by using the amplitude spectrum of the surface waves as we have done so far, the correction for the source effect on the phase spectrum can be easily made. Therefore we can study the regional phase velocity variations by using the phase spectrum observed at a single station.

(2) As demonstrated by the results of our multi-station observations of the same event, the seismic moment can be measured to an accuracy within a factor of 2. Consequently, the surface wave magnitude Ms can be obtained quite accurately. We should be able to establish more precisely the Ms-versus-m_b relationship, or preferably the moment-energy relationship, if measurement of m_b is improved. Such a study will eventually allow us to estimate the stress conditions in various tectonic regions of the Earth.

(3) Although we have studied 32 events from the three major ridge systems, there are still large sections of them not covered in the present study. Extension of a similar study to these sections and to other tectonic regions such as minor ridges and island arcs should be worthwhile.

REFERENCES

Aki, K., Generation and Propagation of G waves from the Niigata earthquake of June 16, 1964, 1, A statistical analysis, Bull. Earthq. Res. Inst., 44, 23-72, 1966.

Aki, K., Generation and Propagation of G waves from the Niigata earthquake of June 16, 1964, 2, Estimation of earthquake moment, released energy, and stress-strain drop from the G wave spectrum, Bull. Earthq. Res. Inst., 44, 73-88, 1966.

Aki, K., Scaling Law of seismic spectrum, J. Geophy. Res., 72, 1217-1231, 1967.

Aki, K., Seismic displacements near a fault, J. Geophys. Res., 73, 5359-5376, 1968.

Aki, K., Seismic efficiency of a moving dislocation source, in press, 1969.

Arkhangel'skaya, V.M., and S. A. Fedorov, Damping of surface Rayleigh waves, Izv. Akad. Nauk, USSR, Ser. Geofiz., English Iransl., No. 8, 738-743, 1961.

Banghar, A. R. and L. R. Sykes, Focal mechanisms of earthquakes in the Indian Ocean and adjacent regions, J. Geophys. Res., 74, 632-649, 1969.

Basham, P. W., and R. M. Ellis, The composition of P codas using magnetic tape seismograms, Bull. Seismol. Soc. Am., 59, 473-486, 1969.

Ben-Menahem, A., Radiation of seismic surface waves from the finite moving sources, Bull. Seismol. Soc. Am., 51, 401-435, 1961.

Ben-Menahem, A. and M.N. Toksöz, Source mechanism from spectrum of long-period surface waves, 2, The Kamchatka earthquake of November 4, 1952, J. Geophys. Res., 68, 5207-5222, 1963.

Ben-Menahem, A. and D.G. Harkrider, Radiation Patterns of seismic surface waves from buried dipolar point sources in a flat stratified earth, J. Geophys. Res., 69, 2605-2620, 1964.

Ben-Menahem, A., Source studies from isolated seismic signals, Proceedings of the VESIAC conference on the current status and future prognosis for understanding the source mechanism of shallow seismic events in the 3 to 5 magnitude range, 85-108, 1967.

Bolt, B. A., C. Lomnitz, and T. V. McEvilly, seismological evidence on the tectonics of Centeral and Northern California and the Mendocino Escarpment, Bull. Seismol. Soc. Am., 58, 1725-1767, 1968.

Brown, R. D., Jr. and J. G. Vedder, Surface tectonic fractures along the San Andreas fault, in the Parkfield-Cholame, California, earthquakes of June-August 1966, U. S. Geologic Survey Professional Paper 579, 2-22, 1967.

Burridge, R. and L. Knopoff, Body force equivalents for seismic dislocations, Bull. Seismol. Soc. Am., 54, 1875-1888, 1964.

Dorman, J., M. Ewing,and J. Oliver, Study of shear velocity distribution in the upper mantle by mantle Rayleigh waves, Bull. Seismol. Soc. Am., 50, 87-115, 1960.

Eaton, J. P., Instrumental seismic studies, U. S. Geologic Survey Professional Paper, 579, 57-65, 1967.

Filson, J. and T. V. McEvilly, Love wave spectra and the mechanism of the 1966 Parkfield sequence, Bull. Seismol. Soc. Am., 57, 1245-1257, 1967.

Gutenberg, B. and C. F. Richter, Magnitude and energy of earthquakes, Ann. Geofisica, 9, 1-15, 1956.

Hagiwara, T., A note on the theory of the electro-magnetic seismograph, Bull. Earthq. Res. Inst. 36, 139-164, 1958.

Harkrider, D. G., Surface waves in multilayered elastic media, 1. Rayleigh and Love waves from buried sources in a multilayered elastic half-space, Bull. Seismol. Soc. Am., 54, 627-679, 1964.

Harkrider, D. G. and D. L. Anderson, Surface wave energy from point sources in plane layered earth models, J. Geophys. Res.,71, 2967-2980, 1966.

Haskell, N. A., The dispersion of surface waves on multilayered media, Bull. Seismol. Soc. Am., 43, 17-34, 1953.

Haskell, N. A., Radiation pattern of surface waves from point sources in a multilayered medium, Bull. Seismol. Soc. Am., 54, 377-393, 1964.

Haskell, N. A., Elastic displacements in the near-field of a propagating fault, Bull. Seismol. Soc. Am., 59, 865-908, 1969.

Healy, J. A., W. W. Rubey, D. T. Griggs, and C. B. Raleigh, The Denver earthquakes, Science, 161, 1301-1310, 1968.

Hirasawa, T., Source mechanism of the Niigata earthquake of June 16, 1964, as derived from body waves, Journ. Phys. Earth, 13, 35-66, 1965.

Iida, K., Earthquake energy and earthquake fault, J. Earth Sci., Nagoya Univ., 7, 98-107, 1959.

Iida, K., Earthquake magnitude, earthquake fault, and source dimensions, J. Earth Sci., Nagoya Univ., 13, 115-132, 1965.

Isacks, B., J. Oliver, and L.R. Sykes, Seismology and the new global Tectonics, J. Geophys. Res., 73, 5855-5899, 1968.

King, C. H. and L. Knopoff, Stress drop in earthquakes, Bull. Seismol. Soc. Am., 58, 249-257, 1968.

Knopoff, L. and F. Gilbert, First motions from seismic sources, Bull. Seismol. Soc. Am., 50, 117-134, 1960.

LaCoss, R. T., A Large-population LASA discrimination experiment, Technical Note, 1969-24, Lincoln Laboratory, M.I.T., 1969.

Liebermann, R. C. and P. W. Pomeroy, Relative excitation of surface waves by earthquakes and Underground explosions, J. Geophys. Res., 74, 1575-1590, 1969.

Maruyama, T., On the force equivalents of dynamical elastic dislocations, Bull. Earthq. Res. Inst., 41, 467-486, 1963.

Major, M. W. and R. B. Simon, A seismic study of the denver (Derby) earthquakes, Colorado School Mines Quart., 63, 9-55, 1968.

McEvilly, T.V., Detailed study of the November 1964 earthquake sequence near Corralitos, California, Proceedings of the VESIAC conference on the current status and future prognosis for understanding the source mechanism of shallow seismic events in the 3 to 5 magnitude range, 165-172, 1967.

McEvilly, T.V., W.H. Bakun, and K.B. Casaday, The Parkfield, California, earthquakes of 1966, Bull. Seismol. Soc. Am., 57, 1221-1244, 1967.

Press, F., Seismic wave attenuation in the crust, J. Geophys. Res., 69, 4417-4418, 1964.

Press, F., Dimensions of the source region for small shallow earthquakes, Proceedings of the VESIAC conference on the current status and future prognosis for understanding the source mechanism of shallow seismic events in the 3 to 5 magnitude range, 155-163, 1967.

Richter, C. F., Elementary seismology, W.H. Freeman and Company, San Francisco, 1958.

Saito, M., Excitation of free oscillations and surface waves by a point source in a vertically heterogeneous earth, J. Geophy. Res., 72, 3689-3699, 1967.

Sato, R., Attenuation of seismic waves, Journ. Physics Earth, 15, 32-61, 1967.

Stauder, W. and G. A. Bollinger, The S wave project for focal mechanism studies — earthquakes of 1962, Bull. Seismol. Soc. Am., 54, 2199-2208, 1964a.

Stauder, W. and G. A. Bollinger, The S wave project for focal mechanism studies — earthquakes of 1962, Rept., Air Force Office Sci. Res. grant AF-AFOSR 62-458, Saint Louis University, 1964b.

Stefansson, R., Methods of focal mechanism studies with application to two Atlantic earthquakes, Tectonophysics, 3, 209-243, 1966.

Sykes, L. R., Mechanism of earthquakes and nature of faulting on the mid-oceanic ridges, J. Geophy. Res., 72, 2131-2153, 1967.

Sykes, L.R. Seismological evidence for transform faults, sea floor spreading, and continental drift, The history of the earth's crust, 120-150, Princeton University Press, 1968.

Takeuchi, H., M. Saito and N. Kobayashi, Study of shear velocity distribution in the upper mantle by mantle Rayleigh and Love waves, J. Geophys. Res., 67, 2831-2839, 1962.

Takeuchi, H., J. Dorman and M. Saito, Partial derivatives of surface wave phase velocity with respect to physical parameter changes within the earth, J. Geophys. Res., 69, 3429-3441, 1964.

Tobin, D. G. and L. R. Sykes, Seismicity and tectonics of the Northeast Pacific Ocean, J. Geophys. Res., 73, 3821-3845, 1968.

Tocher, D., Earthquake energy and ground breakage, Bull. Seismol. Soc. Am., 48, 147-152, 1958.

Toksöz, M. N., A. Ben-Menahem, and D. G. Harkrider, Determination of source parameters by amplitude equalization of seismic surface waves, 1, Underground nuclear explosions, J. Geophys. Res., 69, 4355-4366, 1964.

Trygavasson, E., Dissipation of Rayleigh wave energy, J. Geophys. Res., 70, 1449-1455, 1965.

Tsai, Y. B. and K. Aki, Simultaneous determination of the seismic moment and attenuation of seismic surface waves, Bull. Seismol. Soc. Am., 59, 275-287, 1969.

Wickens, A. J. and J. H. Hodgson, Computer re-evaluation of mechanism solutions, Publ. Dom. Obs., Ottawa, 33, 1-560, 1967.

Wilson, J. T., A new class of faults and their bearing on continental drift, Nature, 207, 343, 1965a.

Wilson, J. T., Transform faults, oceanic ridges and magnetic anomalies southwest of Vancouver Island, Science, 150, 482, 1965b.

Wu, F. T., Parkfield earthquake of June 28, 1966: Magnitude and source mechanism, Bull. Seismol. Soc. Am., 58, 689-709, 1968.

Yanovskaya, T. B., On the determination of the dynamic parameters of the focus and hypocenter of an earthquake from records of surface waves, Izv. Akad. Nauk, USSR, Ser. Geofiz., 289-301, 1958.